

AFRL-SN-WP-TR-1999-1131

**INVESTIGATION OF POLYMER
OPTICAL WAVEGUIDE DEVICES**



**JAMES G. GROTE
JOSEPH E. BRANDELIK**

**AFRL/SNDI
SENSORS DIRECTORATE
AIR FORCE RESEARCH LABORATORY
2241 AVIONICS CIRCLE, STE. 20
WRIGHT-PATTERSON AFB, OH 45433-7322**

NOVEMBER 1999

FINAL REPORT FOR 05/05/1995 – 01/10/1999

APPROVED FOR PUBLIC RELEASE; DISTRIBUTION UNLIMITED

**SENSORS DIRECTORATE
AIR FORCE RESEARCH LABORATORY
AIR FORCE MATERIEL COMMAND
WRIGHT-PATTERSON AIR FORCE BASE OH 45433-7318**

20000525 023

DTIC QUALITY INSPECTED 1

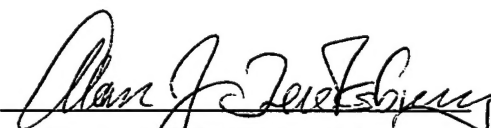
NOTICE

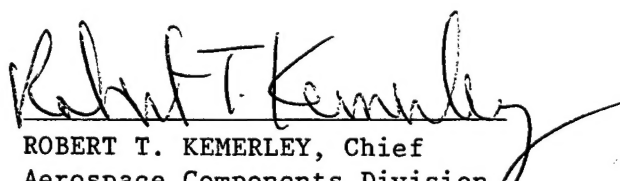
USING GOVERNMENT DRAWINGS, SPECIFICATIONS, OR OTHER DATA INCLUDED IN THIS DOCUMENT FOR ANY PURPOSE OTHER THAN GOVERNMENT PROCUREMENT DOES NOT IN ANY WAY OBLIGATE THE US GOVERNMENT. THE FACT THAT THE GOVERNMENT FORMULATED OR SUPPLIED THE DRAWINGS, SPECIFICATIONS, OR OTHER DATA DOES NOT LICENSE THE HOLDER OR ANY OTHER PERSON OR CORPORATION; OR CONVEY ANY RIGHTS OR PERMISSION TO MANUFACTURE, USE, OR SELL ANY PATENTED INVENTION THAT MAY RELATE TO THEM.

THIS REPORT IS RELEASABLE TO THE NATIONAL TECHNICAL INFORMATION SERVICE (NTIS). AT NTIS, IT WILL BE AVAILABLE TO THE GENERAL PUBLIC, INCLUDING FOREIGN NATIONS.

THIS TECHNICAL REPORT HAS BEEN REVIEWED AND IS APPROVED FOR PUBLICATION.


JOSEPH E. BRANDELIK
Multi-Chip Integration Branch
Aerospace Components Division


ALAN J. TEWKSBURY, Chief
Multi-Chip Integration Branch
Aerospace Components Division


ROBERT T. KEMERLEY, Chief
Aerospace Components Division
Sensors Directorate

Do not return copies of this report unless contractual obligations or notice on a specific document requires its return.

REPORT DOCUMENTATION PAGE			Form Approved OMB No. 0704-0188	
Public reporting burden for this collection of information is estimated to average 1 hour per response, including the time for reviewing instructions, searching existing data sources, gathering and maintaining the data needed, and completing and reviewing the collection of information. Send comments regarding this burden estimate or any other aspect of this collection of information, including suggestions for reducing this burden, to Washington Headquarters Services, Directorate for Information Operations and Reports, 1215 Jefferson Davis Highway, Suite 1204, Arlington, VA 22202-4302, and to the Office of Management and Budget, Paperwork Reduction Project (0704-0188), Washington, DC 20503.				
1. AGENCY USE ONLY (Leave blank)		2. REPORT DATE NOVEMBER 1999	3. REPORT TYPE AND DATES COVERED FINAL REPORT FOR 05/05/1995 - 01/10/1999	
4. TITLE AND SUBTITLE INVESTIGATION OF POLYMER OPTICAL WAVEGUIDE DEVICES			5. FUNDING NUMBERS C IN-HOUSE PE 62204 PR ARPE TA 01 WU 01	
6. AUTHOR(S) JAMES G. GROTE JOSEPH E. BRANDELIK				
7. PERFORMING ORGANIZATION NAME(S) AND ADDRESS(ES) AFRL/SNDI SENSORS DIRECTORATE AIR FORCE RESEARCH LABORATORY 2241 AVIONICS CIRCLE, STE. 20 WRIGHT-PATTERSON AFB, OH 45433-7322			8. PERFORMING ORGANIZATION REPORT NUMBER	
9. SPONSORING/MONITORING AGENCY NAME(S) AND ADDRESS(ES) SENSORS DIRECTORATE AIR FORCE RESEARCH LABORATORY AIR FORCE MATERIEL COMMAND WRIGHT-PATTERSON AFB, OH 45433-7318 POC: JOSEPH E. BRANDELIK, AFRL/SNDI, 937-255-4557 EXT. 3446			10. SPONSORING/MONITORING AGENCY REPORT NUMBER AFRL-SN-WP-TR-1999-1131	
11. SUPPLEMENTARY NOTES THIS IN-HOUSE EFFORT WAS FUNDED IN PART BY DARPA.				
12a. DISTRIBUTION AVAILABILITY STATEMENT APPROVED FOR PUBLIC RELEASE, DISTRIBUTION UNLIMITED.			12b. DISTRIBUTION CODE	
13. ABSTRACT (Maximum 200 words) This report is an initial investigation into polymer waveguides. The CAD program BEAMPROP is utilized for modeling of waveguides. Passive multi-mode and single-mode waveguides are considered. For modeling nonlinear optical polymers, in addition to the BEAMPROPAGATION (BEAMPROP) method, the effective index method and the MARCATILI model are developed. It is shown that a conducting cladding layer for the rectangular waveguides could significantly improve the operation performance of nonlinear optical, poled polymer waveguides.				
14. SUBJECT TERMS Optical Polymers, Waveguides, Waveguide Modeling			15. NUMBER OF PAGES 115	
			16. PRICE CODE	
17. SECURITY CLASSIFICATION OF REPORT UNCLASSIFIED	18. SECURITY CLASSIFICATION OF THIS PAGE UNCLASSIFIED	19. SECURITY CLASSIFICATION OF ABSTRACT UNCLASSIFIED	20. LIMITATION OF ABSTRACT SAR	

TABLE OF CONTENTS

LIST OF FIGURES	v
LIST OF TABLES	viii
FOREWARD	ix
ACKNOWLEDGMENTS	x
SUMMARY	1
1. INTRODUCTION	2
2. THE POINT PROGRAM	5
2.1 Related Program	6
2.2 Program Approach	7
3. THE COMPUTER PROGRAM BEAMPROP	9
3.1 Beamprop Enhancements	10
3.2 Theoretical Background	11
4. BEAMPROP RESULTS	14
4.1 Calculation Of Crosstalk In The Optical Backplane	14
4.2 Simulations On Multimode S-Bends	16
4.3 Simulations For Single-Mode Directional Couplers	18
5. DESIGN AND FABRICATION OF NON-LINEAR OPTICAL POLYMER INTEGRATED OPTICAL DEVICES	20
5.1 Electro-Optic Properties Of Nonlinear Optical Polymers	20
5.1.1 Linear Electro-Optic Effect	22
5.1.2 Index Ellipsoid	26
5.1.3 Electro-Optic Coefficients	29
5.1.4 Induced Refractive Indices and Birefringence	34
5.2 Electro-Optic Modulators	37
5.3 Directional Couplers	40
5.3.1 Zero-Gap Directional Couplers	43
5.3.2 Wavefront Tilt	46
5.3.3 Interaction Length Of The Directional Coupler	47
5.3.4 Rectangular Dielectric Waveguide Model	48

TABLE OF CONTENTS (continued)

5.3.5	Marcatili TE_{pq} Modes	50
5.3.6	Marcatili TM_{pq} Modes	55
5.3.7	Effective Index Method	56
5.3.8	Effective Index Method TE_{pq} Modes	58
5.3.9	Effective Index Method TM_{pq} Modes	64
5.3.10	Beam Propagation Method	66
5.3.11	Refractive Index Of The Waveguide Cladding	72
5.4	Device Fabrication	74
5.4.1	Photobleach	74
5.4.2	Etch And Fill	76
5.4.3	Corona Poling	76
5.5	Practical Nonlinear Optical Polymer Electro-Optic Devices	78
5.5.1	Electrode Separation	79
5.5.2	Passive Zero-Gap Directional Coupler	81
5.5.3	Active Zero-Gap Directional Coupler	84
5.5.4	Nonlinear Polymer To Passive Polymer Coupling	87
6.	CONCLUSIONS	88
7.	REFERENCES	89

LIST OF FIGURES

Figure 1.	Power Requirements for Optical and Electrical Interconnects versus Data Rate [32].	2
Figure 2.	Simulations for an array of five waveguides.	15
Figure 3.	Results for offsets of 1, 2, and 5 μm .	15
Figure 4.	Simulation results for 2.5'S-bends.	17
Figure 5.	Simulation results for 7.5° S-bends.	17
Figure 6.	Simulation results for smooth 7.5° S-bends.	18
Figure 7.	Simulation of a single-mode directional coupler.	19
Figure 8.	Index Surfaces for (a) a Positive Uniaxial Crystal and (b) a Negative Uniaxial Crystal [29].	21
Figure 9.	Inner Ellipse is the Intersection of Index Ellipsoid with the Plane Perpendicular to s [15].	26
Figure 10.	Transverse Electro-Optic Modulator using a Tetragonal 4 Group Crystal.	34
Figure 11.	Operation of a Mach Zehnder Interferometer.	38
Figure 12.	Operation of a Directional Coupler.	40
Figure 13.	Operation of a Zero-Gap Directional Coupler.	46

LIST OF FIGURES (continued)

Figure 14.	Rectangular Waveguide Directional Coupler.	47
Figure 15.	Rectangular Waveguide Directional Coupler Cross Section.	49
Figure 16.	Field Intensity Profiles of the Symmetric and Antisymmetric Modes in a Rectangular Directional Coupler.	52
Figure 17.	Trajectory of a Guided Wave in a Slab Waveguide.	56
Figure 18.	Analytical Model for the Effective Index Method for TE_{pq} Modes.	57
Figure 19.	Amplitudes of the Propagating Fields in an Integrated Optic S-Bend Waveguide.	72
Figure 20.	Schematic of Triple Stack Including Conductive Polymer Charge Sheets.	81
Figure 21.	Schematic of a Passive Zero-Gap Directional Coupler With an NLO Polymer Interaction Region and Passive Polymer Input/Output Channels.	82
Figure 22.	Beam Propagation Model of Passive Zero-Gap Directional Coupler Using NLO and Passive Polymers With Matching Indices.	83
Figure 23.	Beam Propagation Model of Passive Zero-Gap Directional Coupler Using NLO and Passive Polymers With 0.01 Mismatched Indices.	84

LIST OF FIGURES (continued)

Figure 24.	Beam Propagation Model Of Active Zero-Gap Directional Coupler Using NLO And Passive Polymers With Matching Indices.	85
Figure 25.	Beam Propagation Model Of Active Zero-Gap Directional Coupler Using NLO And Passive Polymers With 0.01 Mismatched Indices.	86

LIST OF TABLES

Table 1.	Major Programs On High Speed Parallel Optical Data Links.	8
Table 2.	NLO Materials Comparison.	79
Table 3.	NLO Polymer Comparison.	80

FOREWORD

While passive polymer waveguides are addressed in this manuscript, this report focuses on the modeling and fabrication of practical and competitive non-linear optic (NLO) polymer integrated optic devices for computer based applications. The devices covered will include mach Zehnder interferometers, conventional directional couplers and zero-gap directional couplers. Modeling techniques will include dielectric waveguide, effective index and beam propagation methods. Fabrication techniques, including photobleach, and etch and fill, will be detailed. State-of-the-art design schemes exhibiting the potential to lower the switching voltage of NLO polymer integrated optic devices will be investigated, including the use of conductive polymers. The NLO polymers presented in this manuscript will be those readily available. Coupling techniques used to achieve good coupling efficiency between passive polymers, utilized for general routing, and NLO polymers, used for active switching, will also be addressed.

ACKNOWLEDGMENTS

The optically passive work is based in part on discussions with Yung Liu of General Electric Corporate Research and Development (GECRD), Mario Ghezzi of GECRD, Matthew Nielsen of GECRD and Antonio Crespo of the Air Force Research Laboratory/Sensors Directorate (AFRL/SNDI). The optically active polymer work is based in part on discussions with Julian Bristow of Honeywell, Stephen Caracci of Air Force Research Laboratory/Materials and Manufacturing Directorate (AFRL/MLPO), Bruce Reinhardt of AFRL/MLBP, Mohammad Karim of the University of Dayton (UD), Vincent Dominic of UD, Charles Lee of the Air Force Research Laboratory/Air Force Office of Scientific Research (AFRL/AFOSR), Ray Chen of the University of Texas at Austin, Larry Dalton of the University of Southern California, Paul Ashley of the US Army Missile Command, and Charles Sullivan of Sandia National Laboratories. Their input was both welcomed and invaluable. Sincere appreciation is extended to the members of AFRL/SN for their help and support in device fabrication and test equipment design and fabrication. Members of Technology Scientific Services and Wright State University, working for AFRL/SN also provided assistance in device fabrication, generation of waveguide masks and design and fabrication of the bases and mounts for the test equipment.

This manuscript covers in-house work spanning a number of years and was funded by the Air Force Research Laboratory (AFRL) and the Defense Advanced Research Projects Agency (DARPA).

SUMMARY

This document covers optically passive and optically active polymer waveguides. The passive polymers that are modeled are multimode and the work is an outgrowth of the General Electric POINT program (Air Force contract F33615-94-C-1530). Modeling of the waveguides was through the use of the BeamPROP CAD program. Information transfer using passive polymers requires modulation of a laser. Optically active waveguides can provide their own modulation. The modeling and fabrication of non-linear optic (NLO) polymer integrated optic devices for computer based applications are presented. The devices covered will include Mach-Zehnder interferometers, conventional directional couplers and zero-gap directional couplers. Modeling techniques include the dielectric waveguide, effective index and beam propagation methods. Fabrication techniques, including photobleach, and etch and fill, are detailed. Design schemes that exhibit the potential to lower the switching voltage of NLO polymer integrated optic devices are investigated, including the use of conductive polymers. Coupling techniques used to achieve good coupling efficiency between passive polymers, utilized for general routing, and NLO polymers, used for active switching, are also be addressed.

1.0 INTRODUCTION

As electronic and optical data processing circuits approach multi-gigahertz operation rates, the need for multi-gigahertz communication between these processing circuits becomes essential. This communication includes chip-to-chip on a common multichip module (MCM), MCM to MCM on a common board, and board-to-board through a common backplane. The data rates at which communication through electrical interconnects can be transmitted is limited to the low gigahertz rates, unless one is willing to expend large amounts of power. Electrical wires and striplines possess frequency dependent dissipative losses due to conductive and dielectric properties, and frequency dependent parasitic coupling losses due to radiative and surface wave propagation properties [1]. The higher the frequency, the higher the losses. This is where optics can help provide solutions. Optical interconnects can transmit data at optical frequencies with orders of magnitude lower losses than their electrical counterparts. The power requirements for optical and electrical interconnects versus data rate are illustrated in Figure 1.

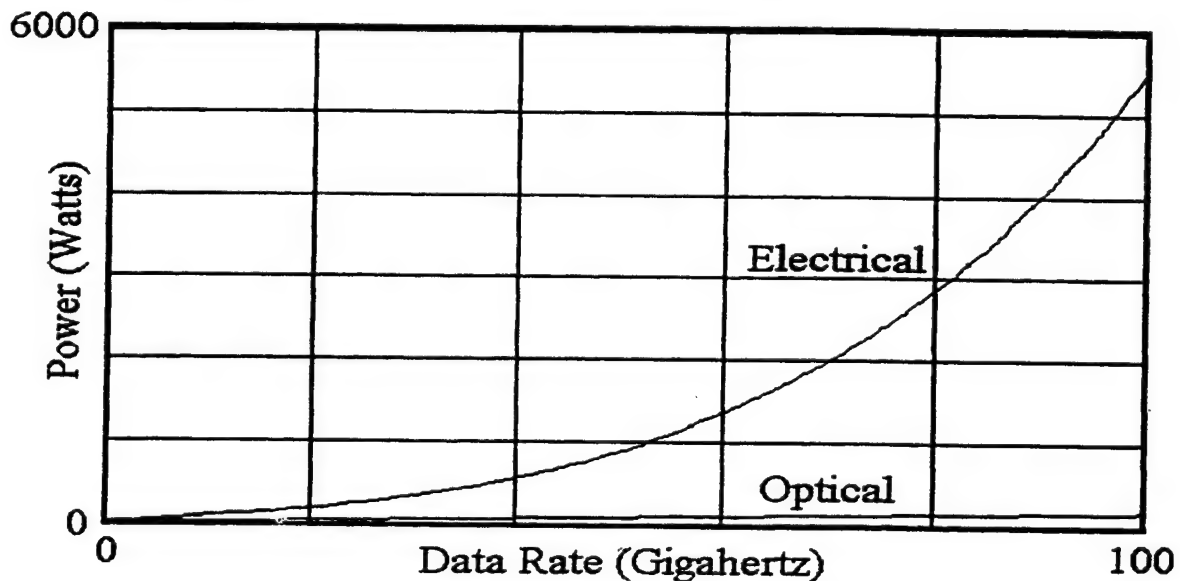


Figure 1. Power Requirements for Optical and Electrical Interconnects versus Data Rate [32].

The criterion used to generate Fig. 1 were as follows: waveguide lengths for both the electronic and optical interconnects were 50 mm. The total number of interconnects was

600 for both types. For electrical interconnects on an alumina substrate, waveguide widths of 25 μm and waveguide heights of 650 μm were assumed. The effective and relative permittivities of the microstrip used were 6.7 and 9.9, respectively [1]. The capacitance used per line was 6 pF and an impedance of 50 Ω was assumed. The power versus data rate for the electrical interconnects was determined with methods given by Edwards [1]. For optical interconnects on a semiconductor substrate, waveguide widths of 3 μm and waveguide heights of 1 μm were assumed. Waveguide propagation loss of 0.2 dB/cm was assumed for 1 GHz growing as 0.08 dB/GHz [2, 3, 4, 5, 6, 7, 8]. The modulator loss was 5×10^{-5} W/channel for 1 GHz growing as 5×10^{-5} W/GHz [3]. The detector capacitance was 0.3 pF and the detector amplifier capacitance used was 1.7 pF [3]. The power, per detector, was 1×10^{-3} W/channel for 1 GHz growing as 1×10^{-3} W/GHz [3]. The laser power was 100 mW for 1 GHz decreasing at the same rate as the waveguide loss was growing per GHz [3]. Finally, 20% electrical efficiency and 50% optical coupling efficiency were assumed for the laser. The power versus data rate was then determined by adding up the power usage of the components.

In addition to the lower power consumption and higher bandwidth, optical interconnects offer isolation from electro-magnetic interference (EMI) [9]. Optical interconnects are starting to be utilized in chassis-to-chassis and board-to-board communication using glass optical fibers [2, 5, 9, 10, 11, 12]. Polymeric optical waveguides are in the early stages of application to interconnects. On the smaller scale of multichip modules and within-module, integrated optics is just beginning to emerge [2, 3, 5, 6, 8-40]. Optics offers the additional advantages of smaller interconnect widths and in-plane crossover capability with very low crosstalk. This eliminates the need for air bridges. Less wafer and board real estate will be required for optical interconnects, which leaves room for additional electronic circuits and devices. Fabrication processes for optical interconnects must be compatible with those processes used for manufacturing electronic interconnects and devices. This is important from the standpoint of practicality and of acceptability. Polymers are attractive materials because they are currently being used for the buffer layers between signal planes in IC's and MCM's. Nonlinear optical (NLO) polymers possess electro-optical effects which can be utilized to fabricate electro-optic (EO) switches.

Optical switches can be incorporated with optical waveguides and other EO switches to realize digital logic operations reconfigurable interconnects. Current research in developing processing techniques for polymer optical waveguides and devices has shown that the processing techniques for these optical circuits are compatible with those techniques used for the fabrication of electronic circuitry [2, 3, 4, 5, 6, 7, 8, 21, 22, 35, 36, 39-65]. By using NLO polymers, one can conceivably house the entire electronic/electro-optic circuit on a single substrate. With the incorporation of NLO polymer electro-optic circuits and polymer optical waveguides, the multichip module or board, currently entirely electronic, could perform more efficiently with less power consumption, move data around faster with less noise, and use less real estate.

There is also the potential to reconfigure the multichip modules to perform entirely different operations, or to route signals around inoperative or defective portions of the module [2, 3, 8-11, 14, 20-22, 32, 35-39, 41, 52, 53].

Nonlinear optic polymers have several attractive characteristics which many researchers have tried to capitalize on over the past decade. These include a high electro-optic coefficient for low voltage operation, a low dielectric constant for high speed modulation, low temperature processing for integration of optics with electronics, excellent index match to optical fibers and the potential to simplify fabrication for lower cost [3, 4, 7, 8, 21, 22, 35, 36, 38-40, 42, 45-47, 49-70]. Current properties of readily available NLO polymers include an electro-optic coefficient $r_{33} = 26 \text{ pm/V}$ at $\lambda = 830 \text{ nm}$, a propagation loss of 1.5 dB/cm at $\lambda = 830 \text{ nm}$ and a long term poling retention temperature stability of 80°C [3, 4, 7, 8, 21, 22, 35, 36, 38-40, 42, 45-47, 49-70]. These properties should be adequate for demonstration of a competitive electro-optic device.

2.0 The Point Program

There have been significant advances in optical materials, devices, and packaging technologies, making optical interconnects the viable wide band interconnect technology of choice [71]. These enabling technologies are:

- 1) Vertical cavity surface emitting lasers (VCSEL) devices and low cost VCSEL packaging
- 2) Polymer based optical waveguide and fiber materials
- 3) Low cost micro-optical components, connectors, and fabrication processes.

Some of these new optoelectronic materials and devices can be handled, processed, and packaged much like IC devices using planar fabrication and batch processing, meeting the key requirements for low cost, large volume manufacturing.

The POINT program was organized in response to DARPA's BAA-94-46, "Affordable Optoelectronic Module Technology," and was under contract on December 1, 1994. The Program kickoff meeting was held on December 15, 1994 at DARPA, and was attended by all Principal Investigators - General Electric, Honeywell, AlliedSignal, AMP, Columbia University, and the University of California at San Diego (UCSD). The goal of the POINT program was to develop affordable optoelectronic packaging technologies utilizing optical polymer media for board and backplane optical interconnect applications in military and commercial systems. The program's technical approach was to leverage electronic packaging and fabrication processes - such as batch process, planar fabrication and passive alignment - to significantly reduce the cost of optoelectronic packaging. The program development focused on:

- 1.) VCSEL devices and the related packaging technology that leverages the electronic planar fabrication process
- 2.) Passive alignment techniques that could reduce significantly the recurrence cost in O/E packaging

- 3.) Planar polymer waveguides that could be used for board and backplane applications for high density
- 4.) High speed optical interconnects to remove the interconnect bottlenecks among multiple processors in a computer system.

2.1 Related Programs

The Optoelectronic Technology Consortium (OETC) [72] was a DARPA sponsored industrial consortium. Originally formed in 1992 by GE (later transferred to Lockheed Martin), ATT, IBM, and Honeywell, OETC aimed at developing key optical interconnect technology for computer applications. This represented the first major R&D effort to develop 32-channel parallel optical links operating at 500 Mbps per channel, with a BER $< 1 \times 10^{-14}$ and average power of 0.25 W/channel dissipated power. The link included 32-channel AlGaAs VCSEL arrays, driver arrays, GaAs MESFET receiver arrays, and fiber ribbon arrays with MAC II connectors. This program is credited with recognizing the significance of VCSEL devices, and it accelerated the development of VCSEL technology from a laboratory novelty at the beginning of the program, to a critical optical component by the time the program ended in 1995, meeting all requirements for short-haul optical communication.

The POLO program [73] consisted of BP, AMP, DuPont, Spectra-Diode Labs (SDL), and University of Southern California (USC), and was sponsored jointly by industry and DARPA. Started in 1994, it aimed to reduce the cost of optoelectronic module technology. POLO led to the development of bi-directional 10-channel parallel optical links operating at 1 Gbps per channel.

The JITNEY program [74], a joint development effort by IBM and 3M, was a NIST-sponsored ATP program to develop low cost, parallel optical modules operating at 20 channels and 1 Gbps/channel. JITNEY used 20-channel VCSEL arrays, CMOS driver ICs, and a 20-channel GaAs MESFET receiver array OEIC. The modules were made of plastic molded optical couplers to interface between VCSEL and large core fibers.

OPTOBUS is a commercial product developed by Motorola. It is available as bi-directional 10-channel transceiver modules operated at 200 Mbps/channel.

2.2 Program Approach

Optical interconnect technologies can be classified broadly into three categories according to the transmission, data rate, and distance:

- 1.) For long-haul communication over several kilometers (such as telecommunication, wide area network, single-mode optic fibers and long wavelength), using InGaAsP edge-emitting lasers at 1.3 at 1.5 μm . Single-channel point-to-point interconnects are typical.
- 2.) For a communication distance ranging between tens and hundreds of meters (such as local area network interconnects between high speed servers, workstation clusters, and supercomputers, using multimode optic fibers and short wavelength). AlGaAs/GaAs semiconductor lasers at 0.85 μm are commonly employed, using either single or multiple channels. The OETC, POLO, OPTOBUS, and JITNEY programs developed the technologies for these applications.
- 3.) For short distance communication less than a few meters (such as within a cabinet, a backplane, or an interconnect between frames and boards), employing multichannel VCSEL arrays at 0.85 μm with multimode fibers or polymer waveguides.

The POINT program approach was to apply emerging enabling technologies with the intent of developing an affordable optical interconnect and packaging technology. In the POINT program, Honeywell's state-of-the-art VCSEL devices were used as the laser source for the development of the parallel optical interconnect links. The VCSEL is the single most important active optical component developed for interconnect applications in short-haul data communication. The POINT was aimed at the development of an affordable optoelectronic packaging and interconnect technologies using optical polymers for board and backplane

applications. See Table 1 for a comparison of programs. The expression, $BER = 0.5 \cdot \text{erfc}(\text{SNR}/(2 \cdot \sqrt{2}))$, was used to determine the bit error rate from the signal to noise ratio.

Table 1. Major Programs On High Speed Parallel Optical Data Links.

Project	OETC	OptoBus	POLO	Jitney	POINT
Sponsor	DARPA	Motorola	DARPA/TRP	NIST/ATP	DARPA
Team	GE (LMC), ATT, IBM, Honeywell	Motorola	HP, AMP, SDL, USC	IBM, 3M	GE, Honeywell, Allied Signal, AMP, Columbia, UCSD
# channels	32	10/10	10/10	20	12/12
Data rate per channel (Mbps)	>500	150	625,1000	500	>350
Total data rate (Gbps)	10020	1.5	6	10	4.2
Max link length (m)	100	30	1-300	<30	Board, backplane<0.1
Size (mm)	33x44x5	38x38x13	40x40	28x18	N?A
Power (W) Tx+Rx	10	1.7	< 3	<3	2
Channel pitch (μm)	140	250	250	500	250/100
Packaging type	Lead frame	Pin grid array	Lead frame	Lead frame SM	User defined
Connector type	MAC II	MT	MT	-	MT
Wavelength	VCSEL (850)	VCSEL (850)	VCSEL (850)	VCSEL (850)	VCSEL (850)
Fiber coupling	Fiber/SiOB 45° mirror	Moulded Plastic couplers	Polyguide 45° mirror	Butt coupled	Polyguide & polymer waveguide 45° mirror
Fiber/pitch dimensions (μm)	62.5/140	62.5	62.5/125	200	50/100 (rectangular waveguides)
Electrical interface	LVDS, ECL	ECL	PECL	LVDS/SCI	Application specific
Target Cost:					
\$/transceiver	\$320 (\$16/Gbps)	\$150 (\$100/Gbps)		\$600 (\$66/Gbps)	Cost added to next line
\$/fiber + connectors				<\$200/10m cable	<\$100/Gbps

The POINT passive polymer effort achieved an interconnect density of 250 lines per board-edge-inch. Each line could operate at up to 1 gigabits per second (Gbps). The total (electrical and optical) insertion loss achieved was -9 dB. The waveguide elements were aligned passively. The fabrication process is MCM foundry compatible.

3. The Computer Program BeamPROP

The BeamPROP software incorporates advanced finite-difference beam propagation techniques for simulation, and a modern graphical user interface for ease of circuit layout and analysis. The benefit of good design and modeling tools is well known in the electronics industry, where both device and circuit simulation programs, such as PISCES and SPICE, have been instrumental in advancing the availability and use of integrated electronic circuits. BeamPROP brings this important capability to the photonics area, and can be an extremely useful tool for research and development groups in both university and industrial environments.

The main program contains a complete CAD layout system for design of waveguide devices and circuits, and controls simulation features such as numerical parameters, input field, and display and analysis options. The simulation program, which can be executed within the main program or as a standalone, performs the actual simulation and provides a graphical display of the field and other quantities of interest for analysis.

The CAD system was designed specifically for photonic circuits, and incorporates a natural, object-oriented input model. Several unique features such as user programmable circuits and optical pathways and monitors allow for rapid parameter variation and ease of analysis. The CAD system allows a smooth transition to the simulation program, with quick startup and easy access to features. The program provides intelligent choices for default numerical parameters, which are problem-dependent. The simulation incorporates integrated, real-time analysis and display of the simulation results, and can be run in the background. Both 2D (one transverse, one longitudinal) and 3D (two transverse, one longitudinal) simulation techniques are available.

One of the key tasks in the POINT program was to develop a software package capable of designing and analyzing multimode waveguide devices for optical interconnects. This outline some of BeamPROP's capabilities and applications.

The software, BeamPROP, was developed at Columbia University and licensed in 1994 to RSoft, Inc., a commercial software firm. During the POINT program, Columbia University worked with RSoft to extend BeamPROP so that it would meet the program's specific needs for multimode devices and for interconnects. The enhanced BeamPROP software, together with the multimode interconnect device templates, forms the CAD tool developed under the POINT program. The software is capable of addressing such problems as:

- Fiber to waveguide coupling
- Source to waveguide and waveguide to detector coupling
- Waveguide transitions
- Bend and routing analysis
- Transmission/loss calculation
- Signal-to-noise, modal noise, and BER estimation

3.1 BeamPROP Enhancements

BeamPROP software is a general purpose waveguide design package. At the start of the POINT program, the software supported the following capabilities:

- CAD layout, simulation, and design of optical waveguide devices and circuits
- Advanced parametric CAD tool
Graphical interface: input material index parameters, waveguide components, mode launch properties, etc.
- 2D and 3D simulation capability
- Enhanced, wide-angle beam propagation
- Integrated dynamic analysis
- Export of standard CAD files
- PC or workstation based (Windows or UNIX)

As the program progressed, Columbia, working with RSoft made the following additions and improvements to the software in response to the POINT team requirements:

- Extended multimode launch options
- Enhanced automatic variable scanning for random sampling
- Added statistical analysis tools for computing modal noise
- Added bit error rate (BER) estimation
- Added a wide-angle transparent boundary condition for multimode problems
- Added vector BPM capability for handling polarization
- Expanded its capability for simulating bends
- Added new optimizations, taking advantage of multimode structures
- Enhanced the wide-angle BPM for multimode problems
- Improved the interface conditions improving the accuracy of high index contrast
- Added new options and utilities for modal decomposition and construction of input fields
- Enhanced the batch capabilities
- Improved the file export capabilities

3.2 Theoretical Background

The objective of BeamPROP is to provide a general simulation package for computing the propagation of light waves in arbitrary waveguide geometries. This is a complex problem, in general, and several assumptions are made at the outset (many of which are subsequently relaxed). We first limit our attention to monochromatic scalar waves, which are described by the Helmholtz equation:

$$\nabla^2 \phi + \frac{\omega^2}{c^2} n^2 \phi = 0$$

Here, the optical field (one component of E or H) has been written as $\phi(x,y,z) e^{-ikz}$ where ϕ is the angular frequency of the light. The refractive index distribution in the domain of interest is assumed to be given by $n(x,y,z)$, and is determined by the geometry of the waveguide circuit.

The BeamPROP software determines an approximate solution to the above equation using several techniques. The computational core of the program is based on a finite difference beam propagation method as described in the paper by R. Scarinozzino and R.M. Osgood, Jr. [75], and references therein. This technique uses finite difference methods to solve the well-known parabolic or paraxial approximation of the Helmholtz equation, which is written as:

$$2ik\bar{u}_z + \nabla_T^2 u + (\bar{k}^2 - k^2)u = 0$$

In this equation we have assumed that the wave is propagating primarily along z, and have factored out the rapid variation in the field by writing $\phi(x, y, z) = u(x, y, z)e^{ikz}$, where \bar{k} is a constant representing the characteristic wavenumber for the propagation. We denote the wavenumber in free space by $k_0 = \omega/c = 2\pi/\lambda$, and have introduced the notation $k(x, y, z) = k_0 n(x, y, z)$ to represent the spatially dependent wavenumber. The above equation is solved numerically using an implicit finite difference scheme as described in reference 1. In addition, the program uses "transparent" boundary conditions following the work of G.R. Hadley [76].

The fundamental physical limitation of the above approach results from the parabolic approximation to the Helmholtz equation, which implies a paraxiality condition on the primary direction of propagation. These limitations can be reduced using more accurate approximations to the Helmholtz equation as outlined by G.R. Hadley [77]. BeamPROP has the option of implementing this technique, and includes (1,0), (1,1), (2,2), (3,3), and (4,4) Padé' approximations.

BeamPROP utilizes vector beam propagation techniques to overcome the limitations of the assumption of scalar waves which prevents polarization effects from being considered. Those

methods are based in part on the approach described by W.P. Huang and C.L. Xu [78, 79] and related references.

BeamPROP uses a bidirectional beam propagation (BPM) algorithm. The algorithm considers coupled forward and backward traveling waves, and can account for reflection phenomenon, including resonant effects as found in grating structures.

The physical propagation problem requires two key pieces of information:

1. The refractive index distribution, $n(x, y, z)$.
2. The input wave field, $u(x, y, z = 0)$.

From these, the physics dictate the wave field throughout the rest of the domain, $u(x, y, z > 0)$.

The software provides a way to specify this information.

The solution algorithm requires additional input in the form of numerical simulation parameters such as:

1. A finite computational domain $\{x \in (x_{\min}, x_{\max})\}, \{y \in (y_{\min}, y_{\max})\}$, and $\{z \in (z_{\min}, z_{\max})\}$
2. The transverse grid sizes, Δx and Δy .
3. The longitudinal step size, Δz .

The software attempts to estimate appropriate values for these parameters, but allows the user to override them. As with any simulation, confidence in the accuracy of the numerical solution requires experimentation to determine the sensitivity to the numerical parameters.

4. BEAMPROP RESULTS

Calculated results for passive waveguides using the CAD software BeamPROP are presented in this chapter. The work on "crosstalk in the optical backplane" and "simulations on multimode S-bends" was conducted on the POINT program by GE [80]. The GE work is based on the use of polymers. One of the polymers used on POINT is UltemTM which is a trademark of the General Electric Company. Another polymer used on the point program was PolyguideTM which is a trademark of Allied Signal. Zero-gap, single-mode, directional couplers simulations were provided by the Air Force Research Laboratory [81]. The single-mode work is based on the use of gallium nitride (GaN).

4.1 Calculation of crosstalk in the optical backplane

During the POINT effort, GE performed a series of simulations to determine an upper bound on the expected level of crosstalk.

GE considered the basic problem of crosstalk between 50 μm wide waveguides in a waveguide array with a 100 μm pitch. There are two sources of crosstalk: evanescent coupling and radiation. In Figure 2, the simulation results for an array of five waveguides using a specific multimode combination launched into the center guide with no offset are shown. Since there is no transition here, no radiation is expected, only evanescent coupling. The results indicate that the evanescent coupling over a 1 cm length is less than 60 dB, and is therefore negligible.

Next, a situation where the input source is misaligned by an offset with respect to the center waveguide is investigated. The results for offsets of 1, 2, and 5 μm (see Figure 3) show that, as the radiation induced by the transition passes through the guide, the crosstalk level in each guide reaches a maximum at a certain distance from the input. Beyond that point, the crosstalk level decays slowly. The peak crosstalk level ranges from about -30 dB for a 1 μm offset, to about -20 dB for a 5 μm offset, giving one an indication of the worst case scenario.

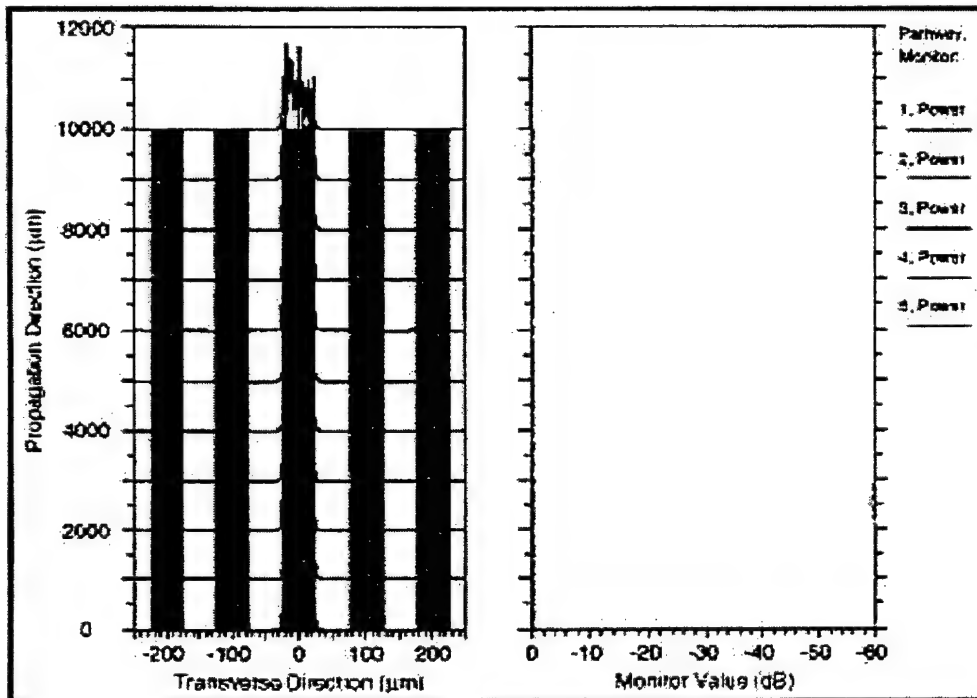


Figure 2. Simulations for an array of five waveguides.

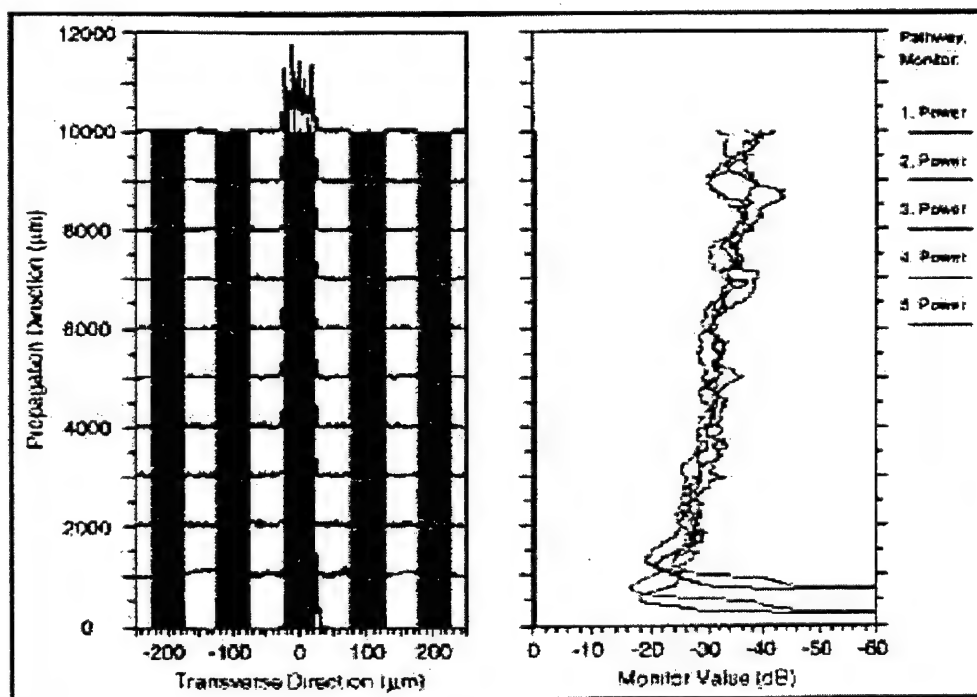


Figure 3. Results for offsets of 1, 2, and 5 μm .

With regard to these results, there are two important points to note:

1. The crosstalk level is not artificial. Instead, the crosstalk level is due to light trapped between the waveguides, which leaks into the adjacent waveguides.
2. These are 2D simulations. One expects the crosstalk levels to be better with 3D simulations because there is an additional dimension in which to diffract.

Simulations showed the beam diffracts rapidly over the 1 cm length, so we expect that the laterally trapped light will dissipate considerably due to vertical diffraction. However, when the vertical field distribution was more like the fundamental mode, diffraction was weak and would not have been sufficient to dissipate the trapped light.

4.2 Simulations On Multimode S-Bends

Beam propagation simulations were performed for 2.5° and 7.5° S-bends in PolyguideTM to determine the expected loss values. The simulation results for 2.5° are shown in Figure 4 and indicate a 0.85 dB loss for the full structure (two angular bends). Figure 5 is a simulation that assumes 7.5° S-bends and indicates a 2.95 dB loss for the full structure. For the simulations that are represented by Figures 4 and 5, abrupt S-bends (also called Z-bends) were used. Note that this is the worst case scenario.

Next, abrupt S-bends (also called Z-bends) are compared with that of smooth S-bends, both. The 7.5° bend angle is the largest angle that would be needed in the POINT receiver module where the waveguides would be used. Having studied this S-bend theoretically in its abrupt form, the smooth version was modeled. The simulation results are shown in Figure 6.

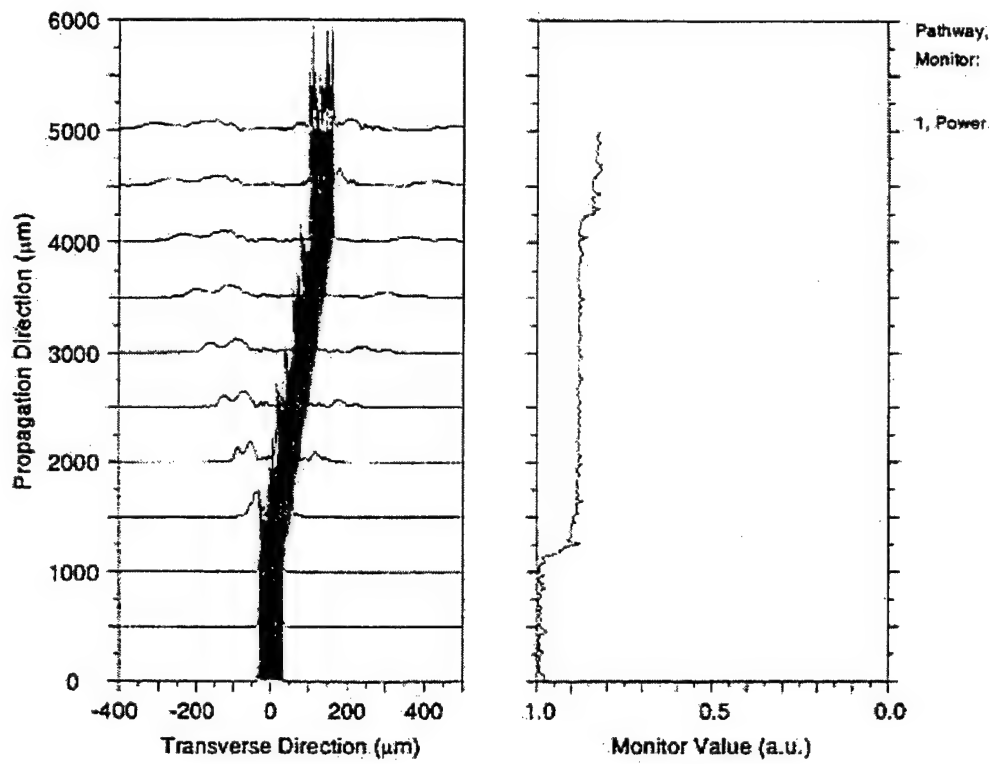


Figure 4. Simulation results for 2.5° S-bends.

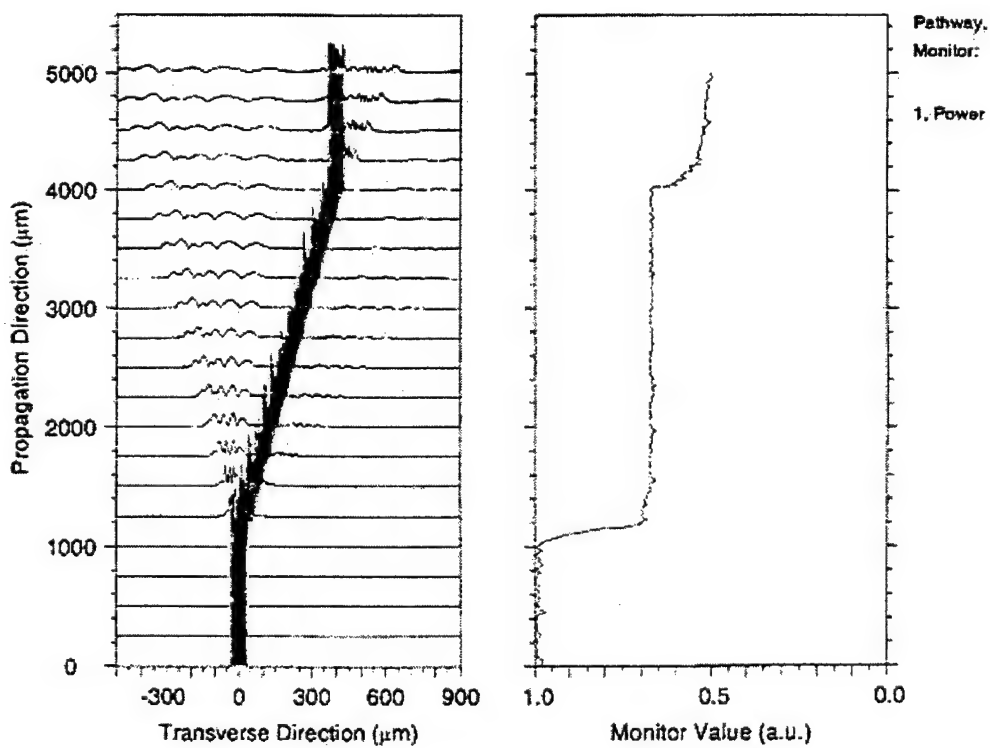


Figure 5. Simulation results for 7.5° S-bends.

The smooth S-bend simulation shown in Figure 6 reveals a bending loss of only 0.38 dB. This confirms that we can considerably improve the loss results by using a non-abrupt design. Note that the power loss in the abrupt structure occurs in two large drops at the bending junctions, whereas the power loss in the smooth structure occurs in two small drops at the first bend and then at the midpoint (the point of maximum curvature). Thus, for a 7.5° effective angle circular arc, the S-bend angle is 15° .

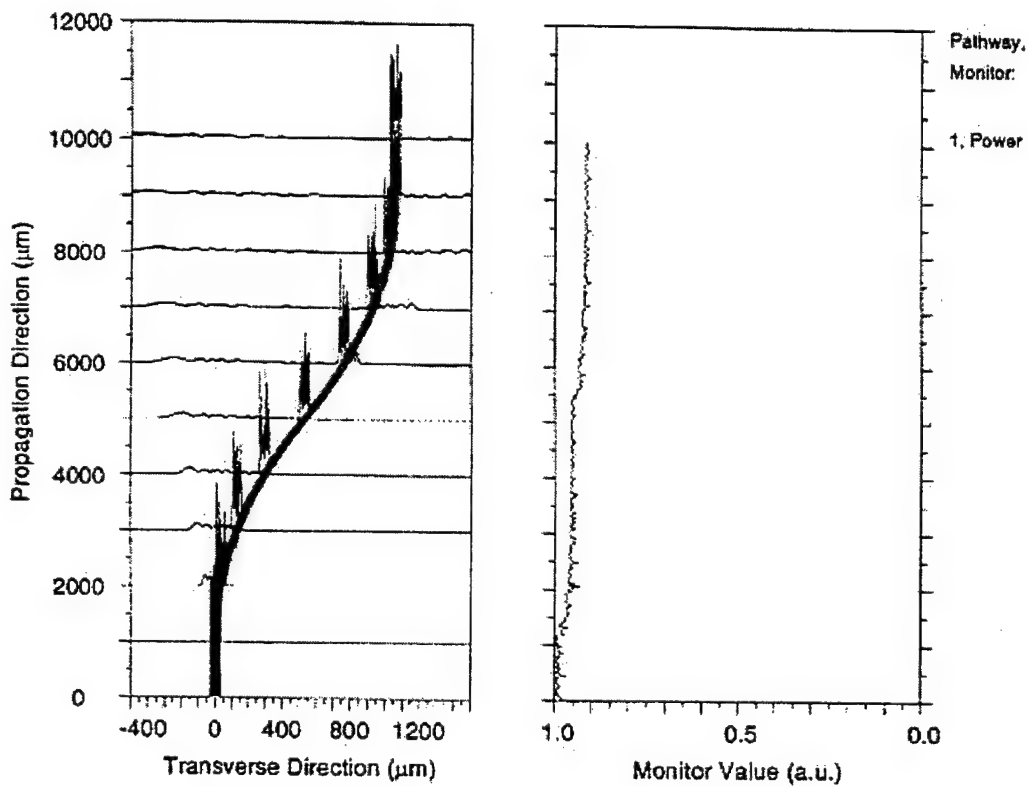


Figure 6. Simulation results for smooth 7.5° S-bends.

4.3 Simulations for single-mode directional couplers

The POINT program utilized multimode passive polymer waveguides. Multimode waveguides do not have the demands on lithography and processing that single-mode waveguides. Passive polymers require individual lasers for every waveguide in order to provide modulated information. Laser diodes are low impedance

current driven, not voltage, driven devices. As the modulation drive frequency increases, the demands on the electronic modulator become formidable because of impedance matching requirements and required drive power. Optically active waveguides can act as modulators. Waveguide modulators are voltage driven devices.

GaN is actively being researched as a high temperature electronic material for amplifiers. GaN is an optically active material with an E-O coefficient for r_{13} of 1.9 pm/V, for r_{33} of 0.5 pm/V, and for r_{51} of 3.1 pm/V. While it has not been demonstrated, both electronic and optical devices may be made on a common substrate using the GaN material. Single-mode GaN directional coupler switches were modeled using BeamPROP at the Air Force Research Laboratory. For an isotropic medium, only the TE mode is propagated. Figure 7 shows the power transfer between two waveguides. The power can be seen to transfer from the input waveguide to the adjacent waveguide and back to the input guide as a function of distance. By controlling the total length of the waveguide, one can decide from which waveguide the optical energy will exit.

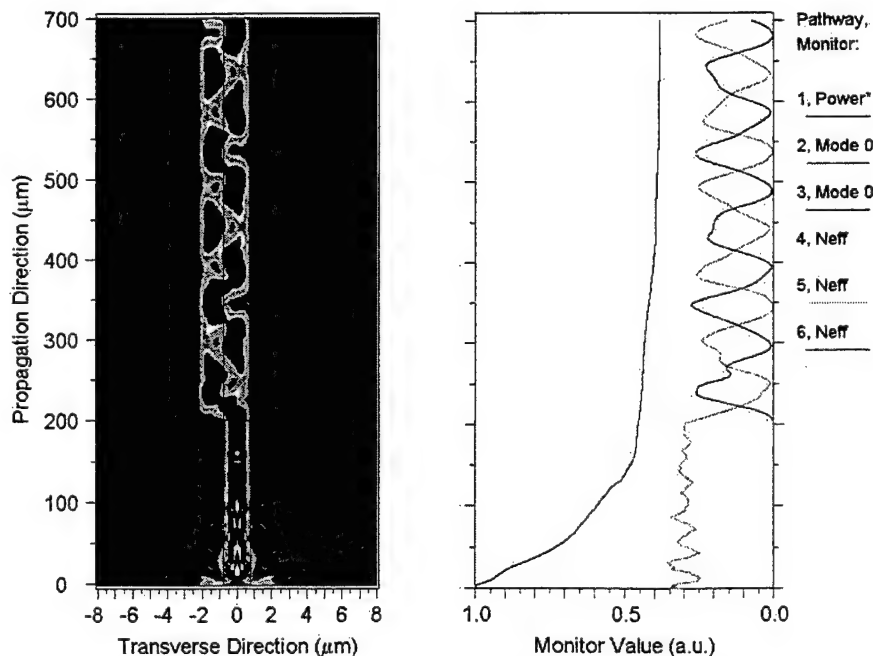


Figure 7. Simulation of a single-mode directional coupler.

Active, single-mode, waveguide modulators are discussed in chapter 5.

5.0 DESIGN AND FABRICATION OF NON-LINEAR OPTICAL POLYMER INTEGRATED OPTICAL DEVICES

The POINT program utilized multi-mode passive waveguides. The multimode waveguides could be manufactured with General Electric's High Density Interconnect (HDI) process. The HDI process does not have the lithographic resolution necessary to realize effective single mode waveguides. In the chapters that follow, single-mode waveguides will be investigated. Single mode waveguides are needed for active devices.

5.1 Electro-Optic Properties Of Nonlinear Optical Polymers

Nonlinear optical polymers in their bulk crystalline form typically behave like biaxial crystals [15, 69, 70, 82]. However, if one takes care to ensure that the material is either amorphous or that the microcrystalline dimensions are very small, undesirable propagation velocity effects, which can introduce phase errors, will be minimized. The NLO polymer can then be treated as a uniaxial crystal [11, 15, 83]. It has been shown that metal particulates embedded in a dielectric material do not show any directional preference or change in dielectric coefficient in the absence of an electric field, when the particulate size is much less than the separation [83]. Application of an electric field in the direction of a chosen axis establishes uniaxial behavior. Care must be taken to ensure that the material does not go through a crystalline material phase during processing. Uniform growth and minimized stress, as well as maximizing spontaneous nucleation sites, are crucial. Realizing a uniaxial crystal structure using NLO polymers is material processing dependent.

For our analysis, we shall assume an NLO polymer belonging to the tetragonal symmetry class 4 [15, 82]. Uniaxial crystals possess EO properties by which a polarization and, hence, a birefringence can be induced when an electric field (E) is applied to the crystal (Pockels effect) [26, 29]. The Pockels effect is a linear EO effect; the induced birefringence is directly proportional to the first power of the applied electric field. Thus, uniaxial crystals exhibit anisotropic behavior.

Figure 8 provides the reference coordinates for uniaxial crystals.

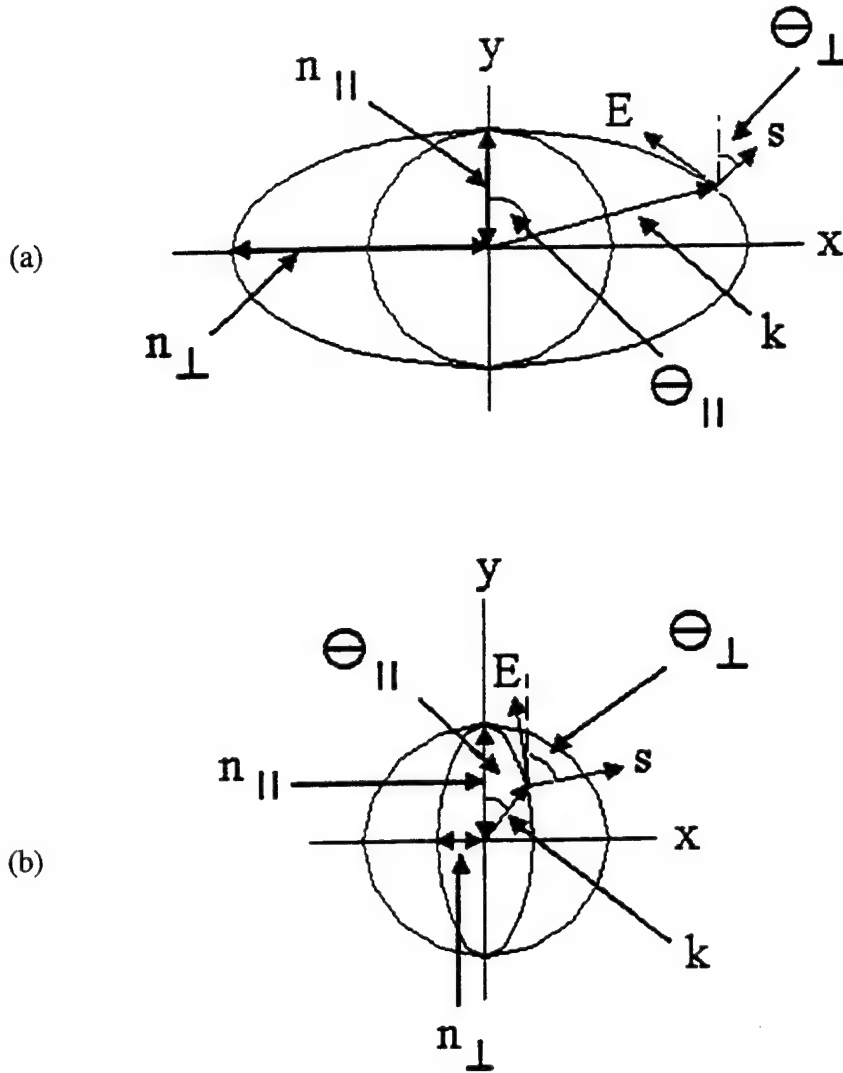


Figure 8. Index Surfaces for (a) a Positive Uniaxial Crystal and (b) a Negative Uniaxial Crystal [29].

In an anisotropic crystal, the polarization induced by E is dependent on the direction of E [26, 29]. Therefore, the speed at which light travels through an anisotropic crystal is dependent upon the direction of propagation. A light beam propagating through an anisotropic crystal along the optic axis (O) is defined as an ordinary ray [26, 29]. The refractive index seen by this propagating beam is defined as the ordinary refractive index ($n_{||}$ or n_o). $n_{||}$ is independent of the direction of the polarization [26, 29]. A light beam propagating through an anisotropic crystal at any other direction to O is defined as an

extraordinary ray [29]. The refractive index seen by this propagating beam is defined as the extraordinary refractive index (n_{\perp} or n_e). n_{\perp} is dependent on the direction of polarization [26, 29]. Hence, n_{\perp} is dependent on the direction E . For our uniaxial crystal, $n_z = n_{\parallel}$ and $n_x = n_y = n_{\perp}$. The index surfaces can, therefore, be represented by a sphere with radius n_{\parallel} an ellipsoid with radius n_{\parallel} parallel to O , and radius n_{\perp} normal to the O [29] (see Figure 8). For $n_{\perp} > n_{\parallel}$, the uniaxial crystal is known as a positive type [29]. For $n_{\perp} < n_{\parallel}$, the uniaxial crystal is known as a negative type [29]. The sphere and ellipse are tangent to each other only at the points along the optic axis. The amount of induced birefringence is defined as the difference between these two refractive indices and, as stated above, is linearly proportional to E [26, 29]. Pockels effect is given mathematically by [26, 29]

$$n_{\parallel} - n_{\perp} = mE, \quad (1)$$

where m is a proportionality constant. Modulating the electric field allows one to modulate the input signal and provide the basis for building an electro-optic switch.

In the next section we will determine the induced birefringence and derive an expression for electro-optic modulation using the EO properties of the tetragonal symmetry class 4 NLO polymer.

5.1.1 Linear Electro-Optic Effect

We will begin our analysis with the constitutive equation [83, 84]

$$\mathbf{D} = \epsilon_0 \mathbf{E} + \mathbf{P}. \quad (2)$$

In Eq. (2), \mathbf{D} is the electric displacement or electric flux density vector, \mathbf{E} is the electric field vector, \mathbf{P} is the electric polarization vector, and ϵ_0 is the permittivity of vacuum. In many isotropic materials the induced polarization is directly proportional to the applied field strength, except for the case of very high fields. We can write [82]:

$$\mathbf{P} = \epsilon_0 \chi \mathbf{E}, \quad (3)$$

where χ is the dielectric susceptibility of the medium. Combining Equations (2) and (3) yields [29, 82]

$$\mathbf{D} = \epsilon \mathbf{E}, \quad (4)$$

where $\epsilon = \epsilon_0(1 + \chi)$ is the permittivity of the medium.

The analysis is similar in anisotropic materials. Equation. (3) can be expressed in its tensor form as [15, 82]

$$P_x = \epsilon_0(\chi_{11}E_x + \chi_{12}E_y + \chi_{13}E_z), \quad (5)$$

$$P_y = \epsilon_0(\chi_{21}E_x + \chi_{22}E_y + \chi_{23}E_z) \quad (6)$$

and

$$P_z = \epsilon_0(\chi_{31}E_x + \chi_{32}E_y + \chi_{33}E_z), \quad (7)$$

where χ_{ij} are the coefficients of a 3x3 array called the dielectric susceptibility tensor of the medium for which $i = 1, 2$ or 3 , and $j = 1, 2$ or 3 . The suffixes i and j designate which axes the coefficients correspond to; 1 represents x , 2 represents y and 3 represents z . Choosing x , y and z so that the diagonal terms vanish gives the principal dielectric axes of the crystal [15]:

$$P_x = \epsilon_0\chi_{11}E_x, \quad (8)$$

$$P_y = \epsilon_0\chi_{22}E_y \quad (9)$$

and

$$P_z = \epsilon_0\chi_{33}E_z. \quad (10)$$

Combining Eq. (2) with Equations (8) - (10) yields [15, 29, 82]

$$d_x = \epsilon_{11}E_x, \quad (11)$$

$$d_y = \epsilon_{22}E_y \quad (12)$$

and

$$d_z = \epsilon_{33}E_z, \quad (13)$$

where

$$\epsilon_{11} = \epsilon_0(1 + \chi_{11}), \quad (14)$$

$$\epsilon_{22} = \epsilon_0(1 + \chi_{22}) \quad (15)$$

and

$$\epsilon_{33} = \epsilon_0(1 + \chi_{33}) \quad (16)$$

are the diagonal coefficients of a 3x3 array ϵ_{ij} , which is referred to as the permittivity tensor of the medium.

If we introduce the phase velocity ($v = (\mu\epsilon)^{-1/2}$), where μ is the permeability of the medium, it becomes evident that for anisotropic crystals, v depends on the direction of the applied field. Thus we have [15, 83, 84]

$$v_x = (\mu\epsilon_{11})^{-1/2}, \quad (17)$$

$$v_y = (\mu\epsilon_{22})^{-1/2} \quad (18)$$

and

$$v_z = (\mu\epsilon_{33})^{-1/2}. \quad (19)$$

For an anisotropic crystal, at least one of the permittivity coefficients is not equal to the other two (i.e., $\epsilon_{11} \neq \epsilon_{22}$ or ϵ_{33}). Only the polarization parallel to the applied electric field and, hence, the permittivity parallel to E , will contribute to the phase velocity. For example,

if an input beam is propagating along the y axis and E is applied parallel to the z axis, ϵ_{33} will be the permittivity, a polarization (P_z) will be induced, and the phase velocity will be v_z (see Equation (19)).

The index of refraction is defined as the reciprocal of the relative phase velocity [29, 83, 84],

$$n = c/v, \quad (20)$$

where c is the speed of light in vacuum. Going to tensor form, we can write the principal refractive indices as [15, 83]

$$n_x = c/v_x = (\mu_r \epsilon_{r11})^{1/2}, \quad (21)$$

$$n_y = c/v_y = (\mu_r \epsilon_{r22})^{1/2} \quad (22)$$

and

$$n_z = c/v_z = (\mu_r \epsilon_{r33})^{1/2}. \quad (23)$$

In Equations (21) - (23), $\mu_r = \mu/\mu_0$ is the relative permeability of the medium, μ_0 is the permeability of vacuum and $\epsilon_{rij} = \epsilon_{ij}/\epsilon_0$ are the coefficients of a 3X3 array called the relative permittivity tensor of the medium. For nonconductive media the relative permeability (μ_r) can be assumed unity [83], and the principal refractive indices then become [15, 83]

$$n_x = (\epsilon_{11}/\epsilon_0)^{1/2}, \quad (24)$$

$$n_y = (\epsilon_{22}/\epsilon_0)^{1/2} \quad (25)$$

and

$$n_z = (\epsilon_{33}/\epsilon_0)^{1/2}. \quad (26)$$

Using the definition for the refractive index along with the analysis for anisotropic crystals given above, it becomes evident that one can induce a change in the refractive index with an applied electric field. This change will, in turn, induce birefringence.

5.1.2 Index Ellipsoid

We will start with the general index ellipsoid for a crystal in its simplest form. This will allow us to determine the direction of polarization as well as the corresponding refractive indices of the crystal. The index ellipsoid is given in the principal coordinate system as [27, 29, 85]

$$x^2/n_x^2 + y^2/n_y^2 + z^2/n_z^2 = 1. \quad (27)$$

In Equation (27), x , y and z are the principal axes (the direction in the crystal along which the electric field vector (\mathbf{E}) and the electric displacement vector (\mathbf{d}) are parallel). $1/n_x^2$, $1/n_y^2$ and $1/n_z^2$ are the principal refractive indices along their respective axes. The lengths of the major axes of the index ellipsoid, represented by Equation (27), are $2n_x$, $2n_y$ and $2n_z$, parallel to directions x , y and z , respectively [15, 85]. The index ellipsoid is used to find the two refractive indices and two corresponding directions of \mathbf{d} associated with the two independent plane waves propagating along an arbitrary direction s in the crystal. These indices are determined using Equation (27). Visually depicted in Figure 9, the major and minor axes of the ellipse are in the directions d_1 and d_2 , respectively, with the length of d_1 equal to $2n_1$, and the length of d_2 equal to $2n_2$.

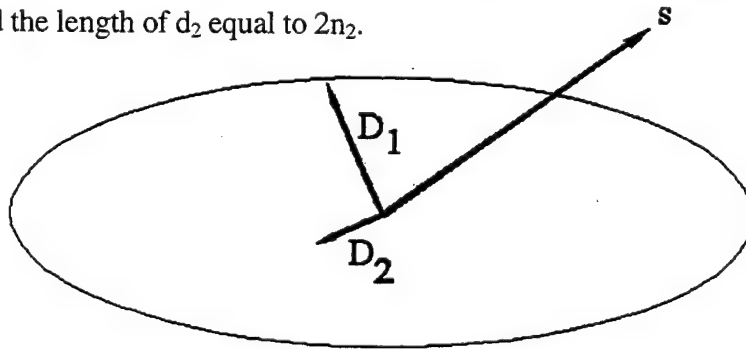


Figure 9. Inner Ellipse is the Intersection of Index Ellipsoid with the Plane Perpendicular to s [15].

Next we will introduce the optical dielectric impermeability tensor of a crystal. The coefficients (η_{ij}) of this tensor depend on the distribution of bond charges in the material [15, 82]. η_{ij} are found by taking the reciprocal of the relative permittivity or dielectric constant [82]. η_{ij} has been defined in terms of the refractive index of the crystal as [82]

$$\eta_{ij} = \epsilon_0 / \epsilon_{ij} = 1/n_{ij}^2 \quad (28)$$

(see Equations (24) - (26)). Application of an electric field E to the crystal results in a redistribution of the bond charges of the crystal, and a possible deformation of the ion lattice. This causes a change in the optical impermeability tensor and, hence, a change in the refractive index of the crystal. This allows us to write the index ellipsoid in the presence of an electric field as [15]:

$$(1/n_x^2)x^2 + (1/n_y^2)y^2 + (1/n_z^2)z^2 + A_1x^2 + A_2y^2 + A_3z^2 + A_4yz + A_5zx + A_6xy + A_7zy + A_8xz + A_9yx = 1. \quad (29)$$

For $E = 0$, A_1 through $A_9 = 0$, and Equation (29) reduces to Equation (27). Introducing the notations for subscripts:

$$\begin{aligned} x^2 &= xx = (11) \rightarrow 1 \\ y^2 &= yy = (22) \rightarrow 2 \\ z^2 &= zz = (33) \rightarrow 3 \\ yz &= (23) \rightarrow 4 \\ zx &= (31) \rightarrow 5 \\ xy &= (12) \rightarrow 6 \\ zy &= (32) \rightarrow 7 \\ xz &= (13) \rightarrow 8 \\ yx &= (21) \rightarrow 9 \end{aligned} \quad (30)$$

And,

$$\begin{aligned}
(1/n^2)_1 &= 1/n_x^2 = A_1 \\
(1/n^2)_2 &= 1/n_y^2 = A_2 \\
(1/n^2)_3 &= 1/n_z^2 = A_3 \\
(1/n^2)_4 &= 1/n_y n_z = A_4 \\
(1/n^2)_5 &= 1/n_z n_x = A_5 \\
(1/n^2)_6 &= 1/n_x n_y = A_6 \\
(1/n^2)_7 &= 1/n_z n_y = A_7 \\
(1/n^2)_8 &= 1/n_x n_z = A_8 \\
(1/n^2)_9 &= 1/n_y n_x = A_9,
\end{aligned} \tag{31}$$

Equation (29) becomes

$$\begin{aligned}
&[1/n_x^2 + (1/n^2)_1]x^2 + [1/n_y^2 + (1/n^2)_2]y^2 + [1/n_z^2 + (1/n^2)_3]z^2 \\
&+ [(1/n^2)_4]yz + [(1/n^2)_5]zx + [(1/n^2)_6]xy + [(1/n^2)_7]zy \\
&+ [(1/n^2)_8]xz + [(1/n^2)_9]yx = 1.
\end{aligned} \tag{32}$$

It has been shown that η_{ij} is symmetric, provided that the medium is lossless and optically active [15]. This allows the permutation of i and j , and the notation presented in Equations (31) and (32) are reduced to:

$$\begin{aligned}
x^2 &= xx = (11) \rightarrow 1 \\
y^2 &= yy = (22) \rightarrow 2 \\
z^2 &= zz = (33) \rightarrow 3 \\
yz &= zy = (23) = (32) \rightarrow 4 \\
zx &= xz = (31) = (13) \rightarrow 5 \\
xy &= yx = (12) = (21) \rightarrow 6,
\end{aligned} \tag{33}$$

with:

$$\begin{aligned}
 (1/n^2)_1 &= 1/n_x^2 \\
 (1/n^2)_2 &= 1/n_y^2 \\
 (1/n^2)_3 &= 1/n_z^2 \\
 (1/n^2)_4 &= 1/n_y n_z = 1/n_z n_y \\
 (1/n^2)_5 &= 1/n_z n_x = 1/n_x n_z \\
 (1/n^2)_6 &= 1/n_x n_y = 1/n_y n_x.
 \end{aligned} \tag{34}$$

Substituting Equations (33) and (34) into Equation (32) yields [27]

$$\begin{aligned}
 &[1/n_x^2 + (1/n^2)_1]x^2 + [1/n_y^2 + (1/n^2)_2]y^2 + [1/n_z^2 + (1/n^2)_3]z^2 \\
 &+ 2[(1/n^2)_4]yz + 2[(1/n^2)_5]xz + 2[(1/n^2)_6]xy = 1.
 \end{aligned} \tag{35}$$

5.1.3 Electro-Optic Coefficients

The electro-optic (EO) coefficients are traditionally defined as [15, 29]

$$\eta_{ij}(E) - \eta_{ij}(0) \Delta\eta_{ij} = r_{ijk}E_k + s_{ijkl}E_kE_l. \tag{36}$$

In Equation (36), E is the applied electric field, r_{ijk} are the coefficients of a 3×9 array called the linear electro-optic (Pockels) tensor of the medium. s_{ijkl} are the coefficients of a 6×6 array called the quadratic electro-optic (Kerr) tensor of the medium, for which $k = 1, 2$, or 3 and $l = 1, 2$, or 3 . In the equation above, we have omitted terms higher than the quadratic. These higher order effects are so weak compared with the linear and quadratic effects, that

they can be neglected for most applications [15, 29]. For centrosymmetric crystals (crystals possessing inversion symmetry for all physical properties), the linear EO effect vanishes [71] (i.e., $r_{ijk} = 0$). This is caused by the spatial inversion symmetry of such crystals. Therefore, the quadratic EO effect will dominate [15]. For noncentrosymmetric crystals (crystals that do not possess inversion symmetry for all physical properties), both the linear and quadratic effects will be present [15]. From the section above, the EO effects will depend on the ratio of the applied electric field (E) to the intra-atomic electric field (E_u) binding the charged particles. This ratio can be estimated by finding the magnitude of E_u at a position (T) arising from a point charge (q) located at a distance (u) from T . E_u at T is given by [83, 84]

$$E_u = (1/4\pi\epsilon_0)q/u^2. \quad (37)$$

The minimum field inside the atom E_u can be determined by substituting the lattice constant a_0 of the crystal for u , and the elementary electron charge for q . If the minimum electric field inside the atom is much larger than the applied field, then the quadratic EO effect should be small enough when compared to the linear EO effect. This will allow us to neglect the s_{ijkl} terms. Equation (36) becomes

$$\eta_{ij}(E) - \eta_{ij}(0) \Delta\eta_{ij} = r_{ijk}E_k. \quad (38)$$

The permutation property, along with Equations (28), (33), (34) and (38), yields [26, 29]

$$\Delta(1/n^2)_i = \sum_{k=1}^3 r_{ik}E_k, \quad (39)$$

where, for example, $\Delta(1/n^2)_5 = r_{51}E_1 + r_{52}E_2 + r_{53}E_3$. Substitution of Eq. (39) into Eq. (35) gives the general index ellipsoid in the presence of an electric field in terms of r_{ik} [15]:

$$\begin{aligned} & [1/n_x^2 + r_{1k}E_k]x^2 + [1/n_y^2 + r_{2k}E_k]y^2 + [1/n_z^2 + r_{3k}E_k]z^2 \\ & + 2[r_{4k}E_k]yz + 2[r_{5k}E_k]xz + 2[r_{6k}E_k]xy = 1 \end{aligned} \quad (40)$$

In order to determine the EO tensor for crystals belonging to the tetragonal 4 class, we will begin with the EO tensor for the triclinic 1 crystal group in matrix form [27]:

$$r_{ijk} = \begin{bmatrix} r_{11} & r_{12} & r_{13} \\ r_{21} & r_{22} & r_{23} \\ r_{31} & r_{32} & r_{33} \\ r_{41} & r_{42} & r_{43} \\ r_{51} & r_{52} & r_{53} \\ r_{61} & r_{62} & r_{63} \end{bmatrix} \quad (41)$$

Neglecting the permutation property for the moment, Equation (41) expands to

$$r_{ijk} = \begin{bmatrix} r_{111} & r_{112} & r_{113} \\ r_{221} & r_{222} & r_{223} \\ r_{331} & r_{332} & r_{333} \\ r_{231} & r_{232} & r_{233} \\ r_{321} & r_{322} & r_{323} \\ r_{131} & r_{132} & r_{133} \\ r_{311} & r_{312} & r_{313} \\ r_{121} & r_{122} & r_{123} \\ r_{211} & r_{212} & r_{213} \end{bmatrix} \quad (42)$$

Since tetragonal crystals have axes of fourfold symmetry, we can let z be the axis of two fold rotation, which can be represented by the matrix [15]

$$a_{ij} = \begin{bmatrix} -1 & 0 & 0 \\ 0 & -1 & 0 \\ 0 & 0 & 1 \end{bmatrix} \quad (43)$$

Equation (43) dictates that the suffixes of the EO coefficients change as follows: $1 \rightarrow -1$, $2 \rightarrow -2$ and $3 \rightarrow 3$ [82]. Substituting this property into Equation (42) yields

$$r_{ijk} = \begin{bmatrix} -r_{111} & -r_{112} & r_{113} \\ -r_{221} & -r_{222} & r_{223} \\ -r_{331} & -r_{332} & r_{333} \\ r_{231} & r_{232} & -r_{233} \\ r_{321} & r_{322} & -r_{323} \\ r_{131} & r_{132} & -r_{133} \\ r_{311} & r_{312} & -r_{313} \\ -r_{121} & -r_{122} & r_{123} \\ -r_{211} & -r_{212} & r_{213} \end{bmatrix} \quad (44)$$

where

$$r_{ijk} = r_{111} \rightarrow r_{(-1)(-1)(-1)} = -r_{111}, r_{ijk} = r_{123} \rightarrow r_{(-1)(-2)(3)} = r_{123}, r_{ijk} = r_{223} \rightarrow r_{(-2)(-2)(3)} = r_{223},$$

etc.

Setting $r_{ijk} = r_{ijk}$ leads to the following condition: $r_{ijk} = -r_{ijk}$, only if $r_{ijk} = 0$ [15]. Equating Equations (42) and (44) with this condition yields

$$r_{ijk} = \begin{bmatrix} 0 & 0 & r_{113} \\ 0 & 0 & r_{223} \\ 0 & 0 & r_{333} \\ r_{231} & r_{232} & 0 \\ r_{321} & r_{322} & 0 \\ r_{131} & r_{132} & 0 \\ r_{311} & r_{312} & 0 \\ 0 & 0 & r_{123} \\ 0 & 0 & r_{213} \end{bmatrix} \quad (45)$$

Since tetragonal 4 class crystals also includes a diad axis parallel to z, the axes transform as follows [71]: $1 \rightarrow -2, 2 \rightarrow 1$ and $3 \rightarrow 3$. Hence,

$$r_{ijk} = \begin{bmatrix} 0 & 0 & r_{113} \\ 0 & 0 & r_{113} \\ 0 & 0 & r_{333} \\ r_{231} & r_{131} & 0 \\ r_{321} & r_{311} & 0 \\ r_{131} & -r_{231} & 0 \\ r_{311} & -r_{321} & 0 \\ 0 & 0 & 0 \\ 0 & 0 & 0 \end{bmatrix} \quad (46)$$

where

$r_{ijk} = r_{113} \rightarrow r_{(-2)(-2)(3)} = r_{223}$, $r_{ijk} = r_{231} \rightarrow r_{(1)(3)(-2)} = -r_{132}$, $r_{ijk} = r_{321} \rightarrow r_{(3)(1)(-2)} = -r_{312}$,
 $r_{ijk} = r_{131} \rightarrow r_{(-2)(3)(-2)} = r_{232}$, $r_{ijk} = r_{311} \rightarrow r_{(3)(-2)(-2)} = r_{322}$, $r_{ijk} = r_{231} \rightarrow r_{(3)(1)(2)} = r_{312}$,
 $r_{ijk} = r_{123} \rightarrow r_{(-2)(1)(3)} = -r_{213}$ and $r_{ijk} = r_{213} \rightarrow r_{(1)(-2)(3)} = -r_{123}$. For $r_{123} = -r_{213}$ and $r_{213} = -r_{123}$,
which proves that

$$r_{123} = r_{213} = 0. \quad (47)$$

Going back to contracted notation, the electro-optic tensor (r_{ik}) for crystals belonging to the tetragonal 4 group can be represented by the well known matrix [15]

$$r_{ik} = \begin{bmatrix} 0 & 0 & r_{13} \\ 0 & 0 & r_{13} \\ 0 & 0 & r_{33} \\ r_{41} & r_{51} & 0 \\ r_{51} & -r_{41} & 0 \\ 0 & 0 & 0 \end{bmatrix} \quad (48)$$

Substituting the EO tensor for tetragonal crystals back into the index ellipsoid (Equation (40)) gives [15]

$$\begin{aligned} & [1/n_x^2 + r_{13}E_z]x^2 + [1/n_y^2 + r_{13}E_z]y^2 + [1/n_z^2 + r_{33}E_z]z^2 \\ & + 2yzr_{41}E_x + 2yzr_{51}E_y + 2x zr_{51}E_x - 2x zr_{41}E_y = 1. \end{aligned} \quad (49)$$

Taking into account that tetragonal 4 crystals are uniaxial allows us to write [85]

$$\begin{aligned} & [1/n_o^2 + r_{13}E_z]x^2 + [1/n_o^2 + r_{13}E_z]y^2 + [1/n_e^2 + r_{33}E_z]z^2 \\ & + 2yzr_{41}E_x + 2yzr_{51}E_y + 2x zr_{51}E_x - 2x zr_{41}E_y = 1, \end{aligned} \quad (50)$$

where n_o and n_e are the ordinary and extraordinary refractive indices, respectively.

5.1.4 Induced Refractive Indices and Birefringence

We need to determine the direction and magnitude of the principal axes of the new ellipsoid represented by Eq. (50), since they may not coincide with x , y , z . For this analysis, we are fabricating a transverse modulated EO switch [15]. This dictates that the electrodes be placed parallel to the waveguides along the optic axis. Propagation of the input beam will be along the y axis through the electro-optic device of length L . The electrodes will be placed on the top and bottom of the coupler running along y and separated by a distance d . The electric field E will be applied along the z axis, normal to y . Figure 9 illustrates a

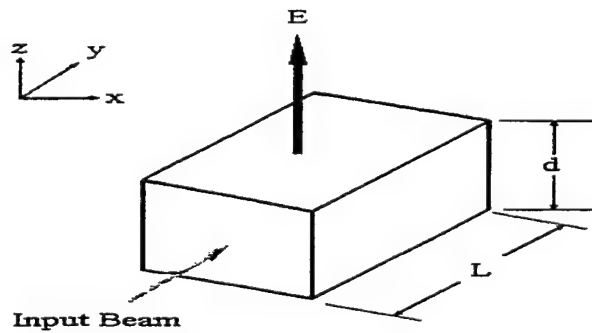


Figure 10. Transverse Electro-Optic Modulator using a Tetragonal 4 Group Crystal.

transverse modulator. Since the electric field is in the z direction, we have

$$E_x = E_y = 0$$

and

$$E_z = E. \quad (51)$$

Substituting Equation (51) into Equation (50) yields the index ellipsoid

$$[1/n_o^2 + r_{13}E]x^2 + [1/n_o^2 + r_{13}E]y^2 + [1/n_e^2 + r_{33}E]z^2. \quad (52)$$

Since no mixed terms appear in Equation (52), the principal axes of the new index ellipsoid remain unchanged. Using Equation (39), we have

$$[(1/n_o^2) + \Delta(1/n_o^2)]x^2 + [(1/n_o^2) + \Delta(1/n_o^2)]y^2 + [(1/n_e^2) + \Delta(1/n_e^2)]z^2 = 1. \quad (53)$$

From Equation (53) we can write

$$1/(n_x)^2 = 1/n_o^2 + \Delta(1/n_o^2), \quad (54)$$

$$1/(n_y)^2 = 1/n_o^2 + \Delta(1/n_o^2) \quad (55)$$

and

$$1/(n_z)^2 = 1/n_e^2 + \Delta(1/n_e^2). \quad (56)$$

Using Equation (1) for Pockels effect along with Equations (52), (38) and (39) yields the induced change in the refractive index

$$\Delta n = m' r_{ik} E = m' \Delta(1/n^2), \quad (57)$$

where m' is a proportionality factor we will use to equate Δn and $\Delta(1/n^2)$. If we assume $r_{ijk}E \ll 1/n^2$, (i.e., $\Delta(1/n^2)$ sufficiently small), it allows us to use the relation [15]

$$\Delta(1/n^2) \approx \partial (1/n^2) = -(2/n^3) \partial n. \quad (58)$$

Multiplying both sides by $-(n^3/2)$ yields

$$\partial n \approx -(n^3/2) \partial (1/n^2). \quad (59)$$

Equating Equations (57) and (59) leads to [15]

$$\Delta n = m' \approx -(n^3/2) \Delta(1/n^2) \quad (60)$$

Using Equation (39) once again, we can write

$$\Delta n \approx -(n^3/2) r_{ik} E. \quad (61)$$

This leads to the indices [15]

$$n_x = n_o + \Delta n_o = n_o - (n_o^3/2) r_{13} E, \quad (62)$$

$$n_y = n_o + \Delta n_o = n_o - (n_o^3/2) r_{13} E \quad (63)$$

and

$$n_z = n_e + \Delta n_e = n_e - (n_e^3/2) r_{33} E \quad (64)$$

The induced birefringence for the new axes with the input beam propagating perpendicular to the applied electric field (i.e., for transverse modulation) can now be given by [15, 26]

$$n_z - n_x = (n_e - n_o) - [(n_e^3/2) r_{33} - (n_o^3/2) r_{13}] E. \quad (65)$$

Equation (65) is the definition for the induced birefringence that we will use to describe the phase retardation experienced by the input beam as it propagates through the crystal.

5.2 ELECTRO-OPTIC MODULATORS

For our analysis we will consider an optical field that is incident and normal to the xz plane propagating along the y axis with E parallel to the z axis. At the input plane $y = 0$, the optical field can be resolved into two mutually orthogonal components polarized along x and z. The x component propagates as [27, 29]

$$E_x = A \exp[i(\omega t - (\omega/c)n_x z)], \quad (66)$$

where ω is the angular frequency, t is time and A is a constant. The z component propagates as [27, 29]

$$E_z = A \exp[i(\omega t - (\omega/c)n_z y)]. \quad (67)$$

The difference in phase between these two components at the output plane $y = L$ is called the phase retardation [27, 29]. It is given by the difference of the exponential terms in Equations (66) and (67). Performing the subtraction yields

$$\Gamma_{xz} = (\omega/c)(n_z - n_x)L, \quad (68)$$

where $[n_z - n_x]$ is the induced birefringence found in the previous section. Substituting for the induced birefringence using Equation (65) gives [27, 29]

$$\Gamma_{xz} = (\omega/c)((n_e - n_o) - ((n_e^3/2)r_{33} - (n_o^3/2)r_{13})E)L. \quad (69)$$

Using the relation $\omega/c = 2\pi/\lambda$ with λ defined as the wavelength, the phase retardation becomes [29, 74]

$$\Gamma_{xz} = (2\pi/\lambda)(n_e - n_o)L - (\pi/\lambda)(n_e^3 r_{33} - n_o^3 r_{13})VL/d, \quad (70)$$

where V is the voltage applied between electrodes separated by a distance d . Due to the natural birefringence term in Equation (70), a Babinet or Soleil phase compensator will be required. This will allow us to adjust the phase retardation, that is present in the absence of the applied voltage, to equal an odd integral multiple of $\pi/2$. We then want a voltage dependant phase retardation of 180° , or $\Gamma_{xz} = \pi$. The voltage necessary to realize a π phase change is defined as half wave voltage [27, 29]. Equating the voltage dependant phase term of Equation (70) to π gives us [15]

$$V_\pi = d\lambda/L(n_e^3 r_{33} - n_o^3 r_{13}). \quad (71)$$

V_π is the voltage necessary to realize half wave polarization in tetragonal crystals.

Figure 11 illustrates a Mach Zehnder (MZ) interferometer.

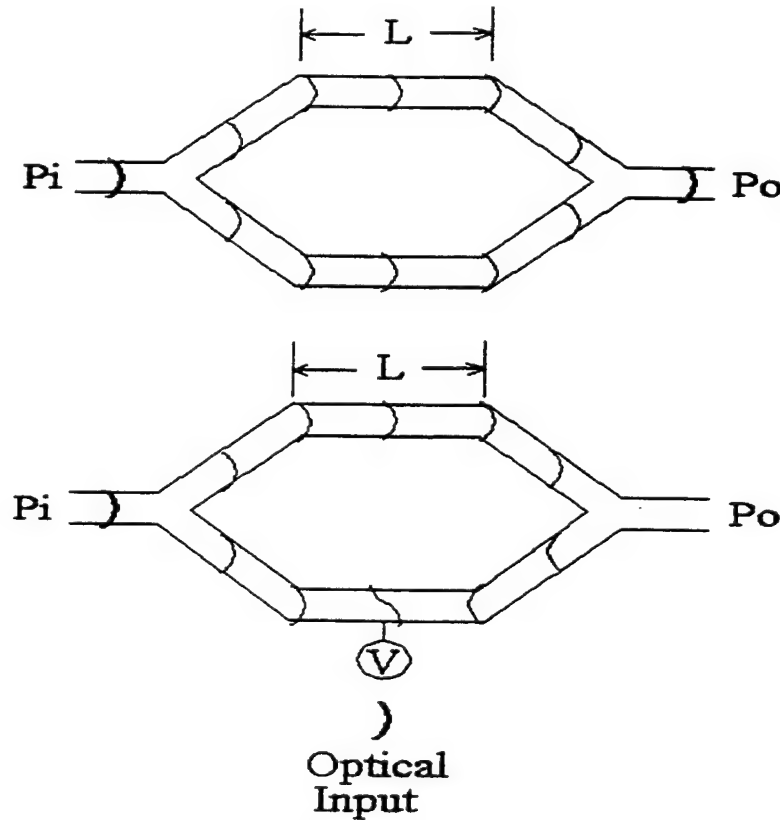


Figure 11. Operation of a Mach Zehnder Interferometer.

interferometer is a form of transverse electro-optic modulator. The input signal is first split equally into two separate channels. These two channels are separated by enough distance to prevent any crosstalk or coupling. The two channels are later recombined back into one channel. Voltage is applied to only one of the separated channels. When voltage is absent, half of the signal propagating in channel one recombines constructively with half of the signal propagating in channel two, and the output equals the that present at the input. Voltage applied to one of the channels results in a phase shift of the propagating beam only in that channel. When enough voltage is applied to shift the phase of the beam in that channel by π , then half of the signal propagating in channel one recombines destructively with half of the signal propagating in channel two, and the output becomes zero. By periodically switching the voltage on and off, one can realize sinusoidal modulation of the optical signal.

5.3 DIRECTIONAL COUPLERS

The directional coupler switch is a device consisting of parallel channel waveguides separated by a finite distance. The coupling between the modes of the parallel waveguides results in an exchange of power between guided modes of adjacent waveguides [15]. This is referred to as directional coupling. The eigenmodes of the coupling region consist of one symmetric and one antisymmetric mode [15, 24, 25, 27, 28, 86-89]. Treatment of waveguide coupling can be performed by coupled-mode theory [15, 27, 28, 86].

A of directional coupler is illustrated in Figure 12. In the figure, s is the separation between the waveguides.

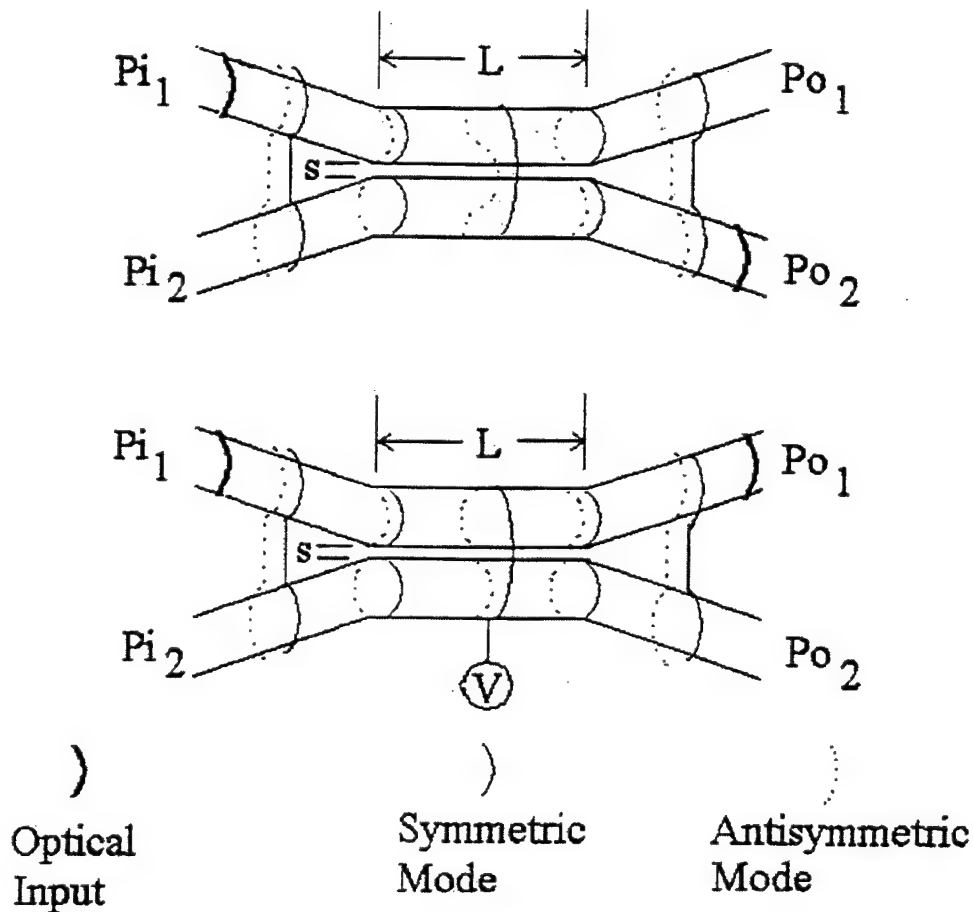


Figure 12. Operation of a Directional Coupler

Consider P_{i1} as the input power to waveguide 1, P_{i2} as the input power to waveguide 2, P_{o1} as the output power from waveguide 1 and P_{o2} as the output power from waveguide 2. Let waveguide 1 propagate through the symmetric mode and waveguide 2 propagate through the antisymmetric mode. Assume that the waveguides are not too close, so that the overlap integral of the mode functions will be small [15, 27, 28, 86]. With a single input to waveguide 1, $P_{i1} = 1$ and $P_{i2} = 0$, the output power from waveguides 1 and 2 are given as [15, 27, 28, 86, 87]

$$P_{o1}(l) = P_{i1} - P_{o2}(l) = P_{i1}(1 - (\kappa^2/(\kappa^2 + \delta^2))(1 - \cos^2[(\kappa^2 + \delta^2)^{1/2}(l)])) \quad (72)$$

and

$$P_{o2}(l) = P_{i1}((\kappa^2/(\kappa^2 + \delta^2))(\sin^2[(\kappa^2 + \delta^2)^{1/2}(l)])), \quad (73)$$

where $2\delta = \beta_1 - \beta_2$ is the difference in the propagation constants between two adjacent uncoupled waveguides 1 and 2, κ is the coupling constant between the two adjacent waveguides. l is the interaction length over which the two waveguides are coupled. By definition, $\kappa = \pi/2L$, where $l = L$ is the length required for complete coupling of the power from one waveguide to the other [15-19, 24, 25, 27, 28, 86-90].

For symmetric waveguides, the phase velocities in the two modes are equal (i.e., $\beta_1 = \beta_2$ or $\delta = 0$). For complete coupling, Eqs. 1.4.1 and 1.4.2 become [15, 27, 28, 86, 87]

$$P_{o1}(L) = P_{i1}(1 - (1 - \cos^2[\pi/2])) = 0 \quad (74)$$

and

$$P_{o2}(L) = P_{i1}(\sin^2[\pi/2]) = P_{i1}. \quad (75)$$

From Eqs. (72) and (73), one can see that the input power P_{i1} into waveguide 1 will exit waveguide 2 as P_{o2} at a distance L . Using Eqs. (74) and (75), complete coupling occurs when $L = \pi/2\kappa$.

Applying an electric field to either waveguide 1 or waveguide 2 over the distance L , where the waveguides are coupled, will change that particular waveguide's propagation constant β . Total switching occurs when $\delta = 3^{1/2}\pi/2L$ [15, 86, 87]. This can be verified by

the substitution of $\delta = 3^{1/2}\pi/2L$ into Eqs. (72) and (73). By doing this, we get [15, 27, 28, 86, 87]

$$Po_1(L) = Pi_1(1 - (1/4)(1 - \cos^2[\pi])) = Pi_1 \quad (76)$$

and

$$Po_2(L) = Pi_1((1/4)(\sin^2[\pi])) = 0. \quad (77)$$

Using the definitions for δ and κ given above, one gets total switching to occur when [15, 27, 28, 86]

$$(\beta_1 - \beta_2) = 3^{1/2}\pi/L. \quad (78)$$

If we apply an electric field (E) over waveguide 2, for instance, this will induce a change in the refractive index of waveguide 2 by an amount proportional to E.

Mathematically, this is given by [15, 27-29, 86]

$$\Delta n_2 = (n_2^3/2)rE, \quad (79)$$

where n_2 is the refractive index of waveguide 2 and r is the electro-optic coefficient of the waveguiding material. To apply an electric field to one of the waveguides, we place electrodes on the top and bottom of the waveguide over the coupling length (L) and apply a voltage (V) to the top electrode. The electric field is then related to the applied voltage by $V = Ed$, where d is the distance between the top and bottom electrode. The total index (n_2') of the waveguide 2 region between the electrodes can be defined by

$$n_2' = n_2 + \Delta n_2 = n_2 + (n_2^3/2)rV/d. \quad (80)$$

By definition, $\beta = 2\pi n/\lambda$, where λ is the wavelength of the source [15, 27, 28, 86]. If we let waveguide 1 and waveguide 2 be identical ($n_1 = n_2 = n$), and substitute Eq. (80) into (78),

along with the definition for β , this yields [15, 27, 28, 86]

$$(2\pi/\lambda)(n' - n)(n^3/2)(rV/d) = (2\pi/\lambda)(n^3/2)(rV/d) = 3^{1/2}\pi/L. \quad (81)$$

We can now find the voltage required to switch the coupling completely. By rewriting Eq. (81), we get

$$V = (3^{1/2}\lambda d)/(n_2^3 r L). \quad (82)$$

The EO coefficient $r = r_{33}$ can be substituted for the assumed crystal orientation presented in the previous section.

5.3.1 Zero-Gap Directional Couplers

As with directional couplers, the interaction region of a zero-gap directional coupler will support two guided symmetric modes, and two guided antisymmetric modes [14, 32, 91-96]. The difference between them, however, results from the fact that we have zero spacing between the two symmetric waveguides in a zero-gap directional coupler. These modes will now be propagating in a single waveguide. We will again have a voltage independent phase difference that accumulates over the interaction length (the two mode section), due to the difference in the phase velocities of the two orthogonal modes, and a phase difference over the two mode section, brought about by the voltage induced change in refractive index (EO effect) [15, 26, 82-84].

The electro-optic dependent phase difference will be denoted by $(\beta_s - \beta_{as})/2 = \Delta\beta/2$, where β_s and β_{as} are the propagation constants of the symmetric and antisymmetric modes, respectively [92]. The value of $\Delta\beta$ required for complete coupling of energy from the top half of the two mode waveguide to the bottom is given by [92]

$$\Delta\beta = \pi/L. \quad (83)$$

$\Delta\beta$ is varied by changing the index of refraction of the waveguiding material in the two-mode section. We will denote the refractive index change, as we did in the last section, as Δn . The change in the difference between the propagation constants of the two modes can then be written as [92]

$$\Delta(\Delta\beta) = \Delta n \partial (\Delta\beta) / \partial n. \quad (84)$$

Equating Eqs. (83) and (84) yields [92]

$$\Delta n = (\pi/L) / (\partial (\Delta\beta) / \partial n). \quad (85)$$

In the last section it was shown that for linear EO materials, the refractive index changes proportionally to the applied voltage. With this relation, it can be seen from Eq. (85) that $\partial (\Delta\beta) / \partial n$ is inversely proportional to the applied voltage. $\partial (\Delta\beta) / \partial n$ is also strongly dependent on the waveguide separation s for the directional coupler [92]. Papuchon and Roy [92] showed that as s decreases, $\partial (\Delta\beta) / \partial n$ increases, and as the value of $\partial (\Delta\beta) / \partial n$ increases, the voltage required for switching decreases. Therefore, the maximum value of $\partial (\Delta\beta) / \partial n$ and, thus, the minimum voltage required to switch the coupling guides, occurs when $s = 0$. When $s = 0$, we have a zero-gap directional coupler [92]. Experiments have shown that the value $\partial (\Delta\beta) / \partial n$ varies by an order of magnitude between the conventional directional coupler and the zero-gap directional coupler [92]. This verifies that zero-gap directional couplers require less voltage to switch the coupling than do conventional directional couplers.

Expressions for the power coupling in zero-gap directional couplers are similar to those used for conventional directional couplers. They are given by [97-99]

$$P_{O1}(L) = P_{i1} \cos^2[(\Delta\beta/2 + \Phi_0)L] \quad (86)$$

and

$$P_{O2}(L) = P_{i1} \sin^2[(\Delta\beta/2 + \Phi_0)L], \quad (87)$$

where Φ_0 is the accumulated, voltage independent phase difference in the phase velocities of the symmetric and antisymmetric modes. With no voltage applied (i.e., $\Delta\beta = 0$), coupling occurs when $\Phi_0 = \pi/2L$. When enough voltage is applied so that $\Delta\beta = \pi/L$, then complete switching occurs. Equating $\Delta\beta$ with Eq. (80) yields

$$(2\pi/\lambda)(n^3/2)(rV/d) = \pi/L. \quad (88)$$

The voltage required for complete switching is then given by

$$V = (\lambda d)/(n^3 r L), \quad (89)$$

where n is the refractive index of the interaction region. Like the directional coupler, the EO coefficient $r = r_{33}$. By comparing Eq. (89) with Eq. (82), one can see that the voltage required to completely switch the optical input from one channel to the other is less for the zero-gap directional coupler. The zero-gap allows us to treat the center interaction region as one waveguide. Operation of the zero-gap directional coupler switch is illustrated in Fig. 13. Another advantage of zero-gap directional couplers, in addition to operating with less voltage, is that the interaction length is much shorter than the interaction length of conventional directional couplers [24, 32-35, 37, 89, 90]. This results in the reduction of real estate required.

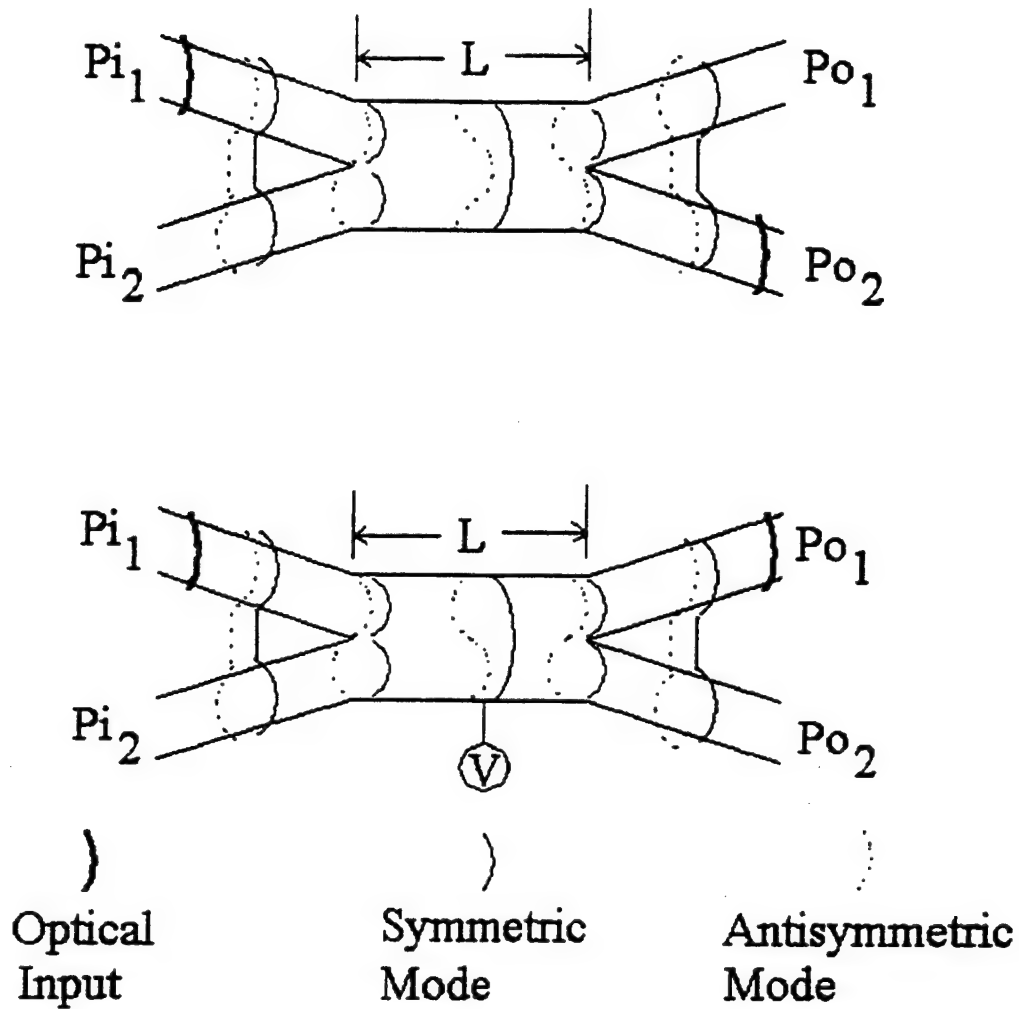


Figure 13. Operation of a Zero-Gap Directional Coupler.

5.3.2 Wavefront Tilt

An additional parameter which needs to be taken into account for directional couplers and zero-gap directional couplers is wavefront tilt, and its affect on waveguide coupling in the branching section. The larger the tilt angle α of the branching section, the less the waveguide coupling [91]. Tilt introduces phase differences that decrease waveguide interaction in the branching section of waveguide coupling. The maximum allowable tilt angle can be obtained by forcing the branching region of waveguide coupling to be within a single lobe of the standing wave generated by the two waves propagating along the tilted

waveguide portions. This gives the limit [91]

$$\sin(\alpha/2) < \lambda/4nw, \quad (90)$$

where w is the width of the waveguides.

5.3.3 Interaction Length Of The Directional Coupler

In this section, the interaction length of a directional coupler is determined by substituting the refractive index of the NLO polymer into several dielectric strip waveguide directional coupler models. Driving the separation between the waveguides to zero allows us to determine the interaction length of the zero-gap directional coupler.

Directional coupling is the exchange of power between the guided modes in adjacent parallel waveguides separated by a finite distance. Fig. 14 is a schematic of a conventional directional coupler device. The index of refraction of the core region is n while that of the clad regions is $n(1 - \Delta)$. This is less than the index of the core region by an amount Δ . The dimensions a , b and c are, respectively, the width, thickness and separation of the waveguides. The interaction length, the distance required for total exchange of power from one guide to the other, is L [77]. The wave is assumed to propagate along the y axis.

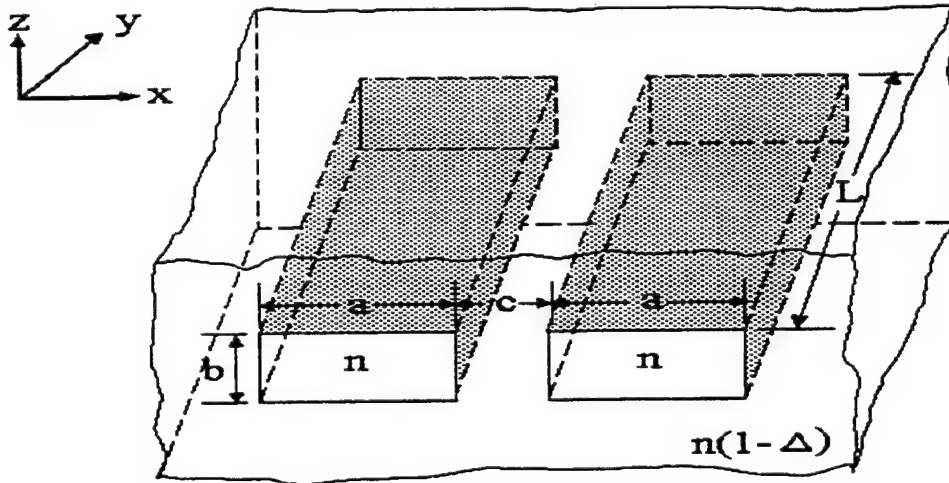


Figure 14. Rectangular Waveguide Directional Coupler.

Extensive treatment of optical waveguide and directional coupler theory has been addressed by many researchers for both continuous two-dimensional film waveguides and dielectric strip waveguides. Various methods, such as dielectric waveguide, coupled mode theory, effective index, beam propagation method and finite-element analysis, have been used [15, 24, 25, 86, 88, 89, 94, 100-125]. Analysis of these methods shows good agreement between all of the different models, provided that we are far from cutoff. This means that the normalized frequency, defined as

$$B = (bk/\pi)[n - n(1 - \Delta)]^{1/2}, \quad (91)$$

is greater than or equal to 1.6 for single mode operation [114, 125]. In Eq. (91), the free-space propagation constant of plane waves is defined as $k = 2\pi/\lambda$, or wave number, where λ is the wavelength. Since the waveguides fabricated for this experiment will be rectangular ridge type structures, we will use several of the dielectric strip waveguide methods to model the devices for this experiment [25, 88, 89, 102-109].

5.3.4 Rectangular Dielectric Waveguide Model

In 1969, Marcatili [88] presented analytical models for integrated optical rectangular dielectric waveguides and directional couplers. Fig. 15 illustrates a directional coupler with the following parameters: n_1 and n_2 are the refractive indices of the core and top clad, respectively; n_3 is the refractive index of the outside clad; n_4 is the refractive index of the bottom clad; n_5 is the refractive index of the center clad; the width and thickness of the individual waveguides are a and b , respectively; and the distance of separation between the two waveguides is c . The modes of the dielectric waveguide are classified as transverse electric (TE_{pq}) and transverse magnetic (TM_{pq}) modes. The variables, $p = (0, 1, 2, \dots)$ and $q = (0, 1, 2, \dots)$, indicate the number of extrema of the electric or magnetic field along the x and z directions, respectively. This gives the order of the mode. For the fundamental "0th order" TE_{pq} mode, $p = q = 0$, and the transverse electric mode is given the designation TE_{00} . TE_{pq} (TM_{pq}) modes have the electric field component polarized predominantly in the z (x)

direction and the magnetic field component polarized predominantly in the x (z) direction. The amplitudes of the fields have only one maximum in each direction.

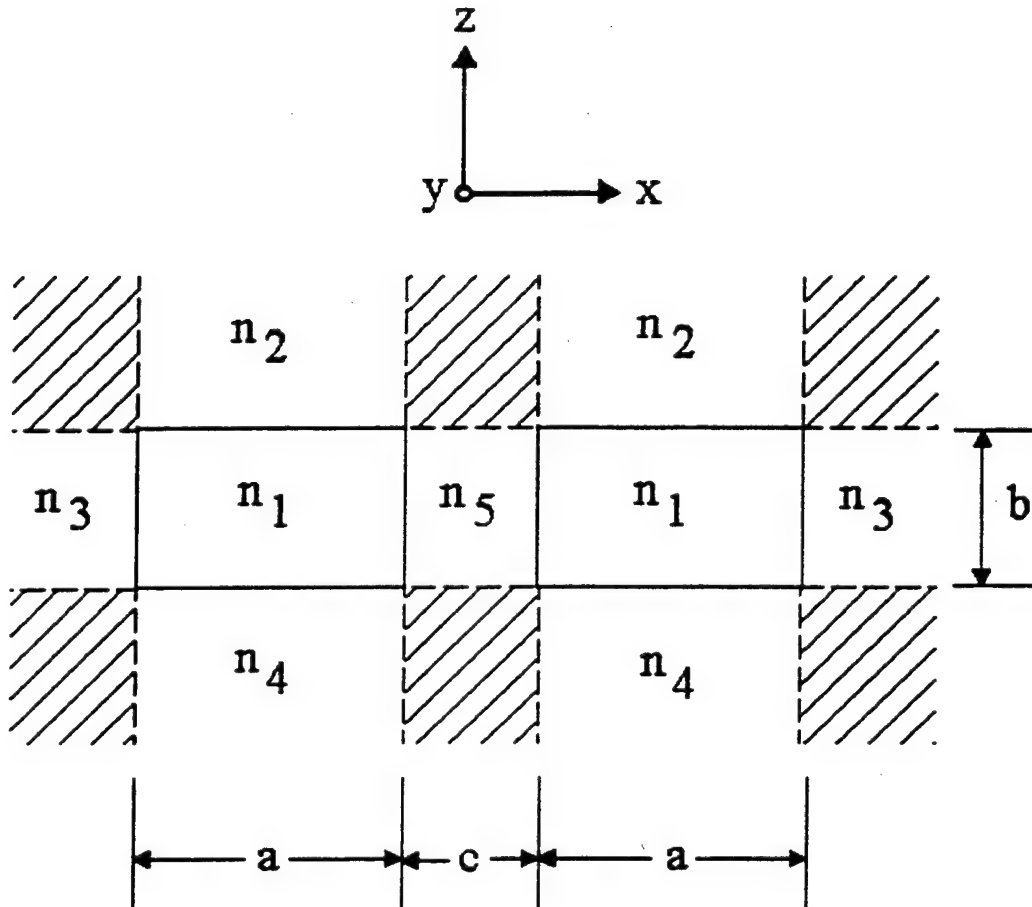


Figure 15. Rectangular Waveguide Directional Coupler Cross Section.

For well-guided modes, the field decays exponentially in the n_2 , n_3 , n_4 and n_5 regions of the directional coupler waveguide structure. Most of the power travels in the n_1 regions while only a small part of the power travels in the n_2 , n_3 , n_4 and n_5 regions. An even smaller portion of the power travels in the shaded areas. Marcatili found that very little error was introduced when the fields along the edges of the shaded regions were not properly matched when calculating the fields in the n_1 regions. This allowed him to neglect the shaded areas from consideration, thus, simplifying the boundary value problem by solving only along the four sides of the core region n_1 .

5.3.5 Marcatili TE_{pq} Modes

For the rectangular dielectric waveguide, illustrated in Fig. 15, the electric and magnetic field components in the five areas are given by [88]

$$H_{x1} = M_1 \cos(k_x x + \alpha) \cos(k_z z + \delta) \exp(-ik_y y + i\omega t), \quad (92)$$

$$H_{x2} = M_2 \cos(k_x x + \alpha) \exp[-(ik_z z + ik_y y - i\omega t)], \quad (93)$$

$$H_{x3} = M_3 \cos(k_z z + \delta) \exp[-(ik_x x + ik_y y - i\omega t)], \quad (94)$$

$$H_{x4} = M_4 \cos(k_x x + \alpha) \exp(ik_z z - ik_y y + i\omega t), \quad (95)$$

$$H_{x5} = M_5 \cos(k_z z + \delta) \sin(k_x x + \gamma) \exp(-ik_y y + i\omega t), \quad (96)$$

$$H_{z1} = H_{z2} = H_{z3} = H_{z4} = H_{z5} = 0, \quad (97)$$

$$H_{y1} = -[(i/k_y) \partial^2 H_{x1} / \partial x \partial z], \quad (98)$$

$$H_{y2} = -[(i/k_y) \partial^2 H_{x2} / \partial x \partial z], \quad (99)$$

$$H_{y3} = -[(i/k_y) \partial^2 H_{x3} / \partial x \partial z], \quad (100)$$

$$H_{y4} = -[(i/k_y) \partial^2 H_{x4} / \partial x \partial z], \quad (101)$$

$$H_{y5} = -[(i/k_y) \partial^2 H_{x5} / \partial x \partial z], \quad (102)$$

$$E_{x1} = -[(1/(\omega \epsilon n_1^2 k_y)) \partial^2 H_{x1} / \partial x \partial z], \quad (103)$$

$$E_{x2} = -[(1/(\omega \epsilon n_2^2 k_y)) \partial^2 H_{x2} / \partial x \partial z], \quad (104)$$

$$E_{x3} = -[(1/(\omega \epsilon n_3^2 k_y)) \partial^2 H_{x3} / \partial x \partial z], \quad (105)$$

$$E_{x4} = -[(1/(\omega \epsilon n_4^2 k_y)) \partial^2 H_{x4} / \partial x \partial z], \quad (106)$$

$$E_{x5} = -[(1/(\omega \epsilon n_5^2 k_y)) \partial^2 H_{x5} / \partial x \partial z], \quad (107)$$

$$E_{z1} = H_{x1} [(k^2 n_1^2 - k_z^2) / \omega \epsilon n_1^2 k_y], \quad (108)$$

$$E_{z2} = H_{x2} [(k^2 n_2^2 - k_z^2) / \omega \epsilon n_2^2 k_y], \quad (109)$$

$$E_{z3} = H_{x3} [(k^2 n_3^2 - k_z^2) / \omega \epsilon n_3^2 k_y], \quad (110)$$

$$E_{z4} = H_{x4} [(k^2 n_4^2 - k_z^2) / \omega \epsilon n_4^2 k_y], \quad (111)$$

$$E_{z5} = H_{x5} [(k^2 n_5^2 - k_z^2) / \omega \epsilon n_5^2 k_y], \quad (112)$$

$$E_{y1} = [(i/\omega \epsilon n_1^2) \partial H_{x1} / \partial z], \quad (113)$$

$$E_{y2} = [(i/\omega \epsilon n_2^2) \partial H_{x2} / \partial z], \quad (114)$$

$$E_{y3} = [(i/\omega \epsilon n_3^2) \partial H_{x3} / \partial z], \quad (115)$$

$$E_{y4} = [(i/\omega \epsilon n_4^2) \partial H_{x4} / \partial z], \quad (116)$$

$$E_{y5} = [(i/\omega\epsilon n_5^2) \partial H_{x5}/\partial z], \quad (117)$$

where $M_{1,2,3,4,5}$ are the amplitudes of the field in each respective medium, α locates the field maxima in the core region n_1 , δ locates the field minima in the core region n_1 , ω is the angular frequency and ϵ is the permittivity of free space. The γ term is necessary because single mode operation of a directional coupler will guide two kinds of TE_{00} modes. One is symmetric when $\gamma = 90^\circ$, and the other is antisymmetric when $\gamma = 0^\circ$ [88]. Both are TEM modes with main field components E_y and H_x . For a symmetric mode, the plane $x = 0$ is a magnetic short circuit. For an antisymmetric mode, the plane $x = 0$ is an electric short circuit. The electric and magnetic field components for both symmetric and antisymmetric modes are depicted in Fig. 16.

The propagation constants k_{xv} , k_y and k_{zv} in each of the five regions are related by [77]

$$k_{xv}^2 + k_y^2 + k_{zv}^2 = \omega^2 \epsilon \mu n_v^2 = k_v^2, \quad (118)$$

where $v = 1, 2, 3, 4, 5$ indicates the region and μ is the permeability of free space. In order to match the fields along the boundaries between the core region n_1 and the top and bottom clad regions (n_2 and n_4) and between the core region n_1 and the outside and center clad regions (n_3 and n_5), Marcatili assumed the following:

$$k_{x1} = k_{x2} = k_{x4} = k_x \quad (119)$$

and

$$k_{z1} = k_{z3} = k_{z5} = k_z. \quad (120)$$

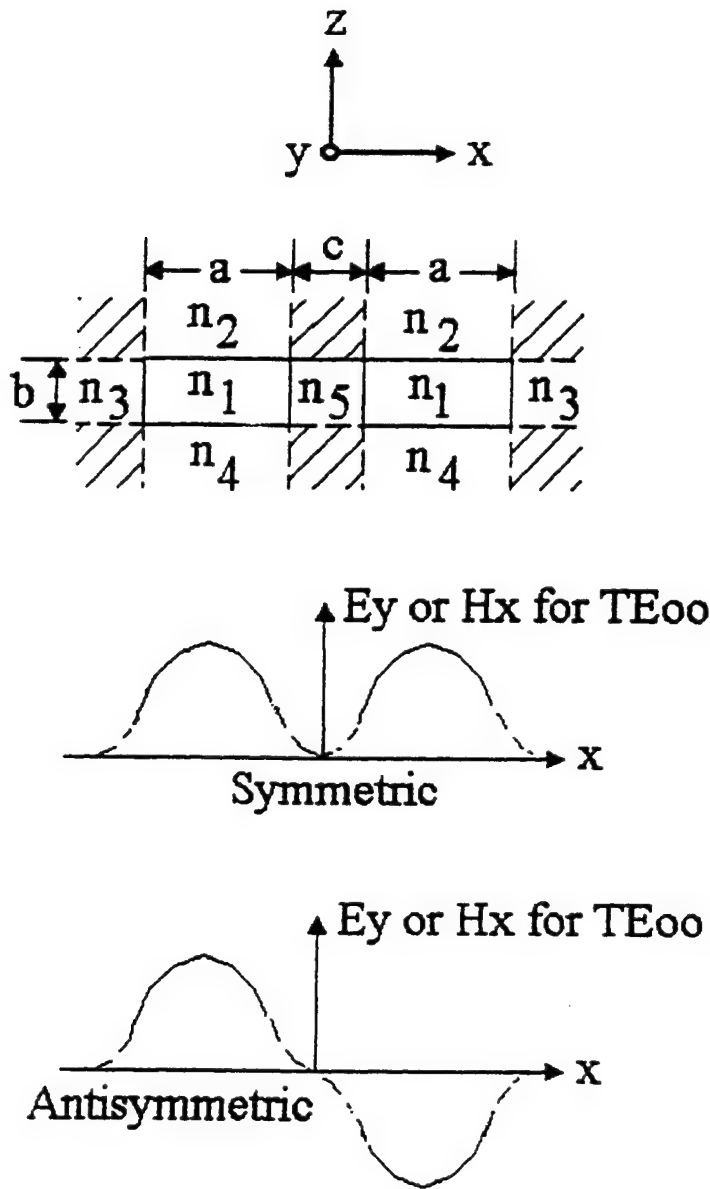


Figure 16. Field Intensity Profiles of the Symmetric and Antisymmetric Modes in a Rectangular Directional Coupler.

Since the refractive index of the core region n_1 is larger than the refractive indices of the cladding regions, only modes of plane wavelets impinging at grazing angles on the surface of the core region n_1 are guided. This implies that $k_x \ll k_y$ and $k_z \ll k_y$ and, therefore, the electric field components E_{x1} , E_{x2} , E_{x3} , E_{x4} and E_{x5} can be neglected.

Matching the remaining field components, H_x and E_z , along the boundaries of the core region n_1 gives the transcendental equations [88]

$$k_x a = k_{x0} a [1 + (2\xi_5/a) \exp(-c/\xi_5 - i2\gamma)/(1 + k_{x0}^2 \xi_5^2)] \quad (121)$$

and

$$k_z b = (q + 1)\pi - \tan^{-1}[(n_2^2/n_1^2)(k_z \eta_2)] - \tan^{-1}[(n_4^2/n_1^2)(k_z \eta_4)], \quad (122)$$

where the transverse propagation constants k_x and k_z are solutions to Eqs. (121) and (122), respectively. k_{x0} is the solution to [88]

$$k_{x0} a = (p + 1)\pi - \tan^{-1}(k_{x0} \xi_3) - \tan^{-1}(k_{x0} \xi_5). \quad (123)$$

A measure of the penetration depths of the field components in the various media are given by [88]

$$\xi_{3,5} = 1/[(\pi/A_{3,5})^2 - k_{x0}^2]^{1/2} \quad (124)$$

and

$$\eta_{2,4} = 1/[(\pi/A_{2,4})^2 - k_z^2]^{1/2}, \quad (125)$$

where

$$A_{2,3,4,5} = \lambda[2(n_1^2 - n_{2,3,4,5}^2)^{1/2}] \quad (126)$$

are the maximum thicknesses of the media for which the slab supports only the fundamental TE_{00} mode.

From Eqs. (118) - (120), the axial propagation constant for each mode of the coupler is determined by [88]

$$k_y = (k_1^2 - k_x^2 - k_z^2)^{1/2}, \quad (127)$$

where $k_1 = kn_1$ is the propagation constant of a plane wave through a medium with a refractive index n_1 at a free-space wavelength λ , and k_x and k_z are obtained from Eqs. (121) and (122).

Substituting γ into Eq. (121) gives slightly different axial propagation constants for the symmetric ($\gamma = 90^\circ$) modes and antisymmetric ($\gamma = 0^\circ$) modes [88].

$$k_{ys} = k_{y0}[1 + 2(k_{x0}^2/k_{y0}^2)(\xi_5/a)\exp(-c/\xi_5)/(1 + k_{x0}^2\xi_5^2)] \quad (128)$$

and

$$k_{ya} = k_{y0}[1 - 2(k_{x0}^2/k_{y0}^2)(\xi_5/a)\exp(-c/\xi_5)/(1 + k_{x0}^2\xi_5^2)], \quad (129)$$

where

$$k_{y0} = (k_1^2 - k_{x0}^2 - k_z^2)^{1/2} \quad (130)$$

is the axial propagation constant of the TE mode of a single dielectric waveguide ($c \rightarrow \infty$) (see Fig. 16.).

The interaction length L for total power transfer from one waveguide to the other and the coupling coefficient K between the two waveguides can then be related to k_{ys} and k_{ya} by [88]

$$-iK = \pi/(2L) = (k_{ys} - k_{ya})/2 = 2(k_{x0}^2/k_{y0}^2)(\xi_5/a)\exp(-c/\xi_5)/(1 + k_{x0}^2\xi_5^2). \quad (131)$$

The interaction length and coupling coefficient for the zero-gap directional coupler are obtained by driving the separation between the two adjacent waveguides to zero and substituting the refractive index n_4 for n_5 , which yields [32]

$$-iK = \pi/(2L) = 2(k_{x0}^2/k_{y0}^2)(\xi_5/a)/(1 + k_{x0}^2\xi_5^2). \quad (132)$$

5.3.6 Marcatili TM_{pq} Modes

The analysis for the TM_{pq} modes is very similar to that used for the TE_{pq} modes. The electric and magnetic field components for TM_{pq} modes are found by substituting E for H , H for E , $-\epsilon$ for μ and $-\mu$ for ϵ into Eqs. (92) - (117). Following Eqs. (119) and (120), the field components E_{zv} and H_{xv} can be neglected for the TM_{pq} analysis.

Matching the field components, E_x and H_z , along the boundaries of the core region n_1 in the same way as was done to match the field components H_x and E_z for the TE_{pq} analysis gives the transcendental equations [88]

$$k_x a = k_{x0} a [1 + (2\xi_5/a) \exp(-c/\xi_5 - 2i\gamma)/(1 + k_{x0}^2 \xi_5^2)] \quad (133)$$

and

$$k_z b = (q + 1)\pi - \tan^{-1}(k_z \eta_2) - \tan^{-1}(k_z \eta_4), \quad (134)$$

where the transverse propagation constants k_x and k_z are solutions to Eqs. (133) and (134), respectively. k_{x0} is the solution to

$$k_{x0} a = (p + 1)\pi - \tan^{-1}[(n_3^2/n_1^2)(k_{x0} \xi_3)] - \tan^{-1}[(n_5^2/n_1^2)(k_{x0} \xi_5)]. \quad (135)$$

η_2 , η_4 , ξ_3 and ξ_5 are obtained from Eqs. (124) - (126).

The interaction length L for total power transfer from one waveguide to the other and the coupling coefficient K between the two waveguides are determined by Eq. (131) using k_{y0} , k_z and k_{x0} obtained from Eqs. (130), (134) and (135), respectively. The interaction length and coupling coefficient for the zero-gap directional coupler are obtained by substituting k_{y0} , k_z and k_{x0} , obtained from Eqs. (130), (134) and (135), into Eq. (132) [32].

Marcuse [89] derived a rectangular dielectric waveguide model following the approach developed by Marcatili. It is also widely used and gives identical results.

5.3.7 Effective Index Method

In a 1975 paper, Burns and Milton discussed mode conversion in planar dielectric separating waveguides [102]. This has since become known as the effective index method, and is treated in detail by Nishihara, Haruna and Suhara for both two and three- dimensional dielectric waveguide structures [25]. The effective index method is based on the concept of the effective index of the guided mode. The guided mode propagating along the z axis sees the effective index (N) defined by [25, 121]

$$\beta = kN, \quad (136)$$

where β is the axial propagation constant, k is the free space propagation constant, and $N = n_1 \cos \theta_1$ (see Fig. 17).

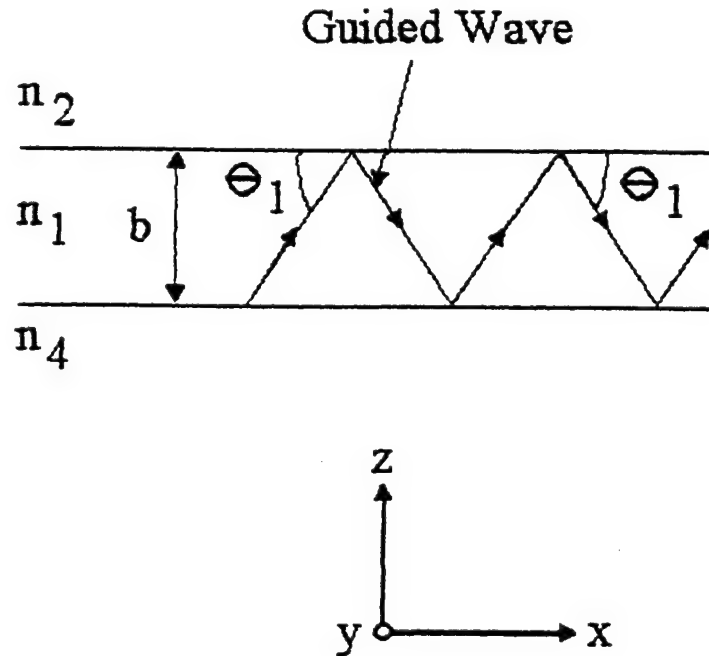
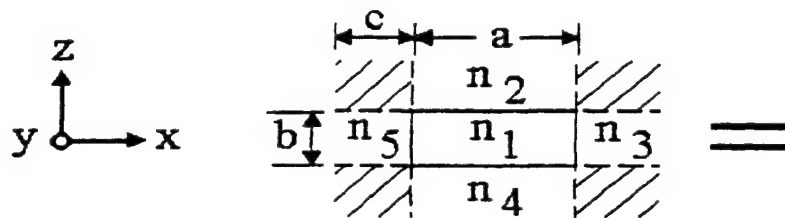
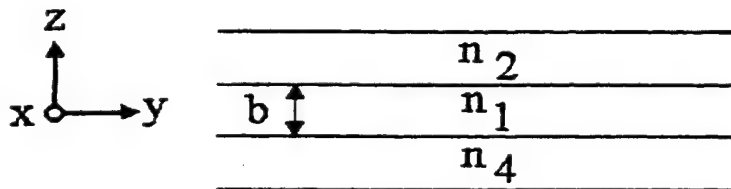


Figure 17. Trajectory of a Guided Wave in a Slab Waveguide.

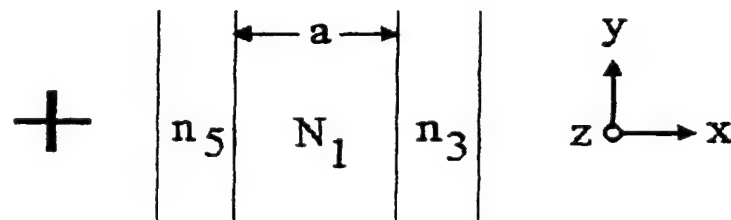
The effective index method used for the dielectric waveguide structure fabricated for this experiment (illustrated in Fig. 15) is performed by dividing the three-dimensional waveguide into two two-dimensional waveguides. The first is 2-D Waveguide 1, with light confinement in the z direction. The second is 2-D Waveguide 2, with light confinement in the x direction (see Fig. 18). The axial propagation constant for the TE_{pq} modes of a three-dimensional waveguide structure is determined using the following procedure: The effective index N_1 of 2-D Waveguide 1 is found by applying TM_{pq} mode analysis to the top and bottom clad regions (n_2 and n_4 , respectively) with waveguide thickness b . Effective index N_1 is used to find the effective index N_2 of 2-D Waveguide 2 by applying TE_{pq} mode analysis to the outside and center clad regions (n_3 and n_5 , respectively) with waveguide width a . The axial propagation constant is obtained by substituting N_2 for N in Eq. (136).



Three-Dimensional Dielectric Waveguide



Two-Dimensional Waveguide 1



Two-Dimensional Waveguide 2

Figure 18. Analytical Model for the Effective Index Method for TE_{pq} Modes.

The axial propagation constant for the TM_{pq} modes is determined in a manner similar to the one used for the TE_{pq} modes. Effective index N_1 of 2-D Waveguide 1 is found by applying TE_{pq} mode analysis to the top and bottom clad regions (n_2 and n_4 , respectively) with waveguide thickness b . Effective index N_1 is then used to find effective index N_2 of a 2-D Waveguide 2 by applying TM_{pq} mode analysis to the outside and center clad regions (n_3 and n_5 , respectively) with waveguide width a .

5.3.8 Effective Index Method TE_{pq} Modes

As outlined in the preceding section, 2-D Waveguide 1 represents the TM_{pq} modes in an infinite slab waveguide of thickness b . 2-D Waveguide 2 represents the TE_{pq} modes in an infinite slab waveguide of width a . Since E_y is the dominant electric field component, the field appears as a TE_{pq} mode with respect to the outside and center clad regions (n_3 and n_5 , respectively). The analysis can be represented by the following [114]:

$$\beta_2 = k[N_2\{TM^b(n_2|n_1|n_4);TE^a(n_3|N_1|n_5)\}], \quad (137)$$

where β_2 is the TE_{pq} axial propagation constant for the three dimensional dielectric waveguide.

First, we start with the wave equation for the TM_{pq} modes of 2-D Waveguide 1, given by [25]

$$\partial^2 H_x / \partial z^2 + (k^2 n^2 - \beta_1^2) H_x = 0, \quad (138)$$

where

$$E_z = (\beta_1 / \omega \epsilon_0 n^2) H_x, \quad (139)$$

and

$$E_y = (1 / i \omega \epsilon_0 n^2) \partial H_x / \partial z, \quad (140)$$

where β_1 is the TM_{pq} axial propagation constant for 2-D waveguide 1.

The field solutions can then be written as [25]

$$H_{x1} = H_1 \cos(k_z z + \phi_2), \quad (141)$$

at $-b < z < 0$ for the core region n_1 ,

$$H_{z2} = H_2 \exp(-\gamma_2 z), \quad (142)$$

at $z > 0$ for the top clad region n_2 , and

$$H_{z4} = H_4 \exp[\gamma_4(z + b)], \quad (143)$$

at $z < -b$ for the bottom clad region n_4 . The variables γ_2 and γ_4 are the transverse propagation constants of a plane wave in the top and bottom cladding regions, respectively. ϕ_2 is the phase shift suffered by a wave polarized with its magnetic field vector parallel to the interface between the core region n_1 and the top clad region n_2 .

In addition to the phase shift due to reflection of the wave from the interface between n_1 and n_2 , there is also a phase shift ϕ_4 suffered by the reflection of the wave from the interface between the core region n_1 and the bottom clad region n_4 . Using Eqs. (138) - (143), these phase shifts can be defined mathematically by [89]

$$\phi_2 = -2\arctan[(n_1^2/n_2^2)(\beta_1^2 - n_2^2 k^2)^{1/2}/(n_1^2 k^2 - \beta_1^2)^{1/2}] \quad (144)$$

and

$$\phi_4 = -2\arctan[(n_1^2/n_4^2)(\beta_1^2 - n_4^2 k^2)^{1/2}/(n_1^2 k^2 - \beta_1^2)^{1/2}]. \quad (145)$$

Using the differences between the phase fronts, which are due to the reflection of the wave at the two interfaces and given mathematically by [89]

$$s_1 = (b \cos \theta_1)[(1/\tan \theta_1) - \tan \theta_1] = (b/\sin \theta_1)(\cos^2 \theta_1 - \sin^2 \theta_1) \quad (146)$$

and

$$s_2 = b/\sin \theta_1, \quad (147)$$

the condition in which both reflected waves contribute to the same plane waves can be expressed by the relation [89]

$$n_1(s_2 - s_1)k + \phi_2 + \phi_4 = 2(q + 1)\pi, \quad (148)$$

where $q = (0, 1, 2, \dots)$ indicates the number of extrema of the magnetic field in the y direction.

The eigenvalue equation, obtained from Eqs. (144) - (148), can then be written as [25]

$$k_z b = (q + 1)\pi - \tan^{-1}[(n_2^2/n_1^2)(k_z/\gamma_2)] - \tan^{-1}[(n_4^2/n_1^2)(k_z/\gamma_4)], \quad (149)$$

where

$$k_z = (n_1^2 k^2 - \beta_1^2)^{1/2}, \quad (150)$$

$$\gamma_2 = (\beta_1^2 - n_2^2 k^2)^{1/2} \quad (151)$$

and

$$\gamma_4 = (\beta_1^2 - n_4^2 k^2)^{1/2} \quad (152)$$

are the transverse propagation constants.

Using Eq. (136), the transverse propagation constants, given by Eqs. (150) - (152), can be expressed in terms of the effective index of 2-D Waveguide 1.

$$k_z = k(n_1^2 - N_1^2)^{1/2}, \quad (153)$$

$$\gamma_2 = k(N_1^2 - n_2^2)^{1/2} \quad (154)$$

and

$$\gamma_4 = (N_1^2 - n_4^2)^{1/2}. \quad (155)$$

Next, the wave equation for the TE_{pq} modes of 2-D Waveguide 2 is given by [25]

$$\partial^2 E_z / \partial x^2 + (k^2 n^2 - \beta_z^2) E_z = 0, \quad (156)$$

where

$$H_x = -(\beta_z / \omega \mu_0) E_z \quad (157)$$

and

$$H_y = -(1 / i \omega \mu_0) \partial E_z / \partial x. \quad (158)$$

The field solutions can be written as [25]

$$E_{z1} = E_1 \cos(k_x x + \phi_3), \quad (159)$$

at $0 < x < a$ for the core region now defined as N_1 ,

$$E_{z3} = E_2 \exp(-\gamma_3 x), \quad (160)$$

at $x < 0$ for the outside clad region n_3 , and

$$E_{z5} = E_5 \exp[\gamma_5 (x + a)], \quad (161)$$

at $x > a$ for the center clad region n_5 . The variables γ_3 and γ_5 are the transverse propagation constants of a plane wave in the outside and center cladding regions, respectively. ϕ_3 is the phase shift suffered by a wave polarized with its electric field vector parallel to the interface between the core region N_1 and the outside clad region n_3 .

In addition to the phase shift due to reflection of the wave from the interface between N_1 and n_3 , there is also a phase shift ϕ_5 suffered by the reflection of the wave from the interface between the core region N_1 and the center clad region n_5 . Using Eqs. (156) -

(161), these phase shifts can be defined mathematically by [25]

$$\phi_3 = -2\arctan[(\beta_2^2 - n_3^2 k^2)^{1/2}/(n_1^2 k^2 - \beta_2^2)^{1/2}] \quad (162)$$

and

$$\phi_5 = -2\arctan[(\beta_2^2 - n_5^2 k^2)^{1/2}/(n_1^2 k^2 - \beta_2^2)^{1/2}]. \quad (163)$$

Using the differences between the phase fronts, which are due to the reflection of the wave at the two interfaces and given mathematically by [25]

$$s_1 = (\cos\theta_1)[(1/\tan\theta_1) - \tan\theta_1] = (a/\sin\theta_1)(\cos^2\theta_1 - \sin^2\theta_1) \quad (164)$$

and

$$s_2 = a/\sin\theta_1, \quad (165)$$

the condition in which both reflected waves contribute to the same plane waves can be expressed with the relation [25]

$$n_1(s_2 - s_1)k + \phi_3 + \phi_5 = 2(p + 1)\pi, \quad (166)$$

where $p = (0, 1, 2, \dots)$ indicates the number of extrema of the electric field in the x direction.

The eigenvalue equation, obtained from Eqs. (162) - (166), can then be written as [25]

$$k_x a = (p + 1)\pi - \tan^{-1}(k_x/\gamma_3) - \tan^{-1}(k_x/\gamma_5), \quad (167)$$

where

$$k_x = (N_1^2 k^2 - \beta_2^2)^{1/2}, \quad (168)$$

$$\gamma_3 = (\beta_2^2 - n_3^2 k^2)^{1/2} \quad (169)$$

and

$$\gamma_5 = (\beta_2^2 - n_5^2 k^2)^{1/2} \quad (170)$$

are the transverse propagation constants.

Using Eq. (136), the transverse propagation constants, given by Eqs. (168) - (170), can be expressed in terms of the effective index of 2-D Waveguide 2.

$$k_z = k(N_1^2 - N_2^2)^{1/2}, \quad (171)$$

$$\gamma_3 = k(N_2^2 - n_3^2)^{1/2} \quad (172)$$

and

$$\gamma_5 = (N_2^2 - n_5^2)^{1/2}. \quad (173)$$

Having solved for β_2 and k_x , the symmetric propagation constant β_s and antisymmetric propagation constant β_a (corresponding to the symmetric and antisymmetric TE_{00} modes of the directional coupler, respectively) are found by [88]

$$\beta_s = \beta_2[1 + 2(k_x^2/\beta_2^2)(1/a\gamma_5)\exp(-c\gamma_5)/(1 + k_x^2/\gamma_5^2)] \quad (174)$$

and

$$\beta_a = \beta_2[1 - 2(k_x^2/\beta_2^2)(1/a\gamma_5)\exp(-c\gamma_5)/(1 + k_x^2/\gamma_5^2)], \quad (175)$$

where c is the distance of separation between the two waveguides.

The interaction length L for total power transfer from one waveguide to the other, and the coupling coefficient K between the two waveguides, can be related to β_s and β_a by [25]

$$-iK = \pi/(2L) = (\beta_s - \beta_a)/2. \quad (176)$$

The interaction length and coupling coefficient for the zero-gap directional coupler are obtained by driving the separation between the two adjacent waveguides to zero and

substituting the refractive index n_4 for n_5 [32]. This yields,

$$\beta_s = \beta_2[1 + 2(k_x^2/\beta_2^2)(1/a\gamma_5)(1/(1 + k_x^2/\gamma_5^2))] \quad (177)$$

and

$$\beta_a = \beta_2[1 - 2(k_x^2/\beta_2^2)(1/a\gamma_5)(1/(1 + k_x^2/\gamma_5^2))], \quad (178)$$

which are then substituted back into Eq. (176).

5.3.9 Effective Index Method TM_{pq} Modes

For TM_{pq} mode analysis, 2-D Waveguide 1 represents the TE_{pq} modes in an infinite slab waveguide of thickness b . 2-D Waveguide 2 represents the TM_{pq} modes in an infinite slab waveguide of width a . With H_y as the dominant magnetic field component, the field appears as a TM_{pq} mode with respect to the outside and center clad regions (n_3 and n_5). The analysis can be represented by the following [114]:

$$\beta_2 = k[N_2\{TE^b(n_2|n_1|n_4); TM^a(n_3|N_1|n_5)\}], \quad (179)$$

where β_2 is the TM_{pq} axial propagation constant for the three dimensional dielectric waveguide. Following the same procedure as was presented in the previous section, the eigenvalue equation for the TE_{pq} modes of 2-D Waveguide 1 can be written as [25]

$$k_x a = (p + 1)\pi - \tan^{-1}[(n_3^2/n_1^2)(k_x/\gamma_3)] - \tan^{-1}[(n_5^2/n_1^2)(k_x/\gamma_5)], \quad (180)$$

where

$$k_x = (n_1^2 k^2 - \beta_1^2)^{1/2}, \quad (181)$$

$$\gamma_3 = (\beta_1^2 - n_3^2 k^2)^{1/2} \quad (182)$$

and

$$\gamma_5 = (\beta_1^2 - n_5^2 k^2)^{1/2}. \quad (183)$$

Using Eq. (136), the transverse propagation constants, given by Eqs. (181) - (183), can be expressed in terms of the effective index of 2-D Waveguide 1.

$$k_z = k(n_1^2 - N_1^2)^{1/2}, \quad (184)$$

$$\gamma_3 = k(N_1^2 - n_3^2)^{1/2} \quad (185)$$

and

$$\gamma_5 = (N_1^2 - n_5^2)^{1/2}. \quad (186)$$

The eigenvalue equation for the TM_{pq} modes of 2-D Waveguide 2 can be written as [25]

$$k_z b = (q + 1)\pi - \tan^{-1}(k_z/\gamma_2) - \tan^{-1}(k_z/\gamma_4), \quad (187)$$

where

$$k_z = (N_1^2 k^2 - \beta_2^2)^{1/2}, \quad (188)$$

$$\gamma_2 = (\beta_2^2 - n_2^2 k^2)^{1/2} \quad (189)$$

and

$$\gamma_4 = (\beta_2^2 - n_4^2 k^2)^{1/2}. \quad (190)$$

Using Eq. (136), the transverse propagation constants, given by Eqs. (188) - (190), can be expressed in terms of the effective index of 2-D Waveguide 2.

$$k_z = k(N_2^2 - N_1^2)^{1/2}, \quad (191)$$

$$\gamma_2 = k(N_2^2 - n_2^2)^{1/2} \quad (192)$$

and

$$\gamma_4 = (N_2^2 - n_4^2)^{1/2}. \quad (193)$$

Having solved for β_2 and k_x , the symmetric propagation constant β_s and antisymmetric propagation constant β_a for the TM_{00} modes of the directional coupler are found by substituting β_2 and k_x , determined here, into Eqs. (174) and (175).

The interaction length L for total power transfer from one waveguide to the other, and the coupling coefficient K between the two waveguides, can be related to β_s and β_a by Eq. (176). The interaction length and coupling coefficient for the zero-gap directional coupler are obtained by using Eqs. (177) and (178), which are then substituted back into the equation for the zero-gap directional coupler, Eq. (176).

5.3.10 Beam Propagation Method

In 1976, Fleck, Morris and Feit proposed a propagating beam method (bpm) for computing fields of an optical beam passing through a medium [114]. The method calculates the characteristics of an input beam as it propagates through a medium over a small distance y , and then corrects for the variations of the refractive index as seen by the beam over this distance y . It has already been applied to several optical fiber and integrated optic applications [104-110, 117, 123, 124].

The beam propagation method is derived for a scalar field. The theory is restricted to small changes in the refractive index. The first part of the derivation assumes the propagation of a high frequency beam through an inhomogeneous medium. It begins with the wave equation [109]

$$\nabla^2 \phi + k^2 n^2(\mathbf{r}) \phi = 0, \quad (194)$$

where ϕ represents the scalar field, k is the free space wave number defined at the beginning of this chapter, and $n(\mathbf{r}) = n_0(\mathbf{r})^2 + \Delta n^2(\mathbf{r})$ is the refractive index of the medium consisting of an unperturbed part ($n_0(\mathbf{r})^2$), and a perturbation ($\Delta n^2(\mathbf{r})$). Splitting $n^2(\mathbf{r})$ into its respective parts, Eq. (194) takes the form [109]

$$\nabla^2 \phi + k^2 n_0^2(\mathbf{r}) \phi = -k^2 \Delta n^2(\mathbf{r}) \phi = s(\mathbf{r}), \quad (195)$$

where the right hand side of the equation, designated as $s(\mathbf{r})$, is considered a source function. Next, the unperturbed part of the index is chosen so that the new wave equation [109]

$$\nabla^2 \psi + k^2 n_0^2(\mathbf{r}) \psi = 0, \quad (196)$$

along with the radiation conditions at $y = \infty$, has a solution. If ψ is known for $y = y_0$, where y_0 is the position $y = 0$, then ψ and its derivative, with respect to y , can be solved for all values of y by use of an operator (\hat{a}). \hat{a} acts with respect to only the transverse coordinates (x, z) . This leads to [109]

$$\partial \psi / \partial y = \hat{a} \psi(x, y_0, z). \quad (197)$$

For $n_0 = \text{constant}$, the scalar field can be represented in the angular spectrum domain by [109, 126]

$$\Psi(k_x, k_z, y) = \int_{-\infty}^{+\infty} \int \psi(x, y, z) \exp[-i(k_x x + k_z z)] dx dz, \quad (198)$$

where $\Psi(k_x, k_z, y)$ is the Fourier transform of the scalar field ($\psi(x, y, z)$), and k_x and k_z are the transverse propagation constants. Taking the derivative of Eq. (198), with respect to y , yields [109, 126]

$$\partial \Psi / \partial y(k_x, k_z, y) = -ik_y \Psi(k_x, k_z, y), \quad (199)$$

where $k_y = (k^2 n_0^2 - k_x^2 - k_z^2)^{1/2}$ is the axial propagation constant. By using Eq. (199), the integral operator \hat{a} can be derived.

For a given coordinate (y), the field (ϕ) is split into two parts. The first part, (ϕ_1), is generated by the sources in the region where $y' < y$. The second part, (ϕ_2), is generated by

the sources where $y' > y$. Using the function [109]

$$\begin{aligned} \{e_1(\mathbf{r}|\mathbf{r}') = 0 \text{ for } y < y' \\ e_1(\mathbf{r}|\mathbf{r}') = 1/2 \text{ for } y = y' \\ e_1(\mathbf{r}|\mathbf{r}') = 1 \text{ for } y > y'\}, \end{aligned} \quad (200)$$

an explicit expression for ϕ_1 and ϕ_2 can be obtained. Defining \mathbf{G} as Greens function of Eq. (196), the wave equation (ϕ_1) can be expressed by [109]

$$\phi_1(\mathbf{r}) = \int \int \int_{-\infty}^{+\infty} \mathbf{G}(\mathbf{r}|\mathbf{r}') e_1(\mathbf{r}|\mathbf{r}') s(\mathbf{r}') dV'. \quad (201)$$

Taking the derivative of ϕ_1 , with respect to y , yields [109]

$$\begin{aligned} \partial \phi_1 / \partial y(\mathbf{r}) = \int \int \int_{-\infty}^{+\infty} \partial \mathbf{G} / \partial y(\mathbf{r}|\mathbf{r}') e_1(\mathbf{r}|\mathbf{r}') s(\mathbf{r}') dV' \\ + \int \int \int_{-\infty}^{+\infty} \mathbf{G}(\mathbf{r}|\mathbf{r}') \delta(y - y') s(\mathbf{r}') dV' \end{aligned} \quad (202)$$

where $\delta(y - y')$ is the step size. The first integral of Eq. (202) represents the unperturbed medium. It can be expressed in terms of \hat{a} using Eq. (197) [109],

$$\hat{a}\phi_1(\mathbf{r}). \quad (203)$$

The second integral of Eq. (202) includes both the unperturbed medium and the perturbation. With the help of Eq. (195), the second integral in Eq. (202) can be written as [109]

$$\int \int_{-\infty}^{+\infty} \mathbf{G}(x, y, z | x', y, z') (-k^2) \Delta n^2(x', y, z') \phi(x', y, z') dx' dz'. \quad (204)$$

Eq. (204) can be expressed in terms of an operator (\hat{u}) acting on ϕ by [109]

$$\hat{u}\phi(x',y,z'), \quad (205)$$

where, like \hat{a} , operator \hat{u} acts with respect to only the transverse coordinates (x,z).

Substitution of Eqs. (203) and (205) into Eq. (202) yields [109]

$$\partial \phi_1 / \partial y(x',y,z') = \hat{a}\phi_1(x',y,z') + \hat{u}\phi(x',y,z'). \quad (206)$$

Neglecting the influence of the reflected field (ϕ_2) on ϕ_1 , ϕ_1 can be substituted for ϕ in Eq. (206). The first-order differential equation for ϕ_1 then becomes [109]

$$\partial \phi_1 / \partial y(x',y,z') = \hat{a}\phi_1(x',y,z') + \hat{u}\phi_1(x',y,z'), \quad (207)$$

where $\hat{u}\phi_1$ is the correction term.

From Eq. (207), the propagation of field (ϕ_1) is given by two terms. One describes propagation in an unperturbed medium ($\hat{a}\phi_1$). The other describes a correction term ($\hat{u}\phi_1$), representing the influence of Δn . Using Fourier transforms and convolution, along with the assumption that the unperturbed media is homogeneous, the correction term in Eq. (207) can be simplified [109]

$$\hat{u}\phi_1(x',y,z') = -(ik/2n_0)\Delta n^2\phi_1(x',y,z'). \quad (208)$$

By combining Eqs. (207) and (208), the first-order differential equation for ϕ_1 becomes [109]

$$\partial \phi_1 / \partial y(x',y,z') = \hat{a}\phi_1(x',y,z') - (ik/2n_0)\Delta n^2\phi_1(x',y,z'). \quad (209)$$

In order to solve Eq. (209), it will be assumed that ϕ_1 is known at position $y = y_0$. If $\Delta n^2 = 0$,

Eq. (209) reduces to [98]

$$\partial \epsilon / \partial y(x, y_0, z) = \hat{a}\epsilon(x, y_0, z), \quad (210)$$

where $\epsilon(x, y_0, z) = \phi_1(x, y_0, z)$ is given. Therefore, ϵ represents the field as it propagates through a medium with a refractive index ($n_0(\mathbf{r})$). Introducing a correction factor ($\exp(\Gamma)$) leads to an approximate solution to the differential Eq. (209). This solution is derived by [109]

$$\phi_1(\mathbf{r}) = \exp[\Gamma(\mathbf{r})]\epsilon(\mathbf{r}), \quad (211)$$

with $\Gamma(x, y_0, z) = 0$. Combining Eqs. (209) and (211) yields [109]

$$\partial \Gamma / \partial y = -(ik/2n_0)\Delta n^2 + [\hat{a}(\exp(\Gamma)\epsilon) - \exp(\Gamma)\hat{a}(\epsilon)]/\exp(\Gamma)\epsilon. \quad (212)$$

It has been demonstrated that the second term in Eq. (212) can be neglected, provided Eq. (212) is integrated over a small distance ($y - y_0$) [109]. This yields

$$\Gamma = -(ik/2n_0)\Delta n^2(y - y_0), \quad (213)$$

for ($y - y_0$) small. Combining Eqs. (211) and (213) yields [109]

$$\phi_1(x, y_0, z + \Delta y) = \epsilon(x, y_0, z + \Delta y)\exp[-(ik/2n_0)\Delta n^2\Delta y], \quad (214)$$

which is the equation for the correction term.

For $n_0(\mathbf{r})$ independent of y , the eigenmode of Eq. (196) can be determined. This allows one to calculate the propagation of ϵ [109].

$$\epsilon(x, y_0, z + \Delta y) = \sum_n A_n \psi_n(x, z) \exp[-(i\kappa_n \Delta y)] \quad (215)$$

where

$$A_n = \int_{-\infty}^{+\infty} \int \varepsilon(x, y_0, z) \psi_n(x, z) dx dz. \quad (216)$$

Using Eq. (215) and multiplication with the correction term, defined by Eq. (214), allows the propagation of light in small steps.

Application of the beam propagation method to media with small refractive index variations allows one to analyze beam propagation through integrated waveguide structures. For this case, the operator \hat{a} can be expressed in terms of Fourier transforms (see Eqs. (198) and (199)). The propagation step defined by Eq. (215) can, thus, be calculated using fast Fourier transforms (FFT's). Performing a two dimensional FFT extends the beam propagation method to three dimensions (3D), allowing one to analyze the dielectric waveguide structure illustrated in Fig. 15.

The beam propagation method for integrated optic waveguide applications is available as computer aided design CAD software tools. It is readily available for personal computers (PCs), Macintosh (MAC) computers and workstations. The BPM CAD tool utilized for this chapter was BeamPROP for PC [127]. Although the BPM does not generate hard numbers for the interaction length of directional couplers, in the way the dielectric waveguide and effective index methods do, the beam propagation method does provide an excellent prediction of device performance. It calculates the amplitudes of the fields as they propagate through the medium. For example, the BPM CAD program was used to generate Fig. 19, which gives a visual prediction of the behavior of a light wave propagating through an integrated optic waveguide with an S-bend. The following parameters were substituted into the BPM software: the waveguide width $a = 3 \mu\text{m}$, the waveguide core thickness $b = 1 \mu\text{m}$, the operating wavelength $\lambda = 830 \text{ nm}$, the refractive index of the core $n_1 = 1.63$, the refractive index of the top and bottom clad regions $n_2 = n_4 = 1.61$, and the refractive index of the outside clad regions $n_3 = n_5 = 1.61$. Zero propagation

loss was assumed for the straight guides. The S-bend was designed using the formula [128]

$$x(y) = (h/l)y - (h/2\pi)\sin[(2\pi/l)y], \quad (217)$$

where l is the longitudinal separation in the y direction and h is the lateral offset in the x direction. Eq. (217) allows one to minimize the radiative loss and maximize the mode confinement. For the S-bend structure illustrated in Fig. 13, $h = 20 \mu\text{m}$ and $l = 500 \mu\text{m}$.

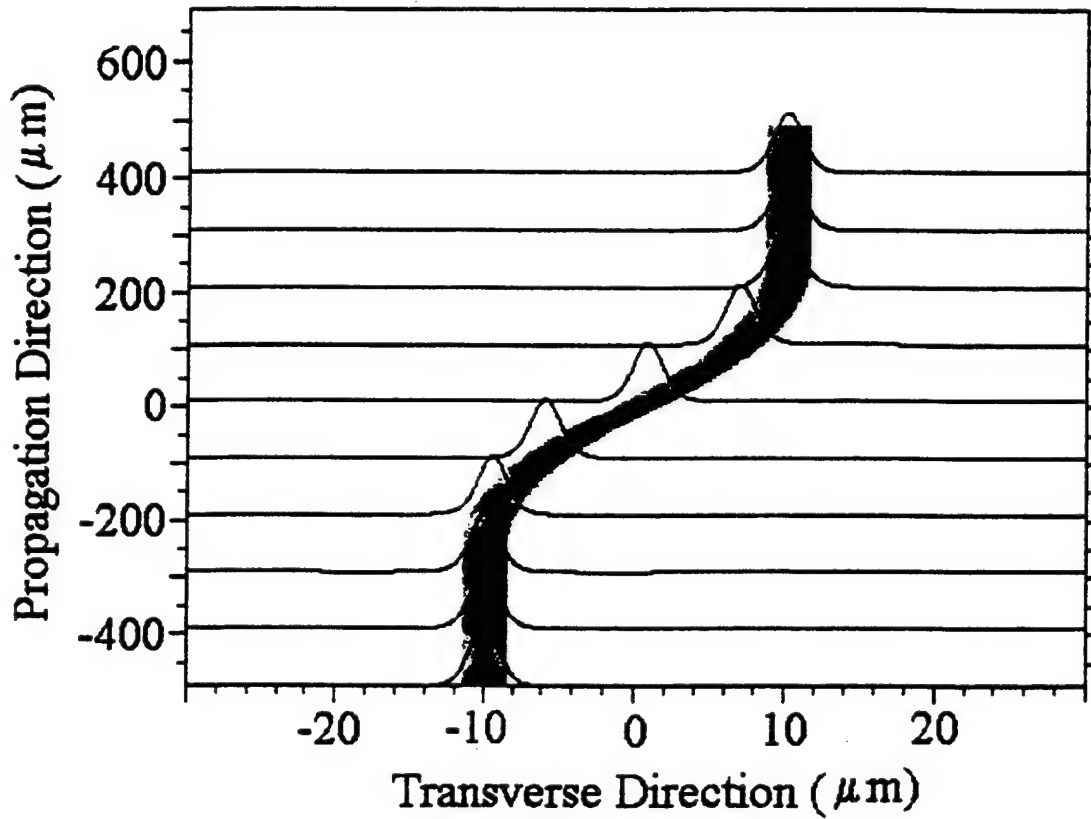


Figure 19. Amplitudes of the Propagating Fields in an Integrated Optic S-Bend Waveguide.

5.3.11 Refractive Index of the Waveguide Cladding

The refractive index of the cladding layer can be found using the relation [16]

$$n_{\text{core}} - n_{\text{clad}} > m^2 \lambda^2 / [4(t_g)^2 (n_{\text{core}} + n_{\text{clad}})], \quad (218)$$

where m is the mode number and t_g is the thickness of the core. Assuming single mode operation ($m=1$), Eq. (218) becomes

$$n_{\text{clad}} > [(n_{\text{core}})^2 - \lambda^2/[4(t_g)^2]]^{1/2}. \quad (219)$$

One can also use a TE/TM mode analysis presented by Ghatak, Thyagarajan and Shenoy [129] to model the loss for a given mode.

The refractive indices and EO coefficients for the various polymers are usually provided by the manufacturer, but they can also be determined experimentally. The parameters used for examples in this chapter are typical values. Now that the basic theory for designing EO devices has been presented, one can address fabrication issues.

5.4 DEVICE FABRICATION

NLO polymers typically come in crystal or powdered form. For our example, we will use an NLO polymer from AdTech Systems Research known as LD-3 [7]. It is composed of a methymethacrylate (MMA) polymer containing 4-[bis (2-hydroxyethyl) amino]-4'-((6-methacryloyl-hexyl) sulfonyl) azobenzene nonlinear optical chromophores. A recipe for reconstituting the polymer into a liquid for spin casting is usually provided by the polymer manufacturer. We will start with LD-3 in powder form. First, grind 0.10 grams of LD-3 into a fine powder and dissolve the powder in 1.0-1.5 ml of pure and dry organic solvent tetrahydrofurane (THF) [7]. Add 0.060 grams of cross-linker 4,4'-diisocyanato-3,3'-dimethoxybiphenyl, which forms 3D networks and locks the dipole aligned chromophores [7]. Stir the mixture for 15 minutes at room temperature. Filter the mixture through a 0.2 μm syringe filter [7]. With the material in its liquid form we are ready to begin fabrication of our EO device. There are several methods that have been employed for fabricating NLO polymer devices. The two most common techniques, namely photobleach [4, 8, 21, 22, 35, 36, 40, 42, 43, 45, 48, 51-62] and etch-and-fill [8, 21, 22, 35, 39, 45-47, 49-54] are described below in 5.4.1.

5.4.1 Photobleach

To begin device processing, we evaporate a thin metal layer on top of a substrate, which can either be glass, polymer or semiconductor. This metal layer will be the ground plane electrode. It can be gold, aluminum, titanium/tungsten/gold or any good conductor; it should be 4000 \AA - 1 μm thick for good conductivity. Deposit a passive polymer bottom cladding material with a refractive index about 0.02-0.04 less than that of the core. The cladding material is usually synthesized to work with the NLO polymer being used. It can be an acrylate, polyimide, or polyetherimide, just to name a few. It must also have a higher glass transition temperature (T_g) than the core material in order to perform the poling step. It is spin cast over the metal layer at an acceleration and a speed to yield a thickness of 3 μm . The cladding layer is then cured by baking on a hot plate until dry. The exact time depends on the type of polymer used. The NLO polymer core layer is then deposited on top

of the cladding layer at an acceleration and speed in order to yield a thickness of 2 μm . It is baked until dry. A passive polymer top cladding layer is deposited in the same manner in order to yield the same thickness as the bottom cladding layer. The top cladding layer is also baked until it is dry. A second metal layer, used for waveguide patterning, is evaporated on top of the top cladding layer. It is a good conductor, typically 500 \AA thick. The metal layer is then patterned with the desired EO waveguide circuit, using standard lithographic techniques, leaving a metal mask. The wafer is then flood exposed with ultraviolet (UV) light. Exposure to UV results in a slight and very controllable reduction in the refractive index of the NLO polymer. This process is called photobleach. Photobleaching defines the side cladding layers of the channel waveguide. Exposures take several hours, and the refractive index of the side cladding can be controlled to the 4th decimal place. The metal mask used for photobleaching is then stripped off. A third 500-3000 \AA metal layer for the electrodes is evaporated on top of the top clad. The top metal layer is patterned with the desired electrode structure using standard IC tools and techniques. After the electrodes have been patterned, the NLO material directly under the electrodes needs to be poled in order to operate as an EO device. Poling is a technique used to align the molecules or moieties of the material in order to maximize the EO properties of the NLO polymer. Poling is performed by heating the EO circuit to a temperature above the glass transition temperature of the material, specified by the manufacturer, and then applying a DC voltage. The higher temperature allows the molecules within the material to move freely. For the NLO polymer LD-3, a poling temperature of 150°C is specified. An electric field is then applied across the electrodes using soft tip probes. The moieties will align in the direction of the electric field, thus, increasing the electro-optic coefficient r_{33} in those regions. The poling voltage is typically 150 VDC/ μm . Thus, for this example, the poling voltage required would be 1200 VDC [3, 4, 7, 8, 21, 22, 35, 36, 39-42, 48-63, 65]. With the voltage still applied, the circuit is cooled to room temperature. This locks the moieties in place. This type of poling is known as selective poling [3, 4, 8, 21, 22, 36, 40, 42, 43, 48, 51-62]; only the NLO material under the electrode is poled. Since the regions along the axis parallel to the applied voltage become birefringent, the electric field of a TM mode will see a higher refractive index in the poled regions than in the un-poled regions, becoming waveguides for TM light [61].

The device is now ready for operation. The parameters for poling and photobleaching are different for the various NLO polymers; one needs to determine optimum conditions through experimentation. The separation between the electrodes for this example is 8 μm . The thicknesses for the cladding and core layers given above have been determined, by several researchers, to provide low propagation loss and are the thicknesses generally used [3, 4, 7, 8, 21, 22, 36, 39-43, 45-47, 48-53, 55-63, 65, 68]. However, an 8 μm separation between electrodes renders long devices not suitable for MCM applications [35]. This will be addressed in a later.

5.4.2 Etch and Fill

For etch and fill, we once again begin by depositing metal onto a substrate for the ground plane. A 5 μm passive polymer cladding layer is spin cast over the metal and heated until dry. Next, the waveguide circuit is patterned onto the cladding layer using standard IC tools and techniques. 2 μm of the cladding layer are etched using either wet or dry etch processes. The NLO polymer is spin cast onto the circuit filling the etched regions and cured by heating. A 3 μm passive polymer cladding layer is spin cast on top of the NLO polymer core layer and cured. Metal is deposited and patterned to provide electrodes over the switching regions. The device is then poled. The difference between the two techniques is that the refractive indices of the passive polymer side cladding layers cannot be controlled as precisely as the refractive indices of the photobleached NLO polymer side cladding layers. This can be important when a precise interaction length L is desired. However, the etch and fill method does eliminate a metalization, patterning and exposure step required for the photobleach method.

5.4.3 Corona Poling

A second poling method commonly used is known as corona poling [7, 8, 39-41, 45-47, 49-54]. After the spin cast films are vacuum dried and heated to 150°C, a small probe tip emitting a high electric field, typically about 5 KVDC, is positioned 2.0 cm over the heated NLO polymer. This provides the 150 VDC/ μm poling voltage. The 150°C

temperature and 5 KVDC poling voltage are maintained for 2 hours. The films are cooled to room temperature, with the electric field still applied. When the films reach room temperature, the voltage can be turned off, and the material is ready for EO device fabrication. The switching electrodes then need to be deposited and patterned. Corona poling is also attractive for material characterization because the NLO polymer can be poled over a large area. For device fabrication, however, care must be taken to deposit the NLO material only in the switching region, when using corona poling. Since a poled NLO polymer exhibits higher propagation loss than the un-poled NLO polymer [3, 4, 8, 21, 22, 36], an EO circuit fabricated using this method will exhibit higher loss if the NLO material is deposited anywhere besides the switching region.

5.5 PRACTICAL NONLINEAR OPTICAL POLYMER ELECTRO-OPTIC DEVICES

Electro-optic modulators and directional couplers using NLO polymers have been modelled, fabricated and/or analyzed extensively over the years by many researchers [4, 7, 8, 21, 22, 35, 36, 39-43, 45-70]. The EO coefficients for various NLO polymers have been measured by several researchers as well [3, 4, 21, 22, 41-43, 45-70, 135].

However, even with the excellent material characteristics that have been demonstrated, several barriers have prevented NLO polymers from progressing much further than being used for research devices. One of these barriers is poling voltage. In order to align the moieties to attain the nonlinearity of the material, one needs to pole the polymer with a high voltage. As stated earlier, the level of this poling voltage can be 1200 VDC or greater. Voltage levels of these magnitudes prevent the ease of integration of optics with electronics. Lift-off techniques are being pursued to allow for integration, but such techniques add to the fabrication cost and can defeat the simplicity claimed for NLO polymer device fabrication. An electronics company that does not utilize lift-off in their current fabrication, might be reluctant to introduce it into their process, unless there were a significant and marketable performance enhancement.

For compatibility with electronic processes, including solder baths, NLO polymers need to be able to retain their nonlinearity at high temperatures. It has been demonstrated that the higher the poling retention temperature stability, the lower the nonlinearity of the material [3, 4, 22]. However, one would like to achieve a high nonlinearity for the material; this is its most attractive characteristic. Due to high poling voltages and lower nonlinearities caused by ruggedization, one should consider using these materials in stand alone EO devices. There is no immediate requirement to monolithically integrate with electronics and/or electronic fabrication processes. This will allow for the relaxation of the high temperature stability requirement, and it will provide a polymer with a higher EO coefficient. It is the belief of this author that for the near term, it is more important to get a

competitive NLO polymer device into the market than to focus on integration with electronics.

5.5.1 Electrode Separation

Substituting the properties of the various competing materials, for example, into Eq. (89) for the zero-gap directional coupler (ZGDC) gives one a good material comparison. These are presented in Table 2. Looking at Table 2, it is clear that the NLO polymer is not being utilized to its full potential. If one could find a way to reduce the electrode separation for NLO polymer devices, the switching voltage could be reduced. For $d = 1 \mu\text{m}$, using the above parameters, $L = 1.5 \text{ mm}$ and the voltage-length is reduced to 7.5 V-mm. Thus, a ZGDC, using the NLO polymers that are currently available, has the potential of having the lowest switching voltage of any integrated optic EO device demonstrated to date. Table 3 illustrates the potential of decreasing the electrode separation. Looking at Table 3, it can be seen that the potential exists to realize extremely short devices.

Table 2. NLO Materials Comparison [4, 7, 8, 12, 32-35, 37-42, 45, 48, 50, 64, 65, 136-150].

Material	V_{π}	λ	n	r_{33}	d	$L \text{ (mm)}$	Voltage- Length
Bulk III-V Semiconductor	5 V	830 nm	3.42	1.5 pm/V	2 μm	5.6 mm	28 V-mm
LiNbO ₃	5 V	830 nm	2.2	32 pm/V	9 μm	4.4 mm	22 V-mm
MQW III-V Semiconductor	5 V	830 nm	3.42	4.7 pm/V	2 μm	1.8 mm	9 V-mm
NLO Polymer	5 V	830 nm	1.63	26 pm/V	8 μm	12 mm	60 V-mm

Table 3. NLO Polymer Comparison [35]

Tolerable Loss	V_{π}	λ	n	r_{33}	d	L (mm)	Voltage- Length
12 dB/cm	5 V	830 nm	1.63	26 pm/V	1 μm	1.5 mm	7.5 V-mm
21 dB/cm	5 V	830 nm	1.63	45 pm/V	1 μm	0.85 mm	4.3 V-mm
187 dB/cm	5 V	830 nm	1.63	400 pm/V	1 μm	96 μm	0.5 V-mm

As a first option, one could decrease the core thickness from 2 μm to 1 μm . Doing this would allow for a 1 μm reduction in the separation between electrodes. However, this would only offer a slight reduction in the switching voltage. In order to reduce the electrode separation any further, one would have to either reduce the thickness of the cladding layers or, as in our proposal, render the cladding layers conductive. Several researchers have recently increased the conductivity of the cladding layers in order to pole the core layer in the triple stack polymer device configuration to its full NLO value [4, 36, 40, 43, 48, 59, 60, 62]. This level of conductivity is not adequate enough to allow the cladding layers to act as switching electrodes. By using conductive polymers, on the other hand, such as HCl doped polyaniline, AsF_5 doped polyacetylene or doped polypyrrole, conductivities of 2×10^2 S/cm to 1×10^5 S/cm can be realized [130-134]. The conductivity of polyaniline is within a factor of 300 of copper. The conductivity of polyacetylene is within a factor of 6 of copper.

Increasing the conductivity of the cladding layers to these conductivity levels, however, increases the dielectric constant of the material. This may produce significant propagation loss [119, 120]. It has been demonstrated, at $\lambda = 632$ nm, that undoped, non-conductive polyaniline, has a dielectric constant $\epsilon = 8.47 + 1.14i$ and conductive, HCl doped polyaniline has a dielectric constant $\epsilon = 13.4 + 2.85i$ [120]. The loss incurred by rendering the cladding material highly conductive may prove too high for practical device operation. One might, therefore, consider a thin charge sheet (< 0.1 μm) of conductive polymer spin casted between the core and cladding layers. This would undoubtedly increase propagation loss, but, not, one would hope, to the levels anticipated from using conductive cladding layers. Fig. 20 is a schematic illustrating the stacked structure under consideration.

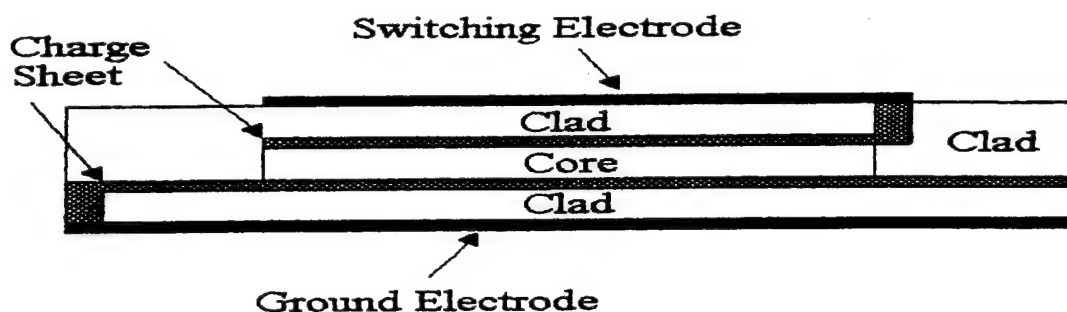


Figure 20. Schematic of Triple Stack Including Conductive Polymer Charge Sheets [35].

5.5.2 Passive Zero-Gap Directional Coupler

We will first analyze our scheme for the passive device (no voltage applied). In anticipation of the higher losses due to the conductive polymer, we would only want to use the NLO polymer for the interaction region of the switch. The input/output channels, as well as the general routing, should be fabricated using a passive polymer, such as General Electric polyetherimide (ULTEM). It has demonstrated losses of 0.24 dB/cm at $\lambda = 830$ nm [2, 23]. Limiting the NLO polymer to the interaction channel of the device only allows one to relax the current low loss requirement for NLO polymers. Fig. 21 is a schematic of the passive zero-gap directional coupler under investigation, with the active polymer making up the interaction region and a passive polymer making up the input/output channels. By using the waveguide and material parameters given in Table 2 and substituting $d = 1$ μm , the predicted optimum interaction length (L) for the passive ZGDC is only 101 μm . Fig. 22 is a BeamPROP beam propagation model representation of this device.

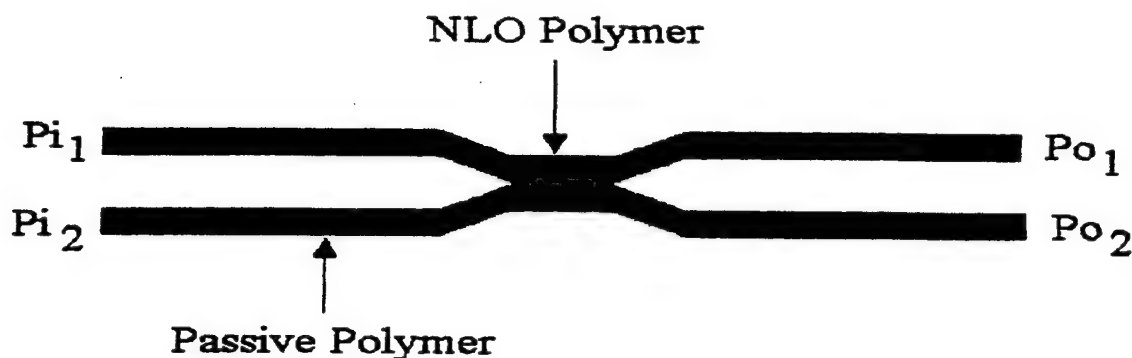


Figure 21. Schematic of a Passive Zero-Gap Directional Coupler With an NLO Polymer Interaction Region and Passive Polymer Input/Output Channels [35].

In addition, the accuracy of the width of the channels for a ZGDC is not too critical. If we can control the accuracy of the width of the interaction channel to within $0.1\ \mu\text{m}$, which is the current tolerance for standard IC fabrication tools, L will only change by $7.6\ \mu\text{m}$. We would be able to control the coupling to within 93% of complete coupling. This would prove very fabrication tolerant.

For our ZGDC, we are also assuming that we will be able to match the refractive indices of the NLO polymer and the passive polymer to within 0.01. Calculating the percentage of coupling with this amount of index tolerance predicts that we could control the coupling to within 93% of complete coupling. This, again, proves very fabrication tolerant. In order to implement this type of structure, we would have to utilize the etch and fill technique. However, with such a fabrication tolerant device, one does not require the precise refractive index control that can be achieved using photobleach. Fig. 23 is a BPM of the device behavior, including the 0.01 refractive index mismatch. Assuming 1.8 dB total loss for this device, corresponding to 1.5 dB/cm propagation loss for the conventional 12 mm long device allows one to tolerate a propagation loss of 178 dB/cm for the $101\ \mu\text{m}$ passive ZGDC.

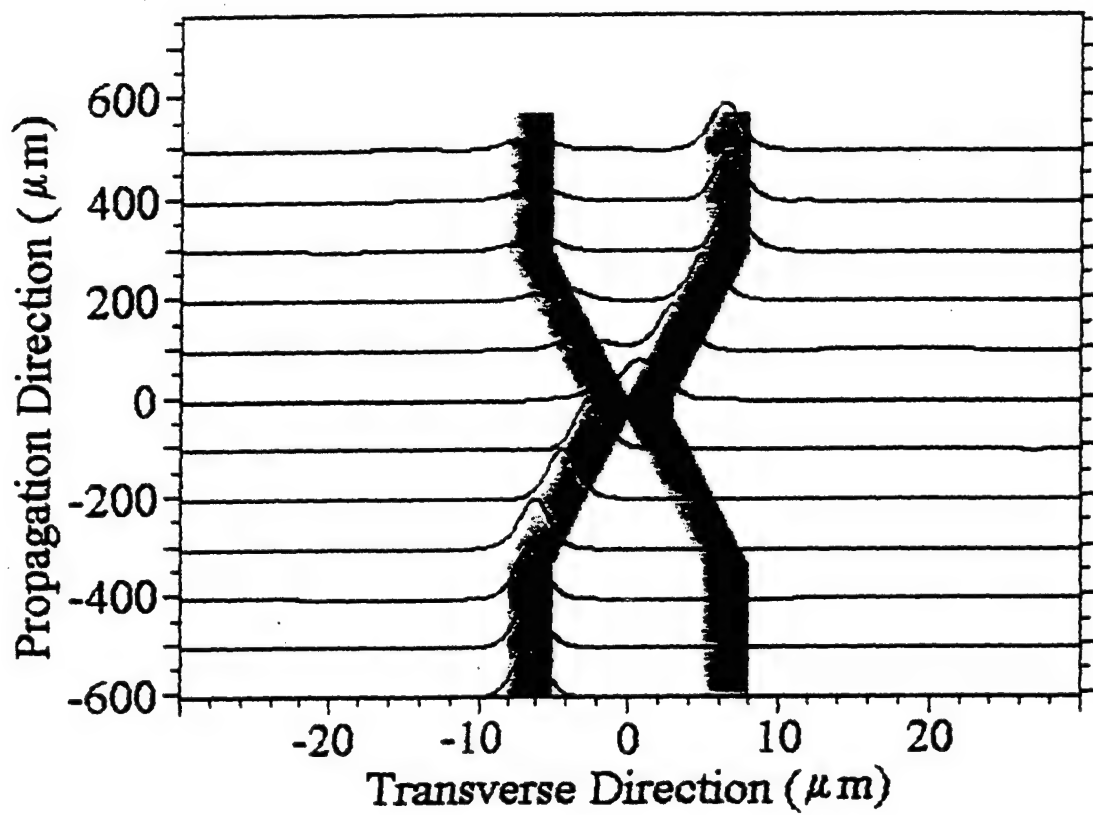


Figure 22. Beam Propagation Model of Passive Zero-Gap Directional Coupler Using NLO and Passive Polymers With Matching Indices.

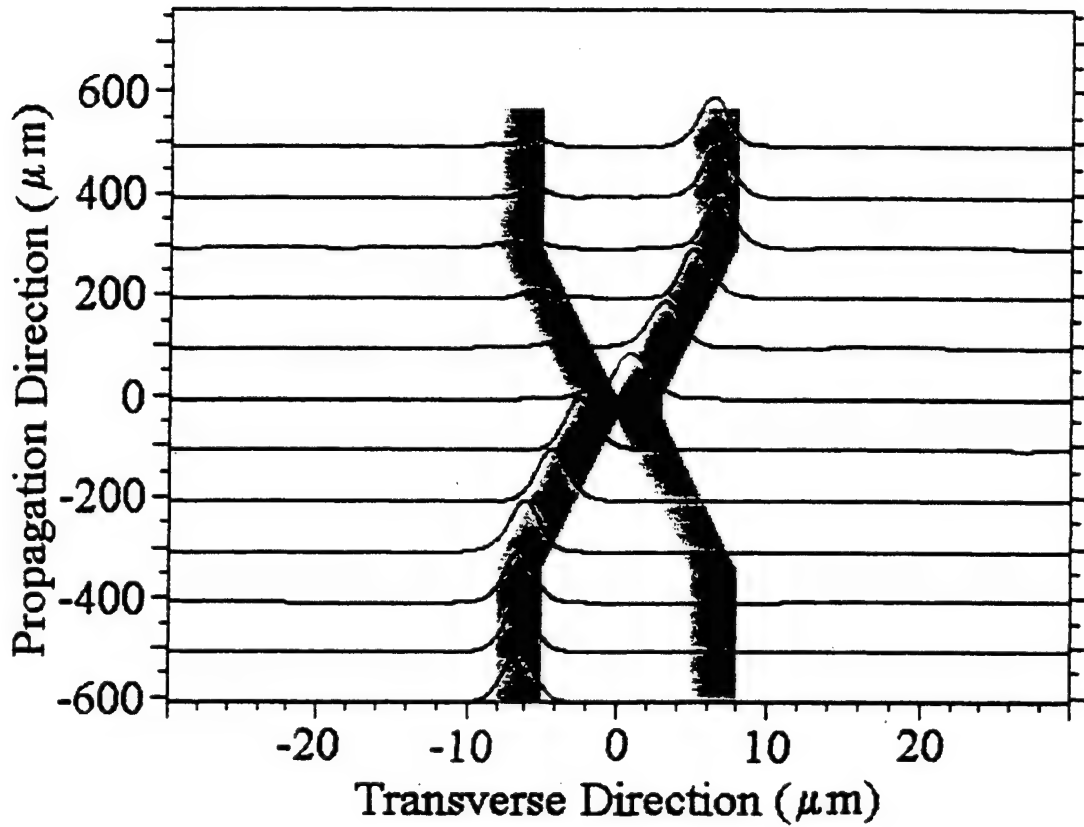


Figure 23. Beam Propagation Model of Passive Zero-Gap Directional Coupler Using NLO and Passive Polymers With 0.01 Mismatched Indices.

5.5.3 Active Zero-Gap Directional Coupler

For switching, we need to implement the active device (voltage applied). In order to keep the switching voltage to a minimum, the active ZGDC will require a longer interaction length than the passive device. The coupling will also be harder to predict, since any error in index matching or width accuracy will be multiplied by a factor determined by dividing the realized active device length by the optimum passive device length. For the active device case, when using the parameters from Table 2 along with $d = 1 \mu\text{m}$ and a 0.01 refractive index difference between the NLO and passive material, our coupling error is still very low. Fig. 24 is a BPM of the behavior of the active ZGDC with perfect index match. Fig. 25 is a BPM of the active ZGDC with 0.01 index mismatch.

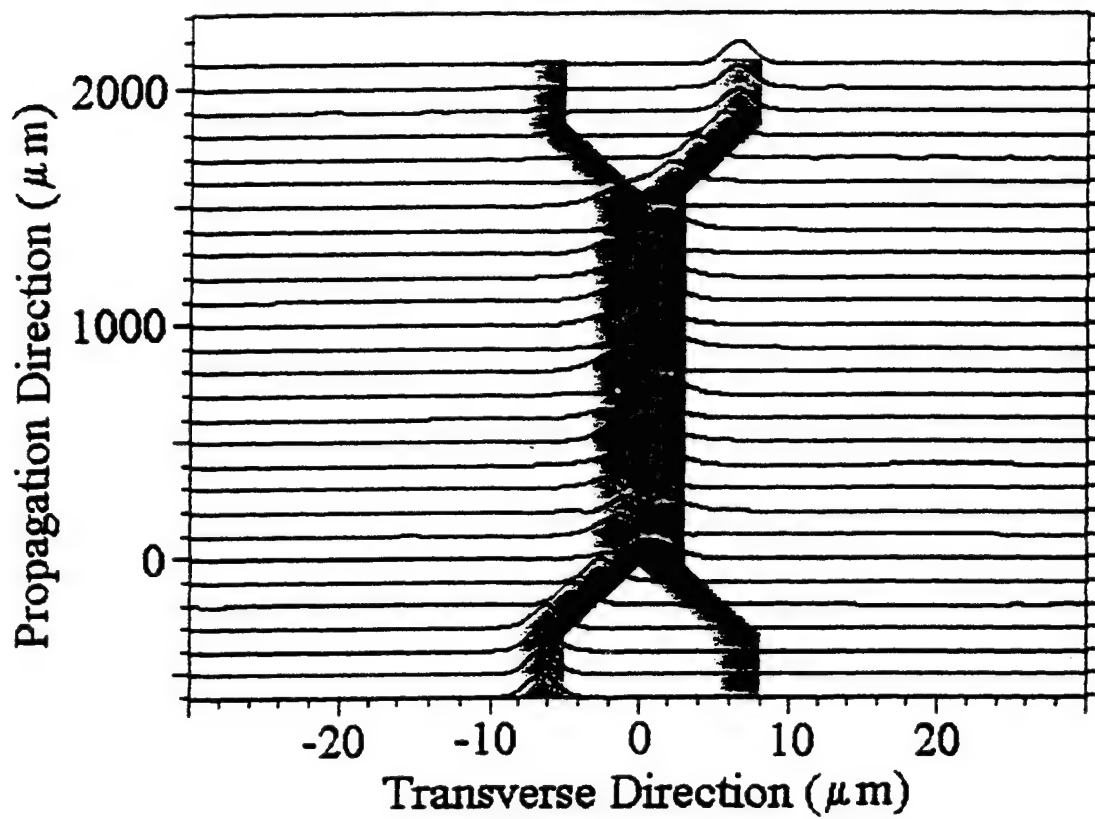


Figure 24. Beam Propagation Model of Active Zero-Gap Directional Coupler Using NLO and Passive Polymers With Matching Indices.

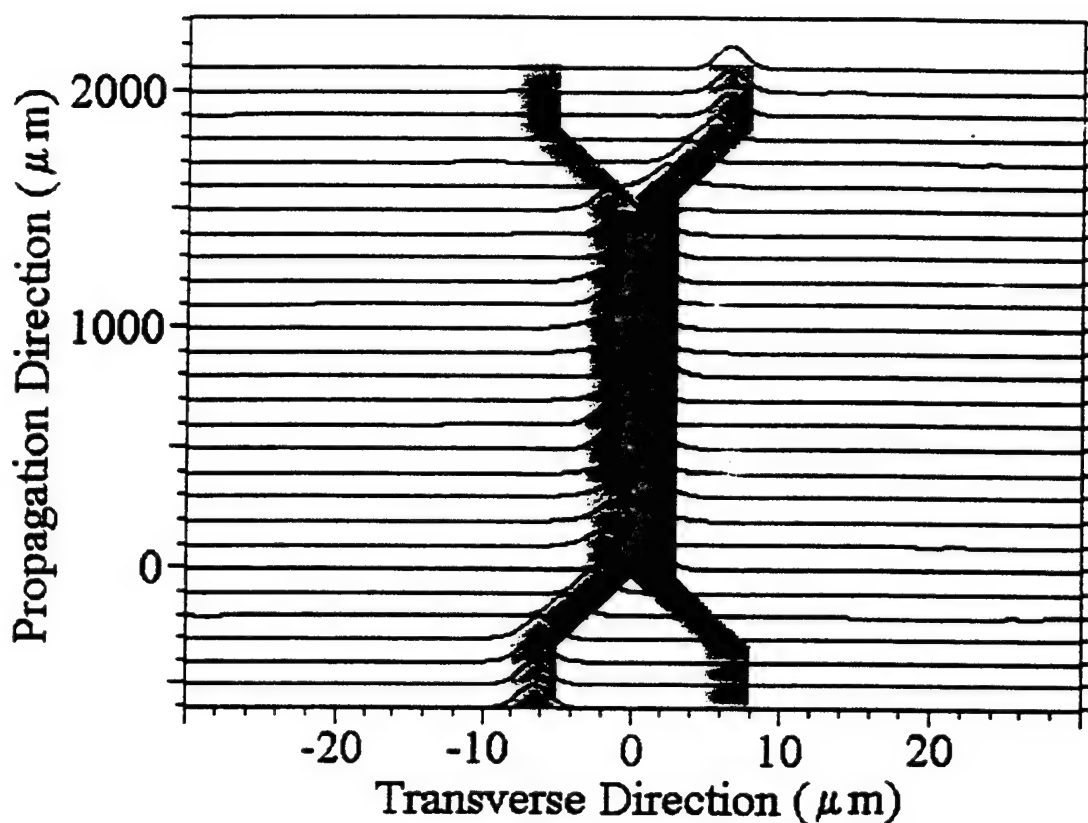


Figure 25. Beam Propagation Model of Active Zero-Gap Directional Coupler Using NLO and Passive Polymers With 0.01 Mismatched Indices.

We would anticipate the coupling to be more difficult to predict when fabricating the actual device, and we would expect the active device to be less fabrication tolerant than the passive device. However, since we will be applying a voltage for switching anyway, we should be able to simply apply a voltage to null the device in the complete coupling state. In any case, this 1.5 mm long device would have the potential for realizing 7.5 V-mm switching. This is a significant benefit, which would offset the inconvenience of having to null the device. Low loss requirements for current NLO polymers could also be relaxed for the active ZGDC. Assuming a 1.8 dB total loss for this device, the same as we did for the passive ZGDC, would allow us to tolerate a propagation loss of 12 dB/cm for the 1.5 mm active ZGDC.

Hence, this length would be short enough to conceivably build an array NLO polymer EO devices within a small chip for placement within a multichip module.

5.5.4 Nonlinear Polymer to Passive Polymer Coupling

Another important issue to be addressed is the coupling efficiency between the NLO polymer material and the passive polymer material. If we wish to use the NLO polymer for the EO device and the passive polymer for the general routing, in order to minimize propagation loss, we need to conceive better coupling techniques than the current butt coupling technique. Butt coupling two waveguides together has proven very lossy, especially between two materials of different refractive indices. It is not efficient enough for coupling the NLO material with the passive material. One possible method may involve tapering the two materials together or blending the two materials. Another may be to utilize the passive zero-gap directional coupler or to use grating couplers. In any event, in order for NLO polymer devices to become practical and competitive for computer applications, good coupling efficiency needs to be achieved.

6. CONCLUSIONS

Passive multimode polymer waveguides are modeled well by the CAD program BeamPROP. Active single-mode waveguides do not give as precise answers as a Maxwell equation based three dimensional finite element method. However, when fabrication tolerances are taken into consideration, BeamPROP is sufficiently accurate. Therefore, in a practical setting, BeamPROP adequately models the behavior of the waveguides.

Polymer waveguides have a greater loss than fiber optical waveguides. However, as the POINT program shows, the losses are low enough for backplane applications. POINT has demonstrated that multimode interconnects are ready for backplane applications at this time. Significant improvements are necessary for active single mode waveguides based on polymers to overcome the lead that lithium niobate based electro-optical modulator waveguides have at this time.

A scheme for realizing 1-2 mm long EO devices, utilizing currently available non-linear optic polymers, was introduced. It offers the potential to achieve the lowest switching voltage of any integrated optic EO device of that length demonstrated to date. The major factors are the propagation loss dependance, using the conductive polymer cladding, and the coupling efficiency between the NLO polymer and passive polymer. If losses are not excessive, these devices have excellent potential for success. If future EO coefficients can then be pushed higher, which would relax the current low loss constraint and the current high temperature stability constraint even further, there exists the potential for 100 μm long active EO devices operating at TTL voltage levels (see Table 3). This would also be a fabrication tolerant device that would not require a nulling voltage. There are undoubtedly other possible methods for reducing the electrode separation, but the ultimate goal should be to reduce that separation. This is the only way to produce practical and competitive electro-optic devices using available non-linear optic polymers.

7. REFERENCES

1. Edwards, T.C., 1985. Foundations for Microstrip Circuit Design. John Wiley and Sons, New York, NY.
2. Bristow, J., 1992-1996. Private Conversations. Honeywell, Inc., Bloomington, MN.
3. Lipscomb, G.F., 1991-1996. Private Conversations. AKZO Electronic Products, Redwood City, CA.
4. Ermer, S., 1992-1996. Private Conversations. Lockheed/Martin Missiles and Space Company, Palo Alto, CA.
5. Liu, Y., Bristow, J., Marta, T., Bounnak, S., Johnson, K., Liu, Y. and Cole, H., 1995. Polymer Waveguide Applications in Multichip Modules (MCMs) and Board Level Optical Interconnects. Organic Thin Films For Photonics Applications. OSA Technical Digest Series, 21, 14.
6. Yardley J.T., Elada, L., Stengel, K.M.T., Shacklette, L.W., Wu, C. and Xu, C., 1995. Toward the Practical Application of Polymeric Optical Interconnection Technology. Organic Thin Films For Photonics Applications. OSA Technical Digest Series, 21, 6.
7. Soni, S., 1995-1996. Private Conversations. AdTech Systems Research, Beavercreek, OH.
8. Chen, R.T., 1992-1996. Private Conversations. University of Texas at Austin, Austin, TX.
9. Husain, A., 1992-1996. Private Conversations. Defense Advanced Research Projects Agency, Arlington, VA.

10. Karim, M.A., 1990-1996. Private Conversations. Center for Electro-Optics, University of Dayton, Dayton, OH.
11. Brandelik, J., 1990-1996. Private Conversations. Electro-Optic Components Branch, Avionics Directorate, Wright-Patterson Air Force Base, OH.
12. Zucker, J., 1995. OSA Annual Meeting, Portland, OR (unpublished).
13. Goodman, J.W., Leonberger, F.I., Kung, S-Y and Athale R.A., 1984. Optical Interconnections for VLSI Systems. Proceedings of the IEEE, Vol. 72, 850.
14. Sullivan, C.T., 1990. III-V Optical Waveguide Technology. United States Air Force Technical Report, WRDC-TR-90-5027, Wright-Patterson Air Force Base, OH.
15. Yariv, A. and Yeh, P., 1984. Optical Waves in Crystals. John Wiley and Sons, New York, NY.
16. Hunsperger, R.G., 1985. Integrated Optics: Theory and Technology, Second edition. Springer-Verlag, New York, NY.
17. Hutcheson, L.D., ed., 1987. Integrated Optical Circuits and Components: Design and Applications. Marcel Dekker, New York, NY.
18. Tamir, T., ed., 1985. Topics in Applied Physics Volume 7: Integrated Optics, Second edition. Springer-Verlag, New York, NY.
19. Martellucci, S. and Chester, A.N., eds., 1983. Integrated Optics: Physics and Applications. Plenum Press, New York, NY.

20. Taylor, G.W., 1992. Three Terminal Opto-Electronic Array. United States Air Force Technical Report, WL-TR-91-5008, Wright-Patterson Air Force Base, OH.
21. Lipscomb, G.F., 1993. Integrated Optical Organic Devices. United States Air Force Technical Report, WL-TR-93-5007, Wright-Patterson Air Force Base, OH.
22. Van Eck, T.E., 1992-1996. Private Conversations. Lockheed Missiles and Space Company, Palo Alto, CA.
23. Sullivan, C., 1990-1995. Private Conversations. Honeywell, Inc., Bloomington, MN.
24. Marcuse, D., 1982. Light Transmission Optics, Second edition. Van Nostrand Reinhold, New York, NY.
25. Nishihara, H., Haruna, M. and Suhara, T., 1985. Optical Integrated Circuits. McGraw-Hill, New York, NY.
26. Young, M., 1992. Optics and Lasers: Including Fibers and Optical Waveguides, Fourth edition. Springer-Verlag, New York, NY.
27. Yariv, A., 1975. Quantum Electronics, Second edition. John Wiley & Sons, New York, NY.
28. Yariv, A., 1985. Optical Electronics, Third edition. Holt, Rinehart and Winston, New York, NY.
29. Karim, M.A., 1992. Electro-Optical Devices and Systems. PWS-Kent Publishing, Boston, MA.
30. Karim, M.A. and Awwal, A.A.S., 1992. Optical Computing: An Introduction. John Wiley & Sons, New York, NY.

31. Hibbs-Brenner, M., 1991-1996. Private Conversations. Honeywell, Inc., Bloomington, MN.
32. Grote, J.G., 1994. Digital Logic and Reconfigurable Interconnects Using Aluminum Gallium Arsenide Electro-Optic Fredkin Gates. PhD Dissertation. University of Dayton, Dayton, OH.
33. Grote, J.G. and Karim, M.A., 1995. Practical Considerations for Fabrication of Active $\text{Al}_x\text{Ga}_{1-x}\text{As}$ Zero-Gap Directional Couplers. SPIE Proceedings-Optoelectronic Interconnects III, 2400, 146.
34. Grote, J.G., 1995. $\text{Al}_x\text{Ga}_{1-x}\text{As}$ Zero-Gap Directional Couplers. 1995. OSA Annual Meeting, Portland, OR (unpublished).
35. Grote, J.G., 1996. Polymer Integrated Optic Zero-Gap Directional Coupler. Materials Research Society Symposium Proceedings on Electrical, Optical and Magnetic Properties of Organic Solid State Materials III, Vol. 413, 231.
36. Van Eck, T.E., 1996. Optical Interconnect Technology-Intra Multichip Module. United States Air Force Technical Report, WL-TR-96-1040, Wright-Patterson Air Force Base, OH.
37. Grote, J.G. and Karim, M.A., 1996. Optical Digital Logic Using $\text{Al}_x\text{Ga}_{1-x}\text{As}$ Zero-Gap Directional Couplers. JSAP/ICO/IEICE Proceedings from the International Topical Meeting on Optical Computing, Vol. 1, 144.
38. Grote, J.G., 1996. Optical Interconnects for Computer Applications. Tri-Service Photonics Coordinating Committee Proceedings from the DoD Photonics Conference, 253.

39. Dalton, L.R., 1994-1996. Private Conversations. University of Southern California, Pasadena, CA.
40. Ashley, P.R., 1992-1996. Private Conversations. U.S. Army Missile Command, Redstone Arsenal, AL.
41. Jen, A., Rao, V., Chen, T., Cai, Y., Drost, K., Liu, Y., Kenney, J., Mininni, R., Bedworth, P., Marder, S. and Dalton, L., 1995. High Performance Chromophores and Polymers for E-O Applications. Organic Thin Films for Photonics Applications. OSA Technical Digest Series, 21, 251.
42. Ermer, S., Anderson, W., Van Eck, T., Girton, D., Marley, J., Harwit, A., Lovejoy, S., and Leung, D., 1995. Progress Toward Practical Polymer Electro-Optic Devices. Organic Thin Films for Photonics Applications. OSA Technical Digest Series, 21, 285.
43. Ashley, P. and Sornsin, E., 1992. Doped Optical Claddings for Waveguide Devices With Electrooptical Polymers. IEEE Photonics Technology Letters, 4, No. 9, 1026.
44. Kagami, M. Hasegawa, K. and Ito, H., 1995. Fabrication of Out-of-Plane Branching Mirrors on Polymer Channel Waveguide. Organic Thin Films For Photonics Applications. OSA Technical Digest Series, 21, 148.
45. Steier, W.H., 1995. Electro-optic Polymer Waveguide Devices - Materials Fabrication and Applications. Organic Thin Films For Photonics Applications. OSA Technical Digest Series, 21, 284.
46. Wang, W., Chen, D., Fetterman, H.R., Shi, Y., Bechtel, H., Kalluri, S., Steier, H.R. and Dalton, L.R., 1995. 60 GHz Electro-optic Modulation by Polymer Waveguide Phase Modulators. Organic Thin Films For Photonics Applications. OSA Technical Digest Series, 21, 293.

47. Kalluri, S., Chen, A., Ziari, M., Steier, W.H., Liang, Z., Dalton, L.R., Chen, D., Jalali, B. and Fetterman, H.R., 1995. Vertical Integration of Polymer Electro-Optic Devices on Electronic Circuits. *Organic Thin Films For Photonics Applications*. OSA Technical Digest Series, 21, 317.
48. Girton, D.G., Anderson, W.W., Marley, J.A., Van Eck, T.E. and Ermer, S., 1995. Current Flow in Doped and Undoped Electro-Optic Polymer Films During Poling. *Organic Thin Films For Photonics Applications*. OSA Technical Digest Series, 21, 470.
49. Steier, W.H., Kalluri, S., Chen, A., Garner, S., Chuyanov, V., Ziari, M., Shi, Y., Fetterman, H., Jalali, B., Wang, W., Chen, D. and Dalton, L.R., 1996. Applications for Electro-optic Polymers in Photonics. *Materials Research Society Symposium Proceedings on Electrical, Optical and Magnetic Properties of Organic Solid State Materials III*, Vol. 413, 147.
50. Kenney, J.T., Nurse, J.C., Chon, J.C., Binkley, E.S., Stiller, M., Ball, D.W. and Jen, A.K-Y., 1996. NLO Polymer Material Systems for Electro-Optic Devices. *Materials Research Society Symposium Proceedings on Electrical, Optical and Magnetic Properties of Organic Solid State Materials III*, Vol. 413, 159.
51. Lytel, R., 1990. Applications of Electro-optic Polymers to Integrated Optics. *SPIE Proceedings on Nonlinear Optical Materials and Devices for Photonic Switching*, Vol. 1216, 31.
52. Lytel, R., Lipscomb, G.F., Binkley, E.S., Kenney, J.T. and Ticknor, A.J., 1990. Electro-optic Polymers for Optical Interconnects. *SPIE Proceedings on Digital Optical Computing*, Vol. 1215, 252.

53. Chen, R.T., 1990. Optical Interconnects: A Solution to Very High Speed Integrated Circuits and Systems. SPIE Proceedings, Vol. 1374, 20.
54. Chen, R.T., 1993. Polymer Based Photonic Integrated Circuits. Optics and Laser Technology, Vol. 25, No. 6, 347.
55. Girton, D.G., Ermer, S., Valley, J.F., Van Eck, T.E., Lovejoy, S., Leung, D. and Marley, J.A., 1994. Poling Considerations for DCM-Polyimide Systems Used in Electro-Optic Devices. ASC/OSA Proceedings on Polymeric Thin Films for Photonic Applications.
56. Ashley, P.R. and Tumolillo Jr., T.A., 1991. New Poling Techniques for Electro-Optic Polymer Devices. IEEE/OSA Proceedings on Integrated Photonics Research, Vol. 8, 87.
57. Tumolillo Jr., T.A. and Ashley, P.R., 1991. Fabrication Techniques of Photopolymer Clad Waveguides for Nonlinear Polymeric Modulators. SPIE Proceedings on Photopolymer Device Physics, Chemistry and Applications II, Vol. 1559, 65.
58. Ashley, P.R. and Tumolillo Jr., T.A., 1990. Single-Mode Nonlinear Channel Waveguides Using Photopolymer Cladding Technique. IEEE/OSA Proceedings on Integrated Photonics Research, Vol. 5, MF4.
59. Ashley, P.R. and Sornsin, E.A., 1992. Doped Optical Claddings for Electro-Optical Polymer Waveguide Devices. IEEE/OSA Proceedings on Integrated Photonics Research, Vol. 10, 246.
60. Tumolillo Jr., T.A. and Ashley, P.R., 1992. A Novel Pulse-Poling Technique for EO Polymer Waveguide Devices Using Device Electrode Poling. IEEE Photonics Technology Letters, Vol. 4, No. 2, 142.

61. Ashley, P.R. and Tumolillo Jr., T.A., 1991. Overview of EO Polymers for Guided Wave Devices. SPIE Proceedings on Integrated Optical Circuits, Vol. 1583, 316.
62. Ashley, P.R. and Tumolillo Jr., T.A., 1991. Channel Waveguides in Electro-Optic Polymers Using a Photopolymer Cladding Technique. Applied Physics Letters, Vol. 58, No. 9, 884.
63. Kaczmariski, P., Van de Capalle, J.-P., Lagasse, P.E. and Meynart, R., 1989. Design of an Integrated Electro-Optic Switch in Organic Polymers. IEEE Proceedings, Vol. 136, Pt. J, No. 3, 152.
64. Lee, C.Y-C., 1992-1996. Private Conversations. Air Force Office of Scientific Research, Bolling Air Force Base, D.C.
65. Prasad, P.N., 1987. Organic Nonlinear Optics. Tutorial Short Course. Department of Chemistry, State University of New York at Buffalo, Buffalo, NY.
66. Williams, D.J., ed., 1983. Nonlinear Optical Properties of Organic Polymeric Materials. American Chemical Society.
67. Garito, A.F. and Singer, K.D., 1982. Organic Crystals and Polymers-A New Class of Nonlinear Optical Materials. Laser Focus, Vol. Feb., 59.
68. Prasad, P.N. and Ulrich, D.R., eds., 1988. Optical Nonlinearities in Organic Materials: Fundamentals and Device Applications. Plenum Press, New York, NY.
69. Lipscomb, G.F., Garito, A.F. and Narang, R.S., 1981. An Exceptionally Large Linear Electro-Optic Effect in the Organic Solid MNA. Journal of Chemical Physics, Vol. 75, 1509.

70. Sigelle, M. and Hierle, R., 1981. Determination of the Electrooptic Coefficients of 3-methyl 4-nitropyridine 1-oxide by an Interferometric Phase-Modulation Technique. *Journal of Applied Physics*, Vol. 52, 4199.

71. Liu, Y. S., Cole, H. S., Bristow, J. and Liu, Yue, "Hybrid integration of electrical and optical interconnects," in *Optical interconnect II*, ed. by Chen, R., Proc. SPIE, 1993. Also, Bristow, J., Sullivan, C., Mukherjee, S., Liu, Yue and Husain, A., "Progress and status of guided wave optical interconnect technology," in *Optical Interconnects*, ed. by Chen, R., vol. 184, Proc. SPIE, pp. 4-10, 1993.

72. Wong, Y.M., Muehlner, D.J., Faudskar, C.C., M. Fishteyn, Gates, J.V., Anthony, R.J., Cyr, G.J., Choi, J., Crow, J.D., Kuchta, D.M., Pepeljugoski, P.K., Stawiasz, K., Nation, W., Engebressen, D., Whitlock, B., Morgan, R.A., Hibbs-Brenner, M.K., Lehman, L., Walterson, R., Kalweit, E., and Marta, T, "Technology development of a high density 32-channel 16 Gbps optical data link for optical interconnect applications for the optoelectronic technology Consortium (OETC)," *Proc. of ECTC'96*, p. 269, 1996.

73. Hahn, K.H., Giboney, K., Wilson, R., Strazicky, J., Wong, E., Tan, M., Kaneshiro, R., Dolfi, D., Mueller, E., Plotts, A., Murray, D., Marchegiano, J., Booth, B. Sano, B., Madhaven, B., Raghavan, V., and Levy, A., "Gigabytes/sec data communications with the POLO parallel optical link," *Proc. of ECTC'96*, p. 301, 1996.

74. Crow, J., Choi, J., Cohen, M., Johnson, G., Kuchta, D., Lacey, D., Ponnappalli, S., Pepeljugoski, P., Stawiasz, K., Trewhella, J., Xiao, P., Tremblay, S., Quimet, S., Lacerte, A., Gauvin, R. Booth, W. Nation, T. Smith, B. DeBaun, G. Henson, S. Igl, N. Lee, A. Piekarczyk, A., Kuczma, A., Spanoudis, S., "The Jitney parallel optical interconnect," *Proc. of ECTC'96*, p.292, 1996.

75. Scarinozzino, R. and Osgood, Jr., R.M., J. Opt. Soc. Amer. A, 8, 724 (1991).
76. Hadley, G.R., J. Quantum Electron., 28, 363 (1992)
77. Hadley, G.R., Optics Letters, 17, 1743 (1992)
78. W.P. Huang , W.P. and Xu, C.L., J. Quantum Electron., 29, 2639 (1993)
79. Xu , C.L., *et al.*, J. Lightwave Tech., 12, 1926 (1994)] and related references
80. Liu, Yung, Ghezzi, Mario, Nielsen, Matthew, "Polymer Optical Interconnect Technology POINT, Volume 1," Final Report for contract F33615-94-C-1530, technical report number AFRL-SN-WP-TR-1999-XXXX.
81. Crespo, Antonio; Air Force Research Laboratory, AFRL/SNDI, Wright-Patterson AFB, OH 45433-7322. This work is part of Mr. Crespo's Ph.D dissertation effort.
82. Nye, J.F., 1985. Physical Properties of Crystals, Second edition. Oxford University Press, New York, NY.
83. Kraus, J.D. and Carver, K.R., 1973. Electromagnetics, Second edition. McGraw Hill, New York, NY.

84. Weidner, R.T. and Sells, R.T., 1975. Elementary Physics: Classical and Modern. Allyn and Bacon, Boston, MA.
85. Namba, S., 1961. Electro-Optical Effect of Zincblende. Journal of the Optical Society of America, Vol. 51, 76.
86. Lee, D.L., 1986. Electromagnetic Principles of Integrated Optics. John Wiley and Sons, New York, NY.
87. Robertson, M.J., Ritchie, S. and Dayan, P., 1985. Semiconductor Waveguides: Analysis of Optical Propagation in Single Rib Structures and Directional Couplers. IEE Proceedings, Vol. 132, Pt. J, 336.
88. Marcatili, E.A.J., 1969. Dielectric Rectangular Waveguide and Directional Coupler for Integrated Optics. Bell System Technical Journal, Vol. 48, 2071.
89. Marcuse, D., 1974. Theory of Dielectric Optical Waveguides. Academic Press, New York, NY.
90. Born, M. and Wolf, E., 1986. Principles of Optics, Sixth edition. Pergamon Press, New York, NY.
91. Forber, R.A., and Marom, E., 1986. Symmetric Directional Coupler Switches. IEEE Journal of Quantum Electronics, Vol. QE-22, 911.
92. Papuchon, M. and Roy, Am., 1977. Electrically Active Optical Bifurcation: BOA. Applied Physics Letters, Vol. 31, 266.
93. Goel, K. and Chang, W.S.C., 1987. Extinction Ratio Degradation Due to Asymmetry in Zero-Gap Directional Coupling and Crossing Channel Switches. IEEE Journal of Quantum Electronics, Vol. QE-23, 2216.

94. Rottmann, F., Neyer, A., Mevenkamp, W. and Voges, E., 1988. Integrated-Optic Wavelength Multiplexers on Lithium Niobate Based on Two-Mode Interference. *Journal of Lightwave Technology*, Vol. 6, 946.
95. De Bernardi, C., Morasca, S., Rigo, C., Sordo, B., Stano, A., Croston, I.R. and Young, T.P., 1989. Two Mode Interference Wavelength Demultiplexer Monolithically Integrated on InP, For 1.5 or 1.3 μm Operation. *SPIE Journal of the 5th European Conference on Integrated Optics: ECIO '89*, Vol. 1141, 238.
96. Goel, K. and Chang, W.S.C., 1987. Effect of Asymmetry on Extinction Coefficient of Crossing Channel LiNbO_3 Waveguide Switches. *SPIE Journal on Integrated Optical Circuit Engineering V*, Vol. 835, 118.
97. Goel, K. and Chang, W.S.C., 1989. Design Considerations for Crossing Channel Switches. *IEEE Journal of Quantum Electronics*, Vol. QE-25, 47.
98. Goel, K., Wooten, E. and Chang, W.S.C., 1988. Design Considerations for Low Switching Voltage Crossing Channel Switches. *Journal of Lightwave Technology*, Vol. 6, 881.
99. Forber, R.A. and Marom, E., 1985. Optimization of Symmetric Zero-Gap Directional Couplers for Large Switch-Array Applications. *Conference of Lasers and Electro-Optics Technology Digest*, 288.
100. Goell, J.E., 1969. A Circular-Harmonic Computer Analysis of Rectangular Dielectric Waveguides. *Bell System Technical Journal*, Vol. 48, 2133.
101. Marcuse, D., ed., 1973. *Integrated Optics*. IEEE Press, New York, NY.

102. Burns, W.K. and Milton, A.F., 1975. Mode Conversion in Planar-Dielectric Separating Waveguides. *IEEE Journal of Quantum Electronics*, Vol. QE-11, 32.
103. Fleck, J.A., Morris, J.R. and Feit, M.D., 1976. Time-Dependent Propagation of High Energy Laser Beams Through the Atmosphere. *Applied Physics*, Vol. 10, 129.
104. Feit, M.D. and Fleck, J.A., 1978. Light Propagation in Graded-Index Optical Fibers. *Applied Optics*, Vol. 17, 3990.
105. Feit, M.D. and Fleck, J.A., 1979. Calculation of Dispersion in Graded-Index Multimode Fibers by a Propagating-Beam Method. *Applied Optics*, Vol. 18, 2843.
106. Feit, M.D. and Fleck, J.A., 1980. Computation of Mode Properties in Optical Fiber Waveguides by a Propagating Beam Method. *Applied Optics*, Vol. 19, 1154.
107. Feit, M.D. and Fleck, J.A., 1980. Computation of Mode Eigenfunctions in Graded-Index Optical Fibers by the Propagating Beam Method. *Applied Optics*, Vol. 19, 2240.
108. Fleck Jr., J.A. and Feit, M.D., 1980. Mode Properties and Dispersion for Two Optical Fiber Profiles by the Propagating Beam Method. *Applied Optics*, Vol. 19, 3140.
109. Van Roey, J., van der Donk, J. and Lagasse, P.E., 1981. Beam-Propagation Method: Analysis and Assessment. *Journal of the Optical Society of America*, Vol. 71, 803.
110. Fleck Jr., J.A. and Feit, M.D., 1983. Beam Propagation in Uniaxial Anisotropic Media. *Journal of the Optical Society of America*, Vol. 73, 920.
111. Mabaya, N., Lagasse, P.E. and Vandebulcke, P., 1981. Finite Element Analysis of Optical Waveguides. *IEEE Transactions*, Vol. MTT-29, 600.

112. Rahman, B.M.A. and Davies, J.B., 1984. Finite-Element Solution of Integrated Optical Waveguides. *Journal of Lightwave Technology*, Vol. LT-2, 682.
113. Rahman, B.M.A. and Davies, J.B., 1985. Vector-H Finite Element Solution of GaAs/GaAlAs Rib Waveguides. *IEE Proceedings*, Vol. 132, Pt. J, 349.
114. Chiang, K.S., 1986. Dual Effective-Index Method for the Analysis of Rectangular Dielectric Waveguides. *Applied Optics*, Vol. 25, 2169.
115. Kendall, P.C., Adams, M.J., Ritchie, S. and Robertson, M.J., 1987. Theory for Calculating Approximate Values for the Propagation Constants of an Optical Rib Waveguide by Weighting the Refractive Indices. *IEE Proceedings*, Vol. 134, Pt. A, 699.
116. Van Der Tol, J.J.G.M. and Baken, N.H.G., 1988. Correction to Effective Index Method for Rectangular Dielectric Waveguides. *Electronics Letters*, Vol. 24, 207.
117. Gribble, J.J. and Arnold, J.M., 1988. Beam Propagation Method and Geometrical Optics. *IEE Proceedings*, Vol. 135, Pt. J, 343.
118. Marcatili, E.A.J. and Hardy, A.A., 1988. The Azimuthal Effective-Index Method. *IEEE Journal of Quantum Electronics*, Vol. 24, 766.
119. Taylor, H.F. and Yariv, A., 1974. Guided Wave Optics. *Proceedings of the IEEE*, Vol. 62, 1044.
120. Hardy, A. and Streifer, W., 1985. Coupled Mode Theory of Parallel Waveguides. *Journal of Lightwave Technology*, Vol. LT-3, 1135.
121. Marcatili, E.A.J., 1986. Improved Coupled-Mode Equations for Dielectric Guides. *IEEE Journal of Quantum Electronics*, Vol. QE-22, 988.

122. Haus, H.A., Huang, W.P., Kawakami, S. and Whitaker, N.A., 1987. Coupled-Mode Theory of Optical Waveguides. *Journal of Lightwave Technology*, Vol. LT-5, 16.
123. Neyer, A., Mevenkamp, W., Thylen, L. and Lagerström, B., 1985. A Beam Propagation Method Analysis of Active and Passive Waveguide Crossings. *Journal of Lightwave Technology*, Vol. LT-3, 635.
124. Boyd, J.T., 1991. *Integrated Optics Devices and Applications*, IEEE Press, New York, NY.
125. Working Group I, COST-216, 1989. Comparison of Different Modeling Techniques for Longitudinally Invariant Integrated Optical Waveguides. *IEE Proceedings*, Vol. 136, Pt. J, 273.
126. Goodman, J.W., 1968. *Introduction to Fourier Optics*. McGraw-Hill, New York, NY.
127. Research Software, 13 Lancaster Ave., Montrose, NY. BeamPROP, Beam Propagation CAD Software.
128. Minford, W.J., Korotky, S.K. and Alferness, R.C., 1982. Low-Loss Ti:LiNbO₃ Waveguide Bends at $\lambda = 1.3 \mu\text{m}$. *IEEE Journal of Quantum Electronics*, Vol. QE-18, 1802.
129. Ghatak, A.K., Thyagarajan, K. and Shenoy, M.R., 1987. Numerical Analysis of Planar Optical Waveguides Using Matrix Approach. *Journal of Lightwave Technology*, Vol. LT-5, 660.
130. Aldissi, M., 1995. *Inherently Conductive Polymers and Engineering Technology*. Advanced Polymer Courses, Winvoski, VT.

131. Foster, M., 1995. Private Conversations. Physical Optics Corporation, Torrance, CA.
132. Passiniemi, P., Laakso, J., Ruuhonen, H. and Väkiparta, K., 1996. Electrically Conducting Polymer Blends Based on Polyaniline. Materials Research Society Symposium Proceedings on Electrical, Optical and Magnetic Properties of Organic Solid State Materials III, Vol. 413, 577.
133. Aleshin, A.N., Mironkov, N.B., Suvorov, A.V., Conklin, J.A., Su, T.M. and Kaner, R.B., 1996. Electrical Properties of Ion Implanted and Chemically Doped Polyaniline Films. Materials Research Society Symposium Proceedings on Electrical, Optical and Magnetic Properties of Organic Solid State Materials III, Vol. 413, 609.
134. Cameron, D.A. and Reynolds, J.R., 1996. Conducting Molecular Composites of Polypyrrole with Electroactive Polymeric Dopant Ions. ACS Proceedings, Vol. 37, No. 1, 684.
135. Ghebremichael, F. and Lackritz, H.S., 1995. Electro-optic and Second Harmonic Generation Studies of Dye-Doped Polymers. Organic Thin Films For Photonics Applications. OSA Technical Digest Series, 21, 458.
136. Properties of Gallium Arsenide, Second edition, 1990. INSPEC, New York, NY.
137. Adachi, S. and Oe, K., 1984. Linear Electro-Optic Effects in Zincblende-Type Semiconductors: Key Properties of InGaAsP Relevant to Device Design. Journal of Applied Physics, Vol. 56, 74.
138. Suzuki, N. and Tada, K., 1984. Elastooptic and Electrooptic Properties of GaAs. Japanese Journal of Applied Optics, Vol. 23, 1011.

139. Hernández-Cabrera, A., Tejedor, C. and Meseguer, F., 1985. Linear Electro-Optic Effects in Zinc Blende Semiconductors. *Journal of Applied Physics*, Vol. 58, 4666.
140. Turner, E.H. and Kaminow, I.P., 1963. Electro-Optic Effect in GaAs. *Journal of the Optical Society of America*, Vol. 53, 523.
141. Ho, L. and Buhrer, C.F., 1963. Electro-Optic Effect of Gallium Arsenide. *Applied Optics*, Vol. 2, 647.
142. Sugie, M. and Tada, K., 1976. Measurements of the Linear Electrooptic Coefficients and Analysis of the Nonlinear Susceptibilities in Cubic GaAs and Hexagonal CdS. *Japanese Journal of Applied Physics*, Vol. 15, 421.
143. Shaldin, Yu.V. and Belogurov, D.A., 1976. Determination of Nonlinear (Quadratic) Optical Susceptibility of GaAs and GaP From Electro-Optic Measurements. *Soviet Journal of Quantum Electronics*, Vol. 6, 897.
144. Bagdavadze, V.N. and Berozashvili, Yu.N., 1978. Electrooptic Effect in Noncentrosymmetric Cubic Semiconductor Crystals With Allowance for Spatial Dispersion. *Soviet Physics-Semiconductors*, Vol. 12, 1115.
145. Kaminow, I.P., 1968. Measurements of the Electrooptic Effect in CdS, ZnTe and GaAs at 10.6 Microns. *IEEE Journal of Quantum Electronics*, Vol. QE-4, 23.
146. Bell, M.I., 1972. Electro-Optic Coefficients of Cubic Semiconductors. 11 *International Conference on the Physics of Semiconductors-Proceedings*, Vol. 2, 845.
147. Pressley, R.J., ed., 1971. *Handbook of Lasers With Selected Data on Optical Technology*. CRC Press, Cleveland, OH.

148. Kumar, A. and Sharma, T.P., 1979. Non-Linear Susceptibility of GaAs. *Indian Journal of Pure Applied Physics*, Vol. 17, 110.
149. Varshney, S.C. and Gundjian, A.A., 1981. First-Order Raman Coefficient as Related to Elasto-Optic, Linear Electro-Optic, and Second-Harmonic-Generation Coefficients in Zinc-Blende Crystals. *Journal of Applied Physics*, Vol. 52, 6301.
150. Adachi, S., 1992. *Physical Properties of III-V Semiconductor Compounds: InP, InAs, GaAs, GaP, InGaAs, and InGaAsP*. John Wiley and Sons, New York, NY.
151. Fisher, R.A., ed., 1983. *Optical Phase Conjugation*. Academic Press, New York, NY.
152. Tsai, C.S., Kim, B. and El-Akkari, F.R., 1978. Optical Channel Waveguide Switch and Coupler Using Total Internal Reflection. *IEEE Journal of Quantum Electronics*, Vol. QE-14, 513.
153. Golshan, R. and Bedi, J.S., 1989. Reversible Nonlinear Interface Optical Computing. *Optical Engineering*, Vol. 28, 683.
154. Schienle, M., Stoll, L., Schulte-Roth, G., Muller-Nawrath, R., Mahlein, H.F., Marz, R. and Cremer, C., 1989. GaInAsP/InP Zero-Gap Directional Couplers as Compact Optical WDM Filters. *Electronics Letters*, Vol. 25, 1180.
155. Betts, G.E. and Chang, W.S.C., 1986. Crossing-Channel Waveguide Electrooptic Modulators. *IEEE Journal of Quantum Electronics*, Vol. QE-22, 1027.
156. Neyer, A., 1983. Electro-Optic X-Switch Using Single-Mode Ti:LiNbO₃ Channel Waveguides. *Electronics Letters*, Vol. 19, 553.

157. Shamir, J. and Caulfield, H.J., 1987. High-Efficiency Rapidly Programmable Optical Interconnections. *Applied Optics*, Vol. 26, 1032.
158. Shamir, J., 1987. Three-Dimensional Optical Interconnection Gate Array. *Applied Optics*, Vol. 26, 3455.
159. Cuykendall, R. and Anderson, D.R., 1987. Reversible Computing: All-Optical Implementation of interaction and Priesse Gates. *Optics Communications*, Vol. 62, 232.
160. Casey Jr., H.C., Sell, D.D. and Panish, M.B., 1974. Refractive Index of $\text{Al}_x\text{Ga}_{1-x}\text{As}$ Between 1.2 and 1.8 eV. *Applied Physics Letters*, Vol. 24, 63.
161. Adachi, S., 1985. GaAs, AlAs, and $\text{Al}_x\text{Ga}_{1-x}\text{As}$: Material Parameters for use in Research and Device Applications. *Journal of Applied Physics*, Vol. 58, R1.
162. Adachi, S. and Oe, K., 1983. Internal Strain and Photoelastic Effects in $\text{Ga}_{1-x}\text{Al}_x\text{As}$ and $\text{In}_{1-x}\text{Ga}_x\text{As}_y\text{P}_{1-y}/\text{InP}$ Crystals. *Journal of Applied Physics*, Vol. 54, 6620.
163. Aspnes, D.E., Kelso, S.M., Logan, R.A. and Bhat, R., 1986. Optical Properties of $\text{Al}_x\text{Ga}_{1-x}\text{As}$. *Journal of Applied Physics*, Vol. 60, 754.
164. Adachi, S., 1989. Optical Dispersion Relations for GaP, GaAs, GaSb, InP, InSb, $\text{Al}_x\text{Ga}_{1-x}\text{As}$, and $\text{In}_{1-x}\text{Ga}_x\text{As}_y\text{P}_{1-y}$. *Journal of Applied Physics*, Vol. 66, 6030.
165. Adachi, S., 1988. Optical Properties of $\text{Al}_x\text{Ga}_{1-x}\text{As}$. *Physical Review B*, Vol. 38, 345.
166. Palik, E.D., ed., 1991. Handbook of Optical Constants of Solids II. Academic Press, San Diego, CA.

167. Selby, S.M., ed., 1975. Standard Mathematical Tables, Twenty-third edition. CRC Press, Cleveland, OH.
168. Van der Ziel, J.P. and Gossard, A.C., 1977. Absorption, Refractive Index, and Birefringence of AlAs-GaAs Monolayers. Journal of Applied Physics, Vol. 48, 3018.
169. Weast, R.C., ed., 1985. CRC Handbook of Chemistry and Physics, Sixty sixth edition. CRC Press, Boca Raton, FL.
170. Sommerfeld, A., 1959. Optics: Lectures on Theoretical Physics, Volume IV. Academic Press, New York, NY.
171. Hecht, E. and Zajac, A., 1974. Optics. Addison-Wesley Publishing, Reading, MA.
172. Brown, E.B., 1965. Modern Optics. Reinhold Publishing, New York, NY.
173. Yariv, A., Mead, C.A. and Parker, J.V., 1966. 5C3-GaAs as an Electrooptic Modulator at 10.6 Microns. IEEE Journal of Quantum Electronics, Vol. QE-2, 243.
174. Somekh, S., Garmire, E., Yariv, A., Garvin, H.L. and Hunsperger, R.G., 1973. Channel Optical Waveguide Directional Couplers. Applied Physics Letters, Vol 22, 46.
175. Faist, J., Reinhart, F.-K., Martin, D. and Tuncel, E., 1987. Orientation Dependence of the Phase Modulation in a p-n Junction GaAs/Al_xGa_{1-x}As Waveguide. Applied Physics Letters, Vol. 50, 68.
176. Somekh, S., Garmire, E., Yariv, A., Garvin, H.L. and Hunsperger, R.G., 1974. Channel Optical Waveguides and Directional Couplers in GaAs-Imbedded and Ridged. Applied Optics, Vol 13, 327.

177. Campbell, J.C., Blum, F.A., Shaw, D.W. and Lawley, K.L., 1975. GaAs Electro-Optic Directional-Coupler Switch Applied Physics Letters, Vol. 27, 202.
178. Faist, J. and Reinhart, F.-K., 1990. Phase Modulation in GaAs/AlGaAs Double Heterostructures: II Experiment. Journal of Applied Physics, Vol. 67, 7006.
179. Donnelly, J.P., DeMeo, Jr., N.L. and Ferrante, G.A., 1983. Three-Guide Optical Couplers in GaAs. Journal of Lightwave Technology, Vol. LT-1, 417.
180. Shelton, J.C., Reinhart, F.K. and Logan, R.A., 1978. Rib Waveguide Switches With MOS Electrooptic Control for Monolithic Integrated Optics in GaAs-Al_xGa_{1-x}As. Applied Optics, Vol. 17, 2548.
181. Walsh, T.E., 1966. Gallium-Arsenide Electro-Optic Modulators. RCA Review, Vol. 27, 323.
182. Shih, C. and Yariv, A., 1982. A Theoretical Model of the Linear Electro-Optic Effect. Journal of Physics C: Solid State Physics, Vol. 15, 825.
183. Shelton, J.C., Reinhart, F.K. and Logan, R.A., 1979. Characteristics of Rib Waveguides in AlGaAs. Journal of Applied Physics, Vol. 50, 6675.
184. Reinhart, F.K., Logan, R.A. and Sinclair, W.R., 1982. Electrooptic Polarization Modulation in Multielectrode Al_xGa_{1-x}As Rib Waveguides. IEEE Journal of Quantum Electronics, Vol. QE-18, 763.
185. Lengyel, G., 1983. GaAlAs p-i-n Junction Waveguide Modulator. Journal of Lightwave Technology, Vol. LT-1, 251.
186. Hutcheson, L.D. and Hall, D.G., eds., 1983. Integrated Optics III-Volume 408. SPIE, Bellingham, WA.

187. Topical Meeting: Integrated and Guided Wave Optics-Technical Digest, 1986. LEOS and OSA, Atlanta, GA.
188. Glick, M., Reinhart, F.K., Weimann, G. and Schlapp, W., 1986. Quadratic Electro-Optic Light Modulation in a GaAs/AlGaAs multiquantum Well Heterostructure Near the Excitonic Gap. Applied Physics Letters, Vol. 48, 989.
189. Sahara, R.T., Steier, W.H., Hummel, S.G. and Dapkus, P.D., 1991. AlGaAs/GaAs Optically Controlled Wave-Plate Modulator. Optics Letters, Vol. 16, 1958.
190. Glick, M., Reinhart, F.K. and Martin, D., 1988. Linear Electro-Optic Effect: Comparison of GaAs/AlGaAs Multi-Quantum-Well Heterostructures With an AlGaAs Solid Solution at 1.1523 μm . Journal of Applied Physics, Vol. 63, 5877.
191. Sze, S.M., 1981. Physics of Semiconductor Devices, Second edition. John Wiley and Sons, New York, NY.
192. Peebles, P.Z., 1987. Probability, Random Variables and Random Signal Principles, Second edition. McGraw-Hill, New York, NY.
193. Parker, E.H.C., ed., 1985. The Technology and Physics of Molecular Beam Epitaxy. Plenum Press, New York, NY.
194. Casey, H.C. and Panish, M.B., 1978. Heterostructure Lasers Part A: Fundamental Principles. Academic Press, New York, NY.
195. Casey, H.C. and Panish, M.B., 1978. Heterostructure Lasers Part B: Materials and Operating Characteristics. Academic Press, New York, NY.

196. Johnson, W.C., 1950. Transmission Lines and Networks. McGraw-Hill, New York, NY.